

1-1-2013

High Power Linearly Polarized Fiber Lasers in a Linear Cavity

Angie Reda Abdelhay Mohamed Ali Eldamak
Ryerson University

Follow this and additional works at: <http://digitalcommons.ryerson.ca/dissertations>

 Part of the [Electrical and Computer Engineering Commons](#)

Recommended Citation

Eldamak, Angie Reda Abdelhay Mohamed Ali, "High Power Linearly Polarized Fiber Lasers in a Linear Cavity" (2013). *Theses and dissertations*. Paper 2079.

This Dissertation is brought to you for free and open access by Digital Commons @ Ryerson. It has been accepted for inclusion in Theses and dissertations by an authorized administrator of Digital Commons @ Ryerson. For more information, please contact bcameron@ryerson.ca.

HIGH POWER LINEARLY POLARIZED FIBER LASERS IN A LINEAR CAVITY

by

Angie Reda Abdelhay Mohamed Ali Eldamak

B.Sc.(2002),M.Sc. (2006), Ain Shams University, EGYPT

A thesis

Presented to Ryerson University

in partial fulfillment of the
requirements for the degree of
Doctor of Philosophy
in the Program of
Electrical and Computer Engineering

Toronto, Ontario, Canada, 2013

©(Angie Eldamak) 2013

AUTHOR'S DECLARATION FOR ELECTRONIC SUBMISSION OF A DISSERTATION

I hereby declare that I am the sole author of this dissertation. This is a true copy of the dissertation, including any required final revisions, as accepted by my examiners.

I authorize Ryerson University to lend this dissertation to other institutions or individuals for the purpose of scholarly research

I further authorize Ryerson University to reproduce this dissertation by photocopying or by other means, in total or in part, at the request of other institutions or individuals for the purpose of scholarly research.

I understand that my dissertation may be made electronically available to the public.

Abstract

HIGH POWER LINEARLY POLARIZED FIBER LASERS IN A LINEAR CAVITY

Angie Reda Abdelhay Mohamed Ali Eldamak

Doctor of Philosophy

Department of Electrical and Computer Engineering

Ryerson University, Toronto, CANADA

2013

This thesis presents two designs for high power linearly polarized all-fiber linear cavity lasers, continuous wave (CW) and mode-locked. The cavity designs use Polarization Maintaining (PM) fibers for both gain medium and Fiber Bragg Gratings (FBGs). The FBG pairs select lasing wavelength and polarization. The fiber lasers incorporating specialty designed FBGs achieve an extinction ratio larger than 23 dB.

Firstly, an all-fiber linear cavity design of a high power picoseconds mode-locked laser is introduced. The proposed configuration is based on Non-Linear Polarization (NPR) using PM Yb-doped active fiber and two matching FBGs to form the laser cavity. The combination of nonlinearity, gain and birefringence in cavity made the laser generate mode-locked pulses in picoseconds range and with high average output power. The output mode-locked pulses amplitude is modulated with an envelope whose mechanism is also investigated in this thesis project.

Experimental data and numerical simulations of the self mode-locking fiber laser are presented. Main parameters affecting mode-locked pulses and its envelope are identified. In addition, a new theoretical model based on Nonlinear Schrödinger Equation (NLSE) is developed and

implemented on the MATLAB® platform. The model explains the self mode-locking mechanism and the source of the pulse envelope. In this model, it is proven that self phase modulation (SPM) plays an essential role in pulse formation and shaping. The theoretical model and experimental results are in a very good agreement at different pumping levels.

A method of regulating the mode-locked pulses is presented. This is achieved by applying a pulsed current to pump diode. This method successfully stabilizes the mode-locked pulses underneath a Q-switched pulse envelope. Further scale-up of average power and pulse energy is realized by adding an amplifier stage.

Secondly, a CW dual-wavelength all-fiber laser is presented. The laser consists of two pairs of FBGs and a PM Er/Yb co-doped fiber as a gain medium. The laser emits at both 1 μm and 1.5 μm wavelengths simultaneously with a stable output. This laser provides a compact fiber-based pumping source that is suitable for mid-IR generation.

Acknowledgements

First, I would like to thank my Creator, for giving me the wisdom and foundation to accomplish this thesis.

I am deeply indebted to my supervisor, Prof. Xijia Gu, for his continuous academic advice, constant encouragement, endless patience, and priceless guidance and support throughout this work. I am really grateful to him, not only for contributing many valuable suggestions and improvements to this thesis, but most importantly for training me to be an independent researcher, with the ability to identify interesting and important research problems and to generate frameworks to solve them. Moreover, I am grateful to him for exposing me to collaboration with different industrial and academic institutions. I feel honoured to have been given the opportunity to work under his supervision.

I would also like to acknowledge my Ph.D. external examiner, Prof. Li Qian and my esteemed internal committee members: Prof. James Smith, Prof. Beau Standish and Prof. Vladislav Toronov for the valuable input they have given into my thesis. I would like also to thank my colleagues in the lab, Yi Lu (Eric), Jiaqi Zhao (Terry) and Lei Zhang for the fruitful scientific discussions. My deepest thanks go to Ms. Jiang Li, for her great help and valuable support especially in FBGs fabrication.

Next, I would like to pay my humble respect and the deepest thanks from my heart to my mother, Hoda Elshehaby, my father, Prof. Reda El-Damak, and my lovely sister, Dina, for their endless support, love, patience, and encouragement. I am extremely grateful to my parents for giving me the best education, the warmest care, the righteous upbringing and the best in everything.

My final warmest thanks from my heart go to my precious husband, Mohamed Kamh, who really changed my life to the best in everything, and supported me throughout this long Ph.D. path. He always lightened my bad days and perfected my good ones. No words can express my gratitude and appreciation to him, and my in-laws, for the kind support and tremendous care.

Dedication

To my lovely son Yousef, my husband Mohamed and my Parents

Table of Contents

List of Tables.....	x
List of Figures	xi
List of Appendices	xvii
Acronyms.....	xviii
Chapter 1. Introduction.....	1
1.1. Applications	2
1.2. Pulsing Mechanisms	2
1.3. Literature Review.....	5
1.3.1. Passively Mode-Locked Fiber Lasers.....	5
1.3.2. Self-Pulsed Fiber Lasers.....	11
1.4. Problem Statement	13
1.5. Thesis Outline	16
Chapter 2. Experimental Characterization.....	17
2.1. General Configuration of Fiber Laser	17
2.2. Optical Components	18
2.2.1. Pump Laser Diodes	18
2.2.2. Optical Fibers	20
2.2.3. Fiber Bragg Gratings on PM fibers.....	25
2.3. Fiber Laser Assembly.....	26
2.4. Fiber Laser Measurements.....	28
2.4.1. Power & Polarization Measurements	28
2.4.2. Pulse Measurements.....	29
2.5. Design Specifications.....	33
Chapter 3. Experimental Results of Mode-Locked all-PM Fiber Laser	35
3.1. Laser Design Overview.....	35
3.2. Characterization of Laser Performance.....	35
3.2.1. Power Measurements	35
3.2.2. Spectrum Measurements	37
3.2.3. Polarization Measurements	39

3.2.4. Pulse Measurements	40
3.3. Scaling Pulse Energy and Average Power	47
3.3.1. Cavity Length Extension	47
3.3.2. Amplifier Stage	48
3.4. Regulation of Mode-Locked Pulses	51
3.4.1. Experimental Setup	52
3.4.2. Experimental Results.....	52
3.5. Summary & Discussions	56
Chapter 4. Numerical Modelling of All-PM Mode-Locked Fiber Laser	58
4.1. Nonlinear Pulse Propagation in Fiber	58
4.1.1. Self Phase Modulation (SPM).....	60
4.1.2. Cross Phase Modulation (XPM).....	61
4.1.3. Nonlinear Polarization Rotation (NPR)	62
4.2. Numerical Modelling.....	64
4.2.1. Nonlinear Schrödinger Equation (NLSE).....	64
4.2.2. Split Step Fourier Method	65
4.3. Numerical Simulations	67
4.3.1. Pulsing origin.....	68
4.3.2. Mode-locked Pulses Simulation.....	70
4.4. Discussions: Mode-locking Mechanism	79
Chapter 5. CW Linearly Polarized ALL-Fiber Laser Sources.....	81
5.1. Introduction	81
5.2. Dual Wavelength all-PM Fiber Laser	83
5.2.1. Experimental setup.....	83
5.2.2. Results & Discussions	85
Chapter 6. Conclusions and Future Directions	89
6.1. Conclusions	89
6.2. Directions for Future Research	91
Appendix. A: Effect of Instruments Bandwidth on Pulse Measurement	92
Appendix. B: Time Dependent Fiber Laser Rate Equations.....	94

Appendix. C: MATLAB Codes.....	96
References	100
Publications.....	108

List of Tables

Table 1.1: Comparison between active and passive mode locking.....	4
Table 1.2: Summary of recent designs for passively mode locked fiber lasers in the 1 μ m band.	11
Table 2.1: 10 W LUMICS multi-mode laser diode specifications	19
Table 2.2: 25 W Ocular multi-mode laser diode specifications.....	20
Table 2.3: Specifications of Yb ³⁺ active fibers used in the thesis.....	23
Table 2.4: Specifications of Er ³⁺ /Yb ³⁺ active fiber used in the thesis	24
Table 2.5: Specifications of passive fibers used in the thesis.....	24
Table 2.6: Specifications of general purpose detectors	31
Table 2.7: Specifications of high speed detectors	32
Table 3.1: Laser output parameters at different repetition rates.....	55
Table 4.1: Simulation parameters for NLSE-based model.....	74
Table B.1: Basic parameters used in fiber laser rate equations.	94

List of Figures

Figure 1.1: Intensity of a periodic pulse train resulting from the sum of M laser modes of equal magnitude and phase (I is the average intensity). 3

Figure 1.2: A schematic diagram for a mode-locked fiber laser using SESAM for (a) A ring cavity [26], and (b) A linear cavity [27]. 6

Figure 1.3: A schematic diagram for a mode-locked fiber laser with NPR technique [28]. 8

Figure 1.4: A schematic diagram for a mode-locked fiber laser using SWNT in a ring cavity form [39]. 10

Figure 2.1: A schematic diagram of the linearly polarized mode-locked high-power fiber laser. 17

Figure 2.2: (a) 10 W LUMICS multi-mode fiber-coupled laser diode, (b) 25 W Oclaro multi-mode laser diode. 19

Figure 2.3: Schematic for double-clad fiber laser. 20

Figure 2.4: Different shapes for polarization maintaining (PM) fibers. 21

Figure 2.5: (a) Absorption and emission spectra for Yb^{3+} in silica [15].(b) Energy level diagram of Er-Yb co-doped fiber [60]. 22

Figure 2.6: Absorption cross section at pump wavelength band for Er^{3+} / Yb^{3+} in silica (a) Ref. [61], (b) Ref. [62] 23

Figure 2.7: Typical Fiber Bragg Grating pair spectra design written on PM fiber at 1064 nm band and used in the proposed fiber laser. 25

Figure 2.8: (a) Schematic for co-splicing two PM fibers. (b) Photo for X-view direction for co-splicing two PM fiber using Fujikura FSM-20PMII machine. .. 26

Figure 2.9: (a) Schematic for cross-splicing two PM fibers. (b) Photo for X-view direction for cross-splicing two PM fiber using Fujikura FSM-20PMII machine. 27

Figure 2.10: (a) Loose nylon tubes (b) Heat shrinkable sleeves with metal support (c) Low index recoating (d) High index recoating.....	27
Figure 2.11: Experimental setup for measuring polarization extinction ratio (PER).	29
Figure 3.1: Measured output power versus pumping power for 5 μ m core module with 5 m active fiber and using different output couplers (a) R=10% (b)R=20%, R=55% and 75%.	36
Figure 3.2: Measured output power versus pumping power for 10 μ m core modules (a) Output coupler reflectivity, R =10% at different active fiber lengths. (b) Active fiber length, L =10 m at R=10% and R=50%.	37
Figure 3.3: (a) Transmission and Reflection spectra for FBG pair with operating wavelength of 1063.4 nm. (b) Output spectrum at 0.46 W and 4.6 W output power of the 5 μ m fiber laser.	38
Figure 3.4: Measurements for 5 μ m core laser module (a) Output spectra at different output power levels, and (b) 20dB bandwidth versus output power at different output coupler reflectivity.....	38
Figure 3.5: Measurements for 10 μ m core laser module with an active fiber length of 10m. (a) Output spectra at maximum power level of 5.4 W and R= 10%. (b) Output spectra at different output power levels using R=50%.	39
Figure 3.6 Measurements for 5 μ m core laser module with an active fiber length of 5m and R= 10%. (a) Extinction ration in (dB) versus laser output power (b) Malus polarization curve: Normalized output power versus polarizer angle in degrees.	39
Figure 3.7: Measured laser spectra at different pumping power with co-spliced output coupler FBG.	40
Figure 3.8: Measurements for 5 μ m core laser module with an active fiber length of 5 m and output coupler of 10% (a) Mode-locked pulse train at output power of 2 W (b) Single pulse width of 83 ps at 2 W output power.....	41

Figure 3.9: Mode-locked pulse train for 5 μ m core laser module with an active fiber length of 5m and R =55% with 54ns round trip time (a) PFL=0.7W. (b) PFL=3W. PFL is the fiber laser output power. 41

Figure 3.10: Measurements for 5 μ m core module with 5m active fiber (a) Envelope width versus output power and R =20%, 46%, 55% and 75%. (b) Measured pulse width versus output power and 55% output coupler. 42

Figure 3.11: Measurements for 10 μ m core laser module with R =10% (a) Pulse width measurements at different output power with active fiber length of 2.55 m and 10 m. (b) Pulse width at 0.8 W and 5 W output power..... 43

Figure 3.12: Measurements for 10 μ m core laser modules. (a) Envelope width versus output power with R=10% and active fiber length of 2.55 m, 4 m and 10 m. (b) Envelope width versus output power with 2.55 m active fiber at R =10% and 82%. (c) Envelope width versus output power using 10 m active fiber at R =10% and R=50 %.(d) Single pulse width versus output power with 10 m active fiber and R=50%. 44

Figure 3.13 Oscilloscope trace for SML pulses with an amplitude envelope. (a) PFL=1 W, P_{pump}=2.5 W. 45

Figure 3.14: All-fiber mode- locked laser schematic with mid cross-splicing point for the active fiber. This module has a total PM Yb-doped active fiber length of 10 m with R= 50%. 45

Figure 3.15: Oscilloscope traces for envelope measurements from 10 μ m core laser module with active fiber length of 10 m with mid cross-splicing and R =50% at different output power levels..... 46

Figure 3.16: Measurements for 10 μ m core laser module with an active fiber length of 10 m with mid cross-splicing and R=50% (a) Envelope width at different output power at R =10%, R =50% without and with active fiber mid cross-splicing. (b) Single pulse width measured at 4W output power. 47

Figure 3.17: Output power versus pumping power for 5 μ m laser module operating at 1 μ m wavelength with 10% output coupler and cavity length of 5 m and 55 m. 48

Figure 3.18: Measurements for 5 μm laser module with 55 m cavity length and 10% output coupler (a) Laser output spectra at different output power (b) Mode-locked pulse train at 1.1 W output power.....	48
Figure 3.19: Amplifier schematic connected to 5 μm core module as seed laser.	49
Figure 3.20: (a) Measurements of seed output power versus seed pump power at different positions before turning on amplifier. (b) Seed laser pulse train at 0.65 W output power.....	50
Figure 3.22: Amplified mode-locked pulse train at 10 W, 16 W and 18.8 W average output power.....	51
Figure 3.23: (a) Average power versus pump power at CW mode. (b) Mode-locked pulses at output power of 6.75W	52
Figure 3.24: (a) Details of Q-switch pulse measured at repetition rate of 10 KHz and electronic pulse width (τ_{EPW}) of 8 μs . (b) Q-switching background height versus τ_{EPW} at different repetition rates.....	53
Figure. 3.25: Pulse measurements where left column is Q-switch pulse train, middle column is QML pulse and the right column is mode-locked pulse width for (a)-(c) $f=10$ KHz, (d)-(f) $f=30$ KHz, (g)-(i) $f=60$ KHz.	54
Figure 3.26: Average power and mode-locked pulse width versus repetition rate.....	54
Figure 3.27: Pulse measurements at $f=100$ KHz (a) Q-switch pulse train. (b) Q-switch pulse with mode-locked pulses (c) single mode-locked pulse width.	55
Figure 3.28: Pulse measurements with current repetition rate of 100 KHz . (a) QML pulse at EPW=8 μs (b) QML at EPW= 9 μs . (c) Q-switched mode-locked pulse train at EPW=9 μs	56
Figure 4.1: MATLAB simulation of a Gaussian pulse after passing through fiber length of 5 m with including SPM with GVD effects (a) $\beta>0$ (Normal dispersion) (b) $\beta<0$ (Anomalous dispersion).....	61

Figure 4.2: The SSFM for one iteration of step h starting at $z = (j-1)h$. The initial pulse $A(0,t)$ enters the medium of length L . The length is divided into $s_L = L/h$ steps of length h	66
Figure 4.3: Measured pulsing start-up near threshold with relaxation oscillation structure.....	68
Figure 4.4: (a) Oscilloscope trace for Self-Q switching pulses at low pumping power near threshold. (b) Details of single Q-switched pulse.....	68
Figure 4.5: Measurement of 5 μ m core fiber laser module with 5 m active fiber and R=46% (a)-(c) Evolution of Q-switched like pulses (d)-(f) Evolution of SML pulses underneath Q-switched pulses.....	69
Figure 4.6 : (a) Fiber laser schematic (b) Simulation model schematic; where SF(1) is the HR-FBG and SF(2) is the OC-FBG.....	70
Figure 4.7: Simulated output pulses (a) without phase shift component (b) with phase shift component.....	74
Figure 4.8: Two polarization simulation using CNLSE and PM FBG reflectivity matrices at $E_{sat}=2$ nJ.....	75
Figure 4.9: (a) Simulation output with phase shift component for $N=10000$ R.T and $E_{sat}=2$ nJ. (b) Single pulse plot underneath the marked envelope shown in Figure4.9 (a).	76
Figure 4.10: (a) Measured pulse envelope at $P_{pump}=1$ W (b) 4 μ s pulse train at $P_{pump}=1$ W (c) Simulated envelope at equivalent $P_{pump}=1$ W, $E_{sat}=2$ nJ (Envelope width=34 μ s). (d). 4 μ s simulated pulse train at equivalent $P_{pump}=1$ W, $E_{sat}=2$ nJ.	76
Figure 4.11: Simulated envelope at equivalent (a) $P_{pump}=2.5$ W, $E_{sat}=4$ nJ (b) $P_{pump}=6$ W, $E_{sat}=12$ nJ (c) $P_{pump}=8$ W, $E_{sat}=16$ nJ.....	77
Figure 4.12: (a) Simulated single pulse width at equivalent $P_{pump}=8$ W, $E_{sat}=16$ nJ. (b) Measured and Simulated envelope widths versus pumping power.....	78
Figure 4.13: Envelope width versus phase factor (K).....	79

Figure 5.1: A schematic diagram of the linearly polarized fiber laser using SP fiber in 1 μ m band [89].....	81
Figure 5.2: A schematic diagram of the dual wavelength linearly polarized Er/Yb-doped fiber laser.....	84
Figure 5.3: Fiber Bragg Grating spectra at 1057 nm show the matching fast and slow axes wavelengths.....	85
Figure 5.4: Output power versus pump power for both wavelengths of 1554 nm and 1057 nm.	86
Figure 5.5: (a) Extinction ratio in dB as a function of the laser total output power (b) Laser output spectrum at 5.3 W pump powers.	86
Figure 5.6: Output spectrum at (a) 1057 nm wavelength and (b) 1554 nm wavelength.....	87
Figure 5.7: (a) Output spectrum tunability by varying temperature of 1057 nm FBG pair (b) Mid-IR spectra tuned at different temperature.	87

List of Appendices

Appendix. A: Effect of Instruments Bandwidth on Pulse Measurement.....	93
Appendix. B: Time-Dependent Fiber Laser Rate Equations.....	95
Appendix. C: MATLAB Codes.....	97

Acronyms

APC	Angle Polished Connector
AQWP	Achromatic Quarter Wave Plates
ASE	Amplified Spontaneous Emission
CFBG	Chirped Fiber Bragg Grating
CW	Continuous Wave
DCF	Dispersion Compensating Fiber
DFG	Difference Frequency Generation
EPW	Electronic Pulse Width
FBG	Fiber Bragg Grating
FC	Flat Connector
FFT	Fast Fourier Transform
FWM	Four-Wave Mixing
GaInNAs	Gallium Indium Nitride Arsenide
GVD	Group Velocity Dispersion
HR	High Reflection
IFFT	Inverse Fast Fourier Transform
InGaAs	Indium Gallium Arsenide
InP	Indium Phosphide
LD	Laser Diode
NOLM	Nonlinear Optical Loop Mirrors
NPR	Nonlinear Polarization Rotation
OC	Output Coupler
OCT	Optical Coherence Tomography
PC	Polarization Controller
PCF	Photonic Crystal Fiber
PER	Polarization Extinction Ratio
PM	Polarization Maintaining
QML	Q-switched Mode-locked
QWP	Quarter Wave Plate
SA	Saturable Absorber
SBS	Stimulated Brillouin Scattering
SESAM	Semiconductor Saturable Absorber Mirror
SHG	Second Harmonic Generation
SMF	Single Mode Fiber
SML	Self Mode-Locked
SNR	Signal to Noise Ratio
SP	Single Polarization
SPM	Self Phase Modulation
SRS	Stimulated Raman Scattering
SWCNT	Single-Wall Carbon Nanotubes
TBP	Time Bandwidth Product
WDM	Wavelength Division Multiplexer
XPM	Cross Phase Modulation

Chapter 1. Introduction

For decades, lasers have been widely applied to numerous applications including electronics, communication, medicine, law enforcement, entertainment and military. Some of applications require the laser power be only in Continuous Wave (CW) while others require high intensity in short time durations, i.e.; pulsed laser systems.

Fiber lasers have gained increasing attention because of their excellent beam quality, high brightness, outstanding efficiency, diverse wavelength selection and good compactness. With the adoption of double-clad fibers and clad-pumping techniques, laser output can be obtained with high power and energy levels at either CW or pulsed regime. Novel applications for fiber lasers are emerging as specialists investigate the performance features and flexibility of the all-fiber solutions.

Fiber lasers have extended their performance capabilities and substitute conventional laser technologies markets. This can be attributed to[1-3]:

- Large gain bandwidth of rare-earth-doped fibers (typically tens of nanometers), compared to gas lasers, allows the generation of pulses down to the femtosecond range.
- High gain efficiency of active fibers compared to Nd:YAG gain medium.
- Extended range of optical wavelengths by using different active dopants including Ytterbium, Erbium, Erbium-Ytterbium, Neodymium, and Thulium.
- Large surface-to-volume ratio of the active-fiber facilitates heat removal and minimizes external cooling requirements.
- Low fabrication costs and compact, rugged setups (particularly if free-space optics is not used) compared to rod or gas lasers with comparable power levels.
- Excellent beam quality.
- Instant turn-on operation without the need for regular tuning and realignment.
- High optical-to-optical, electrical-to-optical and high overall efficiencies compared to Nd: YAG and CO₂ lasers.
- Output-power scalability using multi-port pump injection or fiber-based amplifiers.

1.1. Applications

Fiber lasers are used for wide range of applications in material processing [3-6], military [7], medicine [8], spectroscopy, metrology, communication, LIDAR and GPS satellites [3, 4].

Of particular interest in this thesis are high power pulsed fiber lasers that operate at $1\mu\text{m}$. These lasers are very attractive for several industrial and medical applications including medical devices fabrication, drilling holes in circuit boards, patterning of thin films, processing of solar cells, marking and ablation [3-6, 8-11].

The availability of high power, fiber laser with linearly polarized output open possibilities for applications such as efficient beam combining, interferometer sensing and nonlinear frequency conversion. Second Harmonic Generation (SHG) using $1\mu\text{m}$ linearly polarized pulsed lasers (to realize 532 nm wavelength) acquire higher conversion efficiency [12]. This is because pulsed lasers exhibit higher peak power levels leading to stronger nonlinear interaction [13].

Another application for high power linearly polarized lasers is Differential Frequency Generation (DFG) for Mid-IR applications. These lasers have several industrial applications especially for gas detection [14]. In particular, Methane detection requires generation of $3.3\mu\text{m}$ wavelength. To decrease the overall system cost and sensitivity to environmental disturbances, the use of fiber lasers as pump sources was implemented. Generating $3.3\mu\text{m}$ wavelength is realized using linearly polarized narrow linewidth fiber lasers at wavelengths of $1\mu\text{m}$ and $1.5\mu\text{m}$ [13].

1.2. Pulsing Mechanisms

Fiber lasers are used in many applications which require high peak power and pulse energy. The two most well-established techniques to pulse fiber lasers are Q-switching and mode locking in either active or passive form [13, 15-17]. Q-switching is an effective method to obtain giant short pulses from a laser by spoiling the cavity loss periodically with a modulator inside the resonator cavity [13, 18]. In this technique the pump delivers constant power all time, where the energy is stored as accumulated population inversion during the OFF times (high loss). During the ON-time, the losses are reduced and the accumulated population difference is released as intense pulse of light. Q-Switching allows the generation of pulses of millijoules energy, ns duration and

few Hertz to hundreds kilohertz repetition rate. For shorter pulses in picoseconds range, mode-locking will be the main mechanism. The details of mode-locking definition and techniques are given as follows.

Mode-Locking of a laser produces ultra-short pulses on the order of picoseconds or femtoseconds. This technique induces a fixed phase relationship between the longitudinal modes of the laser's cavity. Interference between these modes causes the laser light to produce a train of pulses. Locking of mode phases enables a periodic variation in the laser output which is stable over time, and with periodicity given by the round trip time of the cavity [17]. Such a laser is said to be *mode-locked* or *phase-locked* as shown in Figure 1.1.

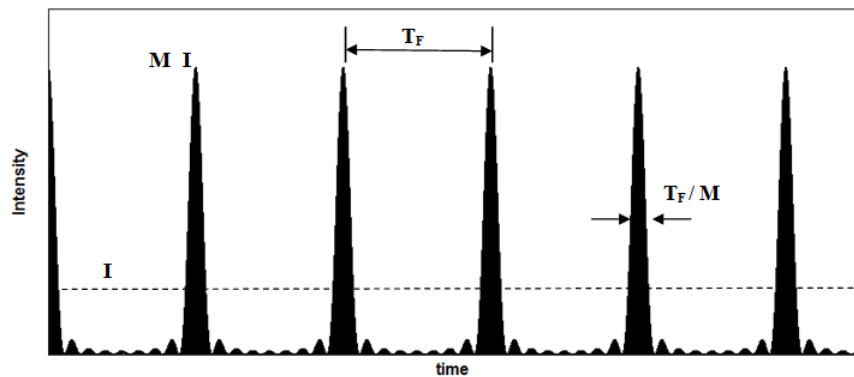


Figure 1.1: Intensity of a periodic pulse train resulting from the sum of M laser modes of equal magnitude and phase (I is the average intensity).

The output pulses are separated in time by $T_F = 2nL/c$, where T_F is the time taken for the light to make exactly one round trip of the linear laser cavity, L is the cavity length, c is the light speed and n is the group refractive index of the medium. The pulse width, τ_{pulse} is approximated by T_F/M ; where, M is the total number of phase locked modes. In a real mode-locked laser, the actual pulse width depends on other factors, such as the pulse shape and the overall dispersion of the cavity.

Fiber lasers can be mode-locked either in active or passive way. Active methods typically use an external signal to modulate the cavity loss and consequently require the use of bulky modulators and drivers. Passive mode-locking depends on incorporating a SA in the laser cavity. A saturable absorber is an optical component with a certain optical loss, which is reduced at high

optical intensities [13]. A comparison between both active and passive techniques is shown in Table.1.1.

Table 1.1: Comparison between active and passive mode locking

	Active Mode Locking	Passive Mode Locking
	Modulation of the cavity loss using external signal at a repetition rate equivalent to the cavity round trip, or one of its harmonics.	Fast modulation of cavity loss by inserting a nonlinear passive element (saturable absorber ‘SA’).
Modulator type	Acousto-optic modulator (AOM), Electro-optic modulator (EOM)	SESAM, Carbon nanotubes Crystals, NLO Artificial SA: Kerr lens mode locking, Additive-pulse mode locking, Nonlinear polarization rotation (NPR).
Advantages	<ul style="list-style-type: none"> • Pulse trains synchronized with an external electronic signal. • Higher repetition rate with harmonic mode-locking 	<ul style="list-style-type: none"> • Shorter pulses of ps and fs pulse width due to short recovery time of SA.
Disadvantages	<ul style="list-style-type: none"> • Longer pulses widths. • Need for an optical modulator or electronic driver. • Require precise matching of modulator driver signal and the laser so that the circulating pulse has minimal losses at the modulator output 	<ul style="list-style-type: none"> • Introduce more losses to the cavity by inserting high loss optical component (SA). • Lower pulse energy.

1.3. Literature Review

1.3.1. Passively Mode-Locked Fiber Lasers

Literature review shows that the most popular SAs in the 1 μ m band are Semiconductor Saturable Absorber Mirrors (SESAMs) [19-27], and Nonlinear Polarization Rotation (NPR) [28-32]. Other modulators such as Single-Wall Carbon Nanotubes (SWCNT) and NOLM are also reported. The following review categorizes the laser designs according to the type of the incorporated SA and analyzes their performance and limitations.

1.3.1.1. Semiconductor Saturable Absorber Mirrors (SESAM)

SESAM is a Bragg mirror on a semiconductor wafer. Most common types of SESAM are in the 1 μ m band, where InGaAs is used as SA. For longer wavelengths as 1.3 μ m or 1.5 μ m, GaInNAs (dilute nitride) or InP is used [13]. The SESAM saturates at a high enough intensity, permitting the majority of the energy in the cavity to pass through the absorbing material to the mirror, and then reflected back into the cavity [13]. SESAMs are known as slow absorbers with recovery time greater than 1 ps.

SESAM exhibits its saturable absorption properties from the interband transition in semiconductor. The energy of the absorbed photons is transferred to the electrons moving from the valence band to the conduction band. At low optical intensity, electronic excitation remains small and absorption is low. At high optical intensity, electrons accumulate in the conduction band while initial states for absorbing transition are depleted, thus the absorption is reduced. After saturation with the pulse, the absorption recovers through interband thermal relaxation and recombination [13].

Examples for laser cavities using SESAMs as SA are shown in Figure 1.2 (a) and (b). They are mainly composed of a piece of active fiber and a wavelength division multiplexer (WDM) to couple pump light in. SESAMs are deployed in the cavity through a 3 port circulator and bulk lenses or butted to the fiber end of a coupler or an active fiber. The laser output is either taken from an output coupler or WDM with an isolator to prevent back reflected light. SESAM-based cavities may also include polarization controllers (PCs), a bandpass filter or a FBG.

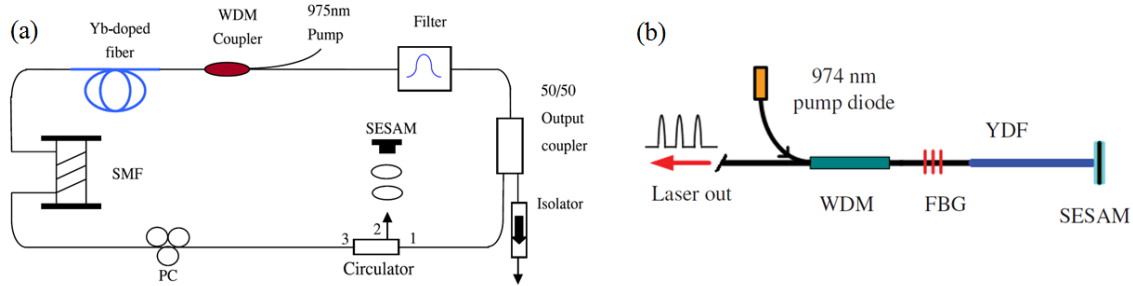


Figure 1.2: A schematic diagram for a mode-locked fiber laser using SESAM for (a) A ring cavity [26], and (b) A linear cavity [27].

Nielsen *et al.* developed passively mode-locked fiber laser using SESAM in [19]. It employs only Polarization Maintaining (PM) fiber in a linear cavity configuration [19]. It uses bulk optics to couple incident and reflected light on SESAM and HR grating. The reported cavity uses a grating compressor and a photonic crystal fiber (PCF) for dispersion compensation. This succeeds to compress the pulse width from 7.2 ps to 240 fs. The laser has a pulse energy of only 0.12 nJ which is enhanced to 1.2 μ J and 21 W average power using two amplifier stages.

Cho *et al.* presented a 0.3 nJ fiber laser with an average power of 10.4 mW in [20]. The laser cavity in [20] acquires a pulse width of 8.3 ps without using any dispersion compensating element. However, the laser output depends on the adjustment of two lenses to focus beam on the SESAM. In addition, Quarter wave plates (QWPs) and a polarizer are used to realize mode-locking in [20]. Using bulk components in [19, 20] will remove the compact advantage of fiber lasers.

Ortac and coworkers introduced a stable all-PM mode-locked fiber laser in a linear cavity using also a SESAM in [21]. The authors compensate cavity dispersion by using hollow-core photonic bandgap fiber and a Chirped Fiber Bragg Grating (CFBG). This all-fiber structure succeeded to compress the pulse width from 15.4 ps to 218 fs. However, core-pumping limits pulse energy to 0.39 nJ and average power to 7.9 mW.

Another SESAM-based design with a PM active fiber in a linear cavity is reported in [22]. It relies on adjustable achromatic quarter wave plates (AQWP) to maximize pulse energy and select the polarization state. The laser achieved relatively high pulse energy of 1 nJ without amplification and a pulse width of 2ps. Wave plates introduce a free space part inside the cavity which may affect the cavity stability. Lian *et al* reported a Fabry Perot cavity using SESAM and

FBG. The FBG provided spectral filtering and pulse shaping. Though the laser has an all-fiber structure; it cannot achieve more than 1nJ of energy and 30mW of average power due to the onset of multi-pulsing operation [23]. It also acquires a relatively broader pulse width of 21 ps.

In literature pulse energy is increased by adding amplifier stages [19, 24, and 25] or extending the cavity length [26]. Turchinovich *et al.* presented a stable all-PM fiber laser using a narrow FBG and SESAM in [24]. The pulse width is compressed down from 5.9 ps to 370 fs using a hollow-core photonic bandgap fiber. The laser achieves a 10 nJ energy level using a series of amplifiers [24]. Tian *et al.* uses 10 m of Yb-doped double cladding active fiber (Yb-DCF) as an amplifier in [25]. It increased the energy of their seed laser from 3 nJ to 4.3 μ J. The laser acquires high average power of 1.27 W but with a broad pulse width of 400ps. This high level of pulse energy is achieved with the aid of polarization controller (PC).

Song *et al.* reported 39 nJ energy level from a ring fiber laser without using an amplifier stage [26]. This is realized using 700 m of single mode fiber (SMF), PC and bandpass filter in addition to SESAM. This long SMF reduces the repetition rate and thus achieves higher pulse energy. On the other hand, the mode-locking operation in [26] depends on the adjustment of polarization controller as well as two lenses used to focus light on SESAM. No information was given on pulse width in [26].

1.3.1.2. Nonlinear Polarization Rotation (NPR)

NPR is another well-known technique for passively mode-locking fiber lasers. It is a very fast SA at which changes in the polarization of light in a fiber depends on the optical intensity. More details on NPR definition and mechanism will be given in Chapter 4.

A laser cavity based on NPR technique is shown in Figure 1.3 . The cavity is composed of an isolator, two PCs and a WDM combining both pump and signal light. The active fiber and output coupler are inserted between WDM and PC. The polarization state of light in the laser cavity is controlled by adjusting the two PCs such that a maximum transmission occurs at the polarizer. The two PCs work with the polarizer to suppress one polarization and realize mode-locked output. However, severe disadvantage is that the optimum polarization settings can drift due to temperature or environmental disturbance.

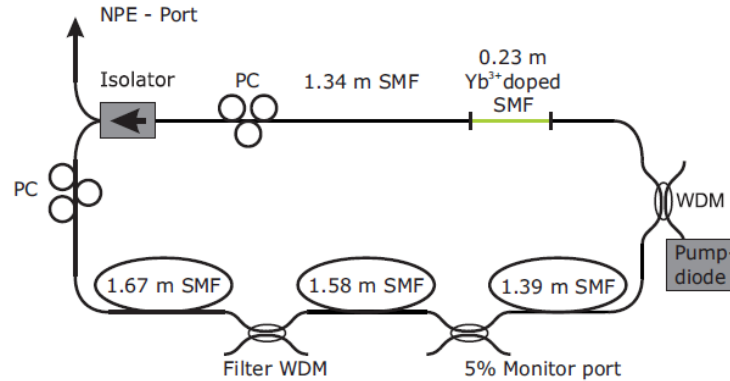


Figure 1.3: A schematic diagram for a mode-locked fiber laser with NPR technique [28].

Pronchnow *et al.* reported a compact all-fiber ring laser. It generates stable output pulses of 10 ps which are further dichirped to 629 fs [28]. Mode locking operation is realized using NPR, saturable Bragg reflectors and two PCs. The laser has a low energy level of 0.8 nJ and 28 mW average power [28].

Ozgoren *et al.* implemented the NPR technique and introduced an angle spliced piece of PM fiber in the laser cavity [29]. The PM fiber, inserted between two PCs and a polarization beam splitter, acts as a Lyot filter. The first polarizer transforms linear polarization, which is decomposed into orthogonal states as it couples to the fast and slow axes of the birefringent medium. The birefringence leads to the accumulation of a relative phase difference between the beams propagating along its main axes, which corresponds to wavelength-dependent rotation of the polarization state. The second polarizer converts this rotation into amplitude modulation, thus realizing mode-locking. The reported filter bandwidth and modulation depth can be controlled by adjusting the PM fiber length, birefringence value and splicing angle. The design with an all-fiber ring configuration generated pulses with a width of 15 ps, average power of 50 mW and pulse energy of 1.5 nJ [29].

A shorter pulse width of 7.6 ps is observed from a ring cavity presented by Schultz *et al.* in [30]. The mode locking operation is based on NPR with additional amplitude modulation using fiber-based spectral filtering and two PCs. The output pulse has energy of 1.8 nJ and compressed pulsed width of 179 fs.

J. Fekete *et al.* developed another mode-locked ring fiber laser cavity using both NPR and SESAM [31]. The design uses a polarization beam splitter between two PCs to acquire mode locking. Combining both NPR and SESAM in a laser cavity achieves no more than 0.2 nJ pulse energy with a 10 ps pulse width. The mode-locking operation in [25, 26, 28-31] is realized by the adjustment of two PCs. Thus, the readjustment for PCs may often become necessary to compensate any operation disturbances.

Nielsen et al. reported in [32] mode-locked fiber laser based on NPR without using PCs. This is achieved by inserting a PM fiber between Faraday mirror (FM) and a polarizer in [32]. The PM fiber is spliced at an angle to the slow axis of the polarizer to realize NPR. The proposed cavity has no free space sections or adjustable components. However, core pumping also limits the output average power to 8 mW and the pulse energy to 1.34 nJ.

1.3.1.3. Carbon Nanotubes

Carbon nanotubes are synthesized by ablating a metal-catalyzed carbon target using Nd: YAG laser in 500 Torr of argon gas. The resulting nanotubes (of mean diameter 1.1 nm) are dispersed in ethanol and sprayed onto on mirrors or fiber-based devices, exhibiting saturable absorption properties of light [13, 33]. Carbon nanotubes serve as fast saturable absorbers, owing to their sub-picosecond recovery time, low saturation intensity and polarization insensitivity [13].

Mode-locked fiber lasers with carbon nanotubes are mostly reported in a ring structure as shown in Figure 1.4. The cavity is composed of an active fiber, pumped with 980 nm laser diode through WDM. An isolator is placed to ensure unidirectional propagation of light. The single-wall nanotube (SWNT) is placed between photonic crystal fiber (PCF) and PC as shown in Figure 1.4. PCF is used for dispersion compensation and further compressing pulse width.

Fewer designs use nanatoubes as SA in the 1 μ m band compared to 1.5 μ m [34-38]. A 22 pJ mode-locked fiber laser using nanotube and photonic crystal fiber (PCF) in 1070 nm range is reported in [39]. The laser acquires a short pulse width of 543 fs by optimizing cavity dispersion.

The laser in [39] uses two lenses to focus light on nanotube and yet introducing a free space section in the fiber laser cavity. A PC is also used in [39] to fix the polarization state in the cavity.

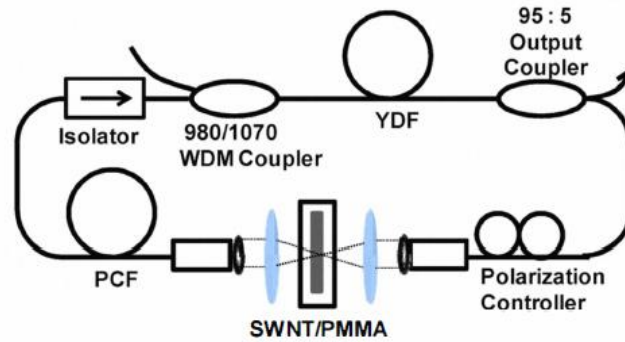


Figure 1.4: A schematic diagram for a mode-locked fiber laser using SWNT in a ring cavity form [39].

Kiew *et al.* used both inline carbon nanotubes and SESAM to realize mode-locking in a ring cavity. The output pulse has 1.5 ps width which is compressed to 250 fs using a grating pair outside the cavity. Using two absorbers offers no more than 3nJ energy level. Also the chosen carbon nanotubes performance was reported to degrade with time. The laser performance in [40] is also sensitive to the settings of the PC.

1.3.1.4. Nonlinear Optical Loop Mirror (NOLM)

NOLM is also used to passively mode-lock fiber lasers. It is constructed from an output coupler whose output ports are spliced together, while counter-propagating intensities are made unequal by having a coupler splitting ratio not 50%. It offers fast recovery time and wide bandwidth compared to SESAMs. However, it is hard to characterize or customize its device parameters. The fastest mode-locked pulse with pulse width 128fs [41] was achieved by combining nonlinear NPR and a nonlinear amplifying loop mirror. The total cavity length is of 12 m and no information on power or energy was given.

This review mainly concentrates on recent designs for passively mode-locked fiber using modulators such as SESAM, NPR, nanotubes and NOLM in the 1 μ m band. The performance parameters are summarized in Table 1.2 in terms of achieved average power, pulse energy, pulse width, repetition rate and operating wavelength. The main limitations of the modulation techniques and the reviewed designs will be summarized in Sec 1.4.

Several fiber laser modules had been also reported with self-pulsed output without using conventional SAs. This type of lasers had been also an attractive topic to study and will be reviewed in the following section.

Table 1.2: Summary of recent designs for passively mode locked fiber lasers in the 1 μ m band.

Ref.	[19]	[20]	[21]	[22]	[23]	[24]	[25]	[26]
Pulse width (ps)	7.2	8.3	15.4	2	15	5.9	400	-
After dichirp (fs)	240	-	218	-	-	370	-	-
Repetition rate (MHz)	17	36	20.3	117	30	34-80	0.87	0.282
Average power (mW)	2	10.4	7.9	117	30	-	1270*	11
Pulse energy (nJ)	1200*	0.3	0.39	1	1	10*	4300*	39
Wavelength (nm)	1030	1062	1035	1030	1064	1065	1073	1064
Laser cavity	linear	ring	linear	linear	linear	linear	ring	ring
Mode-lock method	SAM	SESAM QWP	SAM	SAM, AQWP	SESAM	SESAM	SESAM	SESAM
Ref.	[28]	[29]	[30]	[31]	[32]	[39]	[40]	
Pulse width (ps)	10	10-15	7.6	10	5.6	-	1.5	
After dichirp (fs)	629	230	179	200	-	543	250	
Repetition rate (MHz)	34.8	34	33.3	27.7	5.96	15.1	50	
Average power (mW)	28	50	59	5.5	8	0.33	155	
Pulse energy (nJ)	0.8	1.5	1.8	0.2	1.34	0.022	3	
Wavelength (nm)	1032	1031	1040	1033	1030	1070	1030	
Laser cavity	ring	ring	ring	ring	linear	ring	ring	
Mode-lock method	NPR	NPR, Lyot filter	NPR, spec. filter	NPR, SESAM	NPR, FM	nanotube	SAM, nanotube	

* Amplifier

1.3.2. Self-Pulsed Fiber Lasers

Two kinds of self-pulsing are mainly observed; sustained self-pulsing (SSP) and self-mode locking (SML) [42]. SSP is the emission of laser pulses at a repetition rate associated with relaxation oscillations and observed at specific pumping ranges. Most often, SSP has irregular repetition periods with pulses in microsecond and nanosecond ranges. Alternatively, more

interests are into SML with pulse widths in the range of nanosecond down to picoseconds. In SML, the laser signal modulation period corresponds to the cavity round-trip time.

Various mechanisms may cause self-pulsing in fiber lasers [43] including ion-pairing [44], re-absorption of laser photons in un-pumped part of fiber [45], scattering processes such as SBS or SRS [46-48] and Kerr effect [49]. In References [44-49], self pulsing were investigated only experimentally without numerical verification.

In order to generate stable mode-locked pulses, self pulsing should be characterized both experimentally and numerically. Unadhyaya et al. analyzed numerically in [50] the effect of steady-state conditions on SSP in Yb-doped fiber lasers. Their analysis is based on solving time-independent rate equations for a linear cavity composed of two broadband mirrors. The study revealed that gain peaking along the active fiber is the source of self-pulsing. The model in [51] did not include terms for SBS or SRS that were observed in the experimental measurements.

Brunet et al. developed a time-dependent model describing both SML and SSP for Yb-doped ring fiber laser in [51]. It is based on the repetitive amplification of an optical pulse circulating in the cavity with homogenous gain saturation. The model explains the fiber laser dynamics and transitions between SSP and SML. Though the model matches with the experimental results, it over-estimated the pumping thresholds required to pass from one dynamical regime to the other [52]. This disagreement is attributed to the lack of nonlinear terms in the theoretical model.

Lee and Agrawal added a nonlinear term to the time-dependent laser rate equations in [52] to study SSP and SML in Yb-doped fiber laser. The laser cavity has a Fabry Perot configuration with two FBGs as cavity mirrors. The model succeeds to prove that Self Phase Modulation (SPM) plays important role for the SML output. The simulation results shown in [52] were not compared to experimental data.

Recently, Bedyakova et al. studied in [53] the pulsing dynamics of Yb-doped linear fiber laser. The model is based on NLSE and includes both nonlinear and dispersion effects. Numerical simulations show good agreement for power and spectrum measurements. Yet, the model addresses only a narrow time scale of the self-pulsed output.

1.4. Problem Statement

It is evident from the above literature review that

(a) Current Passively mode-locked fiber lasers are limited by:

- ***Low damage threshold of saturable absorbers***

SESAM limits the pulse energy and peak power due to its low damage threshold and saturation intensity [19-26]. Nanotubes were reported with performance degradation with time in [39]. The highest pulse energy achieved from an all-fiber structure is 1 nJ using SESAM [23], 1.8 nJ using NPR [30] and 3 nJ using nanotubes [40].

- ***Use of core-pumped fibers***

Core pumping sets a limit on the maximum allowable pumping power which impedes scaling output power levels.

- ***Performance susceptibility to environmental changes***

Several fiber lasers especially those using nanotubes [39, 40] or NPR [28-31], use PCs in their designs. Using adjustable components such as PCs even in fiber coupled version may affect continuous stable operation if the alignment is disturbed or the laser is moved.

- ***Use of bulk optics***

Using bulk optic in designing a mode-locked laser can offer polarization selection and optimization for output power. Having a free space section in the fiber laser cavity doesn't allow building compact and rugged laser cavities using fiber.

(b) Current Studies of self-pulsed fiber lasers lack the following:

- Investigation of self-pulsing from all-PM fiber laser cavities.
- Development of time-dependent numerical model to explain the output of self mode-locked fiber lasers at both large and narrow time scales.

Several high power fiber lasers operating at 1 μ m and 532 nm wavelengths are offered in market and literature. They are mainly composed of a seed laser followed by multi-stage amplifiers. Designing an all-fiber seed laser with high average power, short pulse width and suppressed

nonlinear effects is challenging. Such as a laser will reduce the required number of amplifier stages as well as providing compact laser modules with considerably low prices.

In order to design a robust compact all-fiber mode-locked laser with high average and peak powers, the above stated limitations have to be overcome.

First, the use of SESAMs and nanotubes should be avoided. They have low damage threshold which will limit the maximum realized pulse energy and peak power from the laser cavity. In this thesis, the developed mode-locked fiber laser relies on NPR mechanism with no damage threshold condition.

Second, in order to achieve high average power levels, core pumped fibers and components should be replaced with their double-clad counterparts. Cladding pumping gives high potential of scaling up average output power and pulse energy without using numerous amplifier stages. That's why double-clad fibers and components are used to design the mode-locked fiber laser.

Third, the fiber laser should be environmentally stable. Environmentally stable means that the output from the laser is not susceptible to changing environmental conditions or polarization. This is could be realized by using Polarization Maintaining (PM) fibers to build the fiber laser.

Furthermore, the fiber laser should be implemented with no sections of bulk optics or adjustable components (PCs) to make it as stable, compact and cheap as possible.

The developed mode-locked laser is composed of double-clad PM active fibers and specialty designed PM-FBGs in a Fabry Perot structure. Double-clad pumping scales the realized average output power levels. The cavity with a combination of a birefringent medium (PM active fiber) and a polarization selection mechanism generates an output with mode-locked pulses. The mode locking operation is based on Non-linear Polarization Rotation (NPR) technique. The output pulses from proposed cavity are in picoseconds range.

The self mode-locked fiber laser achieved also a linearly polarized output with an extinction ratio up to 30 dB. The design generates mode locked pulses at either $1\mu\text{m}$ or $1.5\mu\text{m}$ regions with a repetition rate determined by its cavity length. The output pulses amplitude is observed with an

envelope modulation. The width of the envelope is reduced with increasing the pumping level. This phenomenon is investigated in this thesis project and methods to regulate it are reported.

The specially designed PM-FBG pair has been also used to develop a compact fiber-based pumping source for Mid-IR generation. Conventionally mid-IR wavelengths are generated using two separate fiber laser sources [54-57]. The output from these two sources are combined at the nonlinear crystal using WDM or combiner as well as using two PCs to adjust their polarization. For further cost and size reductions, comes the motivation to extend using the PM-FBG pair to design a compact DFG pumping source. This source should have high power, linearly polarized, narrow linewidth output with simultaneous emission at both 1 μm and 1.5 μm wavelengths.

The developed dual-wavelength laser consisted of two pairs of Fiber Bragg gratings fabricated on a PM fiber to form a cavity and an Er/Yb co-doped fiber as a gain medium. The laser emits simultaneously two wavelengths with wavelength interval of 500 nm. The compact laser with an output of 23 dB PER ratio and 26pm narrow linewidth is well suited for 3.3 μm wavelength generation.

The thesis main objectives are to:

1. Identify the key parameters that control the mode-locked laser output. . In this parametric study, different design components such as output coupler reflectivity, active fiber length and core diameter will be varied.
2. Explain the mechanism of mode-locking for the proposed design.
3. Develop theoretical model to explain the pulse amplitude envelope.
4. Scale-up the average output power and pulse energy.
5. Explore using modulated current sources to pump laser diodes and study its effect on temporal output.
6. Build a linearly polarized all-fiber laser source using PM FBGs and with a dual-wavelength output.

1.5. Thesis Outline

The rest of the thesis goes as follows:

Chapter 2 describes the experimental setup of the fiber laser including all optical components, their assembly and operations. The description of measurement setups used to characterize the pulsed laser output parameters and the equipment specifications are also included.

Chapter 3 presents experimental results of self mode-locking all-PM fiber laser in a linear cavity. This includes power, spectrum, polarization and pulse measurements. Scaling pulse energy using cavity length extension or amplifier stage is also investigated. It also presents the implementation of pulsed current sources and its effect on output performance.

Chapter 4 discusses theory for mode-locking mechanisms and fiber nonlinearities. Numerical modelling techniques including solving Nonlinear Schrödinger Equation (NLSE) and Split Step Fourier Method (SSFM) will be also illustrated. Characterization and modeling for the observed self mode-locking pulses and its amplitude envelope are included.

Chapter 5 shows development for all-fiber CW lasers with high extinction ratio. It presents novel design for linearly polarized dual wavelength fiber laser.

Finally In **Chapter 6**, conclusions and proposed directions for future work are presented.

Chapter 2. Experimental Characterization

This chapter describes the experimental details of the mode-locked fiber laser including components used and related measurement setups. In Sec 2.1, the basic configuration for the laser will be illustrated. In Sec.2.2 details of all optical components involved in building laser modules will be shown. This includes specifications of pump laser diodes, active and passive fibers used and Fiber Bragg Gratings (FBGs). The optical components assembly operations including fiber splicing and recoating will be described in Sec.2.3. Different measurement setups used to characterize the laser output parameters, such as power, polarization and pulse width will be presented in Sec.2.4. This section will include the details of the measurement techniques as well as the equipments specifications. Details of design specifications and parameters will be given in Sec.2.5.

2.1. General Configuration of Fiber Laser

The schematic of the proposed Self Mode-Locked (SML) all-PM fiber laser, with all fiber connections fusion spliced, is shown in Figure 2.1.

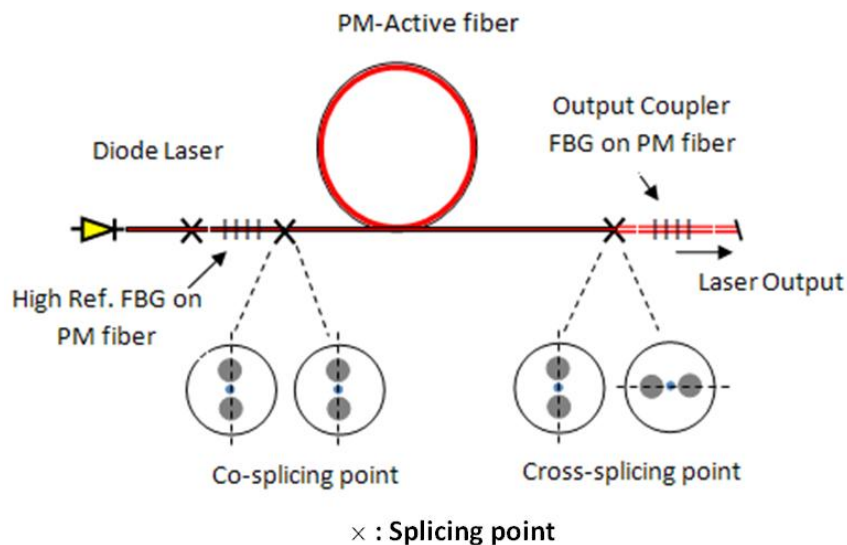


Figure 2.1: A schematic diagram of the linearly polarized mode-locked high-power fiber laser.

The fiber laser was pumped by a fiber-coupled laser diode at 975 nm wavelength. Laser diodes of 10 W and 25 W were used and which have a multi-mode output fiber. In some configurations,

the laser diode was connected to a low pass filter to pass pump wavelength and attenuate longer back-reflected wavelengths that can burn the laser diode. Though the filter introduced around 10% loss to the input pump power, it provided protection to the laser diode at high power levels.

The fiber laser cavity consists of an active fiber spliced between a FBG pair. Both active fiber and FBG fiber are of PM type. The FBG pair is formed of two gratings; one end of the highly reflective FBG is spliced to the laser diode or the filter and the other end is co-spliced (where both PM fibers axes are parallel to each other) to the active fiber.

The other FBG is used as the cavity output coupler with reflectivity value ranges from 7% up to 82%. In order to select polarization, the output coupler grating is cross-spliced (where the slow axes of both PM fibers are perpendicular to each other) to the active fiber. Most of the laser modules have a PM APC-pigtail co-spliced to the output coupler FBG for reducing back reflection. The above schematic is the basic configuration of the developed mode-locked all-fiber laser with some design modifications introduced later in Chapter 3. The mechanism of the mode-locking will be explained in Chapter 4.

2.2. Optical Components

2.2.1. Pump Laser Diodes

There are several kinds of laser diodes used in pumping such as low-power lasers (up to 200 mW), broad area laser diodes with few watts outputs and high power diode bars with tens of watts [13]. The two latter kinds are selected to pump fiber lasers. Using fiber coupled laser diodes as a pump source has several advantages among which are:

- High electrical to optical efficiency (up to 50%),
- Narrow optical bandwidth for laser diodes, allows pumping at certain transition levels in the active medium, without losing power in other transitions and consequently increases the overall efficiency.
- Allowing end pumping for lasers with good overlap between pump and active fiber.
- Long life time for laser diodes, can reach up to 10,000 hours.
- Small foot print can minimize the heat dissipation and develop compact laser module.

In most cases, the pump diodes are operated continuously. This applies to all CW and mode-locked lasers, and also to many Q-switched lasers. However, pulsed operation is also used for

some Q-switching lasers with high pulse energy and low pulse repetition rate. In this thesis, 10W (LUMICS, LU0975T100 from Lumics GmbH company in Berlin, Germany) and 25W (Oclaro, BMU25-975-01 from Oclaro Inc in San Jose, CA,USA or LUMICS, LU975-T250) fiber-coupled pumping laser diodes at 975 nm wavelength are used. Both diodes deliver optical power through 105 μm core, N.A. of 0.15 or 0.22 multimode fibers. Photos for pumping laser diodes (LDs) are shown in Figure 2.2. The diode specifications will be summarized in the following two tables.

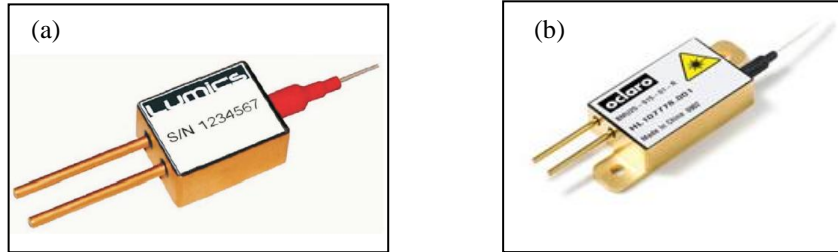


Figure 2.2: (a) 10 W LUMICS multi-mode fiber-coupled laser diode, (b) 25 W Oclaro multi-mode laser diode.

(a) 10 W LUMICS multimode laser diode (LU0975T100)

This laser diode does not have back-reflection protection coating, so normally is followed by a fiber-coupled multimode low pass filter. This filter passes pump wavelengths from 915 to 980 nm and attenuates other reflected back wavelengths in the range from 1020 to 1100 nm. This is needed to protect the laser diode from ASE at 1080-1090 nm wavelengths or any sporadically lasing component that can travel in both directions and damage the laser diode. This fiber-coupled filter has a typical insertion loss around 0.24 to 0.6 dB with maximum power handling of 10 W in the pump wavelength band.

Table 2.1: 10 W LUMICS multi-mode laser diode specifications

Parameter	Value
CW output power (W)	10
Peak wavelength (nm)	975
Spectral width (FWHM) (nm)	4
Maximum operating current (A)	11.5
Power conversion efficiency (%)	45
Maximum heat sink temperature ($^{\circ}\text{C}$)	35
Wavelength shift vs. temperature (nm/K)	0.35

(b) 25 W Oclaro multimode laser diode module (BMU25-975-01)

Oclaro's laser diode is a multi-mode single emitter based laser diode designed to provide an output power of 25 W. The module has feedback protection coating that blocks the reflected back light in the range from 1030 nm to 1200 nm.

Table 2.2: 25 W Ocular multi-mode laser diode specifications

Parameter	Value
CW output power (W)	25
Peak wavelength (nm)	975
Spectral width (FWHM) (nm)	6
Maximum operating current (A)	11
Operating temperature (°C)	25±5
Feedback protection (1030-1200nm) (dB)	45

2.2.2. Optical Fibers

Double-cladding fibers: are class of fiber that have three layered structure instead of two. The inner one is the core, followed by the inner cladding and then an outer cladding layer, with the three layers having different refractive indices.

In double-clad fiber, it becomes easier to couple pump light of high power levels, and low brightness, into the inner cladding. The inner cladding with higher index than the outer cladding acts as a waveguide to the pump light which is gradually absorbed by the doped core. This will allow high multimode pump power to be efficiently converted (sometimes more than 80%) to a high brightness output laser beam as illustrated in Figure 2.3. To achieve such a performance, the outer cladding should have the lowest refractive indices of the three layers.

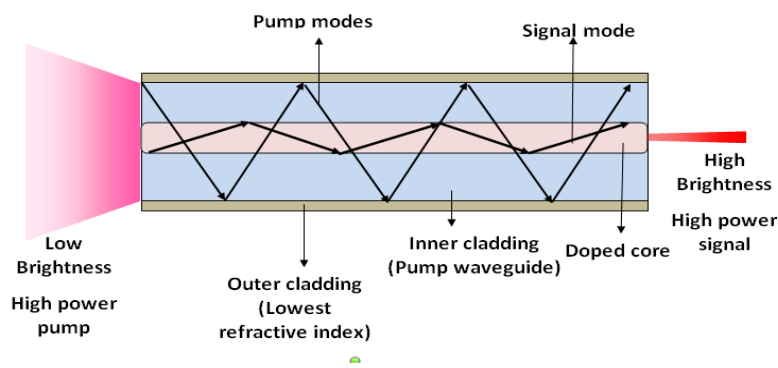


Figure 2.3: Schematic for double-clad fiber laser.

In this thesis, in order to achieve high average output power, most of the fibers used are of double-clad type. The fiber laser designs not only offers high output power but also a linearly-polarized beam. This is realized by using PM fibers.

Polarization maintaining (PM) fibers: are optical fibers in which linearly polarized light, if properly launched to one of the fiber axes, it can preserve its polarization with little or no cross-coupling between the two polarization modes. Its construction is based on either introducing stress rods of different material into the cladding or via non-symmetrical cladding shapes. Polarization maintaining or also known as polarization preserving fibers can be manufactured in different forms [58] as shown in Figure 2.4.

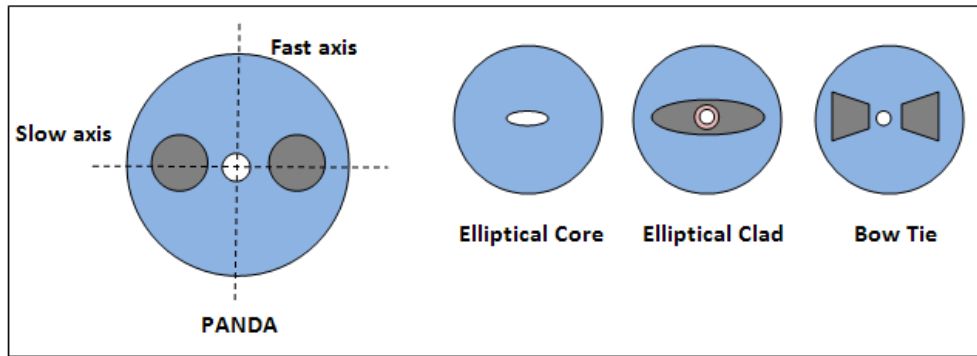


Figure 2.4: Different shapes for polarization maintaining (PM) fibers.

One of the most common configurations for PM fibers, also used in this thesis, is the PANDA-style PM fiber with the cross section shown in Figure 2.4. PM fibers have two perpendicular axes, slow and fast axis. The axis along which the polarization mode index is smaller is called the fast axis because the group velocity is larger for the light propagating; and for the same reason; the axis with larger mode index is called the slow axis. The slow axis connects the centers of two stress rods.

For PM fibers, modal birefringence is an important property when designing the mode-locked fiber laser. The modal birefringence, B_m is defined as [59]:

$$B_m = \frac{|\beta_x - \beta_y|}{k_o} = |n_x - n_y| = \Delta n \quad (2.1)$$

where n_x and n_y are the modal refractive indices for the two orthogonally polarized states. β_x and β_y are the propagation constant for the two orthogonally polarized while k_o , is equal to $2\pi \lambda_o^{-1}$ where λ_o is the center wavelength.

For a given value of birefringence, B_m , the two modes exchange their powers in a periodic fashion as they propagate inside the fiber with period called the beat length [59]:

$$L_B = \frac{2\pi}{|\beta_x - \beta_y|} = \frac{\lambda}{B_m} \quad (2.2)$$

One of these two parameters is given in the PM-fiber data sheet. All of the fibers used in building the proposed laser modules are of double-clad PM type either the active or passive. The specifications of the active and passive fibers will be presented in the two following sections.

(a) Active fibers

Two types of active fiber are used in this thesis, Ytterbium (Yb^{3+}) and Erbium-Ytterbium co-doped ($\text{Er}^{3+}/\text{Yb}^{3+}$). Ytterbium ions are one of the most versatile ions to be doped in silica-based fibers. It offers several advantages of wide absorption band from 850 nm to 1070 nm. It can be also pumped with wide selection of solid-state laser diodes (850 nm, 980 nm, 1047 nm and 1064 nm). In addition, ytterbium co-doped fibers have impressive emission spectra in the range from 970 to 1200 nm [15]. Both absorption and emission spectra for Yb^{3+} in silica are shown in Figure 2.5(a). In the thesis, all of our Yb-doped active fibers are pumped with 975 nm laser diodes with an emission in the 1 μm band.

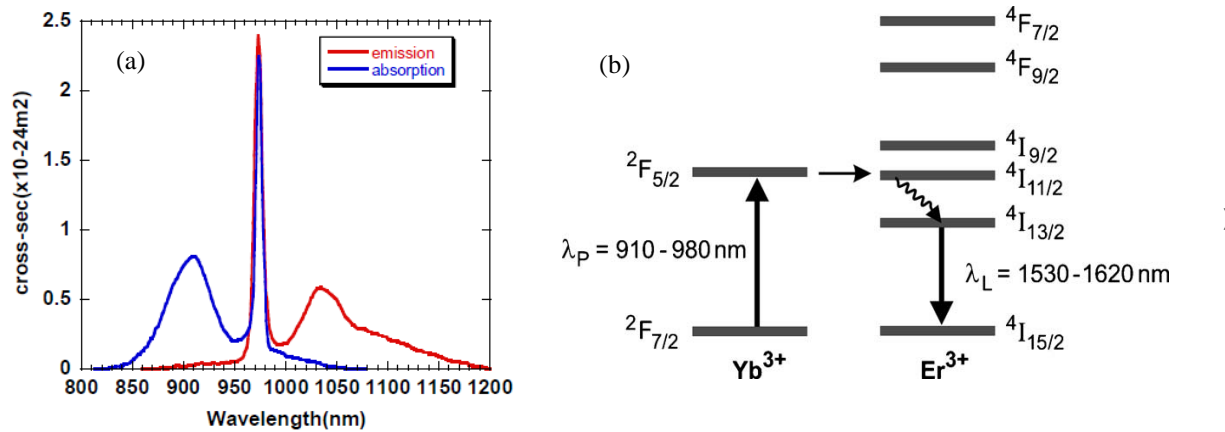


Figure 2.5: (a) Absorption and emission spectra for Yb^{3+} in silica [15]. (b) Energy level diagram of Er-Yb co-doped fiber [60].

Another type of active fiber is Er/Yb co-doped active fiber for emission at 1.5 μm band (C-band). Yb^{3+} is used to heavily co-dope the active Er^{3+} fiber to enhance absorption at 980 nm band which is not available for Erbium ions. As shown in Figure 2.5(b), the higher excitation level of Yb^{3+} ($^2\text{F}_{5/2}$) matches the erbium level ($^2\text{I}_{11/2}$). The Er^{3+} ions will be indirectly excited with the energy transfer from the Yb^{3+} ions. The erbium ions with $^4\text{I}_{13/2}$ - $^4\text{I}_{15/2}$ transition will provide emission at 1.5 μm wavelength [51, 52]. The emission and absorption spectra in pump spectrum for $\text{Er}^{3+}/\text{Yb}^{3+}$ are shown in Figure 2.6.

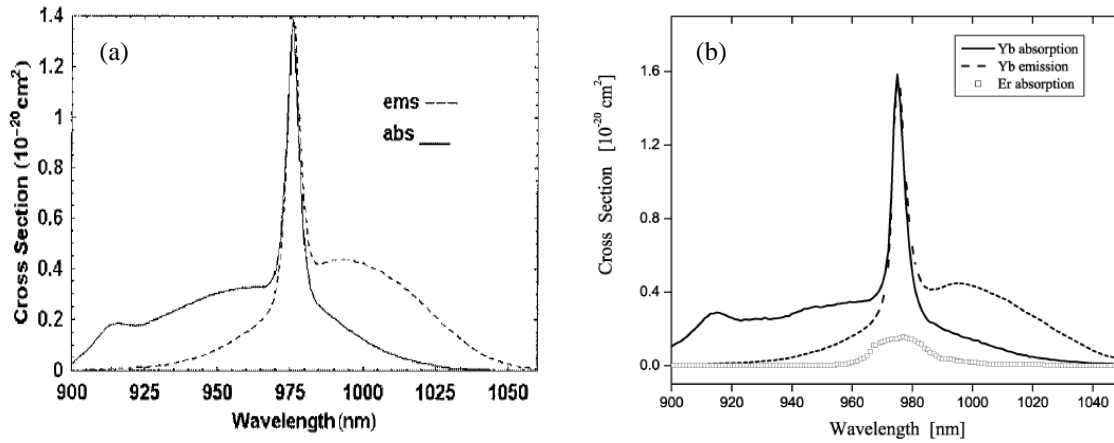


Figure 2.6: Absorption cross section at pump wavelength band for $\text{Er}^{3+}/\text{Yb}^{3+}$ in silica (a) Ref. [61], (b) Ref. [62]

Table 2.3: Specifications of Yb^{3+} active fibers used in the thesis

Parameter	Yb^{3+} -doped active fiber (5/130)	Yb^{3+} doped active fiber (10/125)
Fiber part number	Nufern PM-YDF-5/130	Nufern PLMA-YDF-10/125
Fiber type	PM (PANDA), Double-clad	PM (PANDA), Double-clad
Core diameter/ Cladding diameter	5 μm /130 μm	10 μm /125 μm
Mode field diameter	6.9 μm	11 μm
Core N.A.	0.13	0.075
Birefringence	0.00037	0.0003
Cladding absorption @975nm	1.7 dB/m	5 dB/m

One of the most important parameters for active fiber is the absorption per meter at the pump wavelength. Most of the active fiber data sheets list the absorption per meter at 915nm wavelength. The ratio between the absorption at 975 nm and 915nm could be estimated from the absorption spectra. The absorption coefficient at 975 nm is about three times the one at 915 nm for Yb^{3+} while for $\text{Er}^{3+}/\text{Yb}^{3+}$ co-doped fiber, the ratio varies from 5-7 [61, 62]. This coefficient is important to estimate the length of the active fiber needed to build an efficient cavity. A minimum of 10-12 dB absorption of a gain fiber is required to build an efficient laser. The main specifications for active fibers used in the thesis are shown in both Table.2.3 and Table.2.4.

Table 2.4: Specifications of $\text{Er}^{3+}/\text{Yb}^{3+}$ active fiber used in the thesis

Parameter	$\text{Er}^{3+}/\text{Yb}^{3+}$ co-doped active fiber (6/125)
Fiber part number	Nuferm PM-EYDF-6/125-HE
Fiber type	PM (PANDA), Double-clad
Core diameter/ Cladding diameter	6 μm /125 μm
Mode field diameter	6.7 μm
Core N.A.	0.18
Birefringence	0.00034
Cladding absorption @915nm	0.89dB/m

(b) Passive fibers

Passive fibers either single or double cladding, matching active fibers, are used mainly for Fiber Bragg Gratings (FBGs) and also for output pigtails. Table.2.5 shows the specifications of passive fibers (product also of Nufern Company) used in the thesis.

Table 2.5: Specifications of passive fibers used in the thesis

Fiber part number	PM980-HP	PM1060-GDF	PM085-LNA-FA
Fiber type	PM (PANDA), Single Clad	PM(PANDA), Double Clad	PM(PANDA), Double Clad
Core/Clad Diameter	6/125 μm	5/130 μm	10/125 μm
Mode field diameter	6.7 μm	Not Available	10.6 μm
Core N.A.	0.11	0.12	0.085
Beat length	2.6 mm	Not Available	3 mm
Matching Active fiber	Nuferm PM-YDF- 5/130,NufermPM- EYDF-6/125-HE	Nuferm PM-YDF- 5/130,NufermPM- EYDF-6/125-HE	Nuferm PLMA-YDF- 10/125

2.2.3. Fiber Bragg Gratings on PM fibers

FBGs inscribed on a PM fiber are used in this thesis to build fiber laser cavities with a linearly polarized output. When the PM fiber is exposed to UV- light for grating inscription, the resulting index modulation gives rise to two spectrally separated Bragg reflective peaks because of fiber's birefringence [63]. The wavelength difference between the two peaks ($\Delta\lambda_B$) can be calculated as follows:

$$\Delta\lambda_B = 2B_m\Lambda \quad (2.3)$$

where B_m is the PM fiber birefringence and Λ is the grating period, which is expressed as:

$$\Lambda = \frac{\lambda_B}{2 * n} \quad (2.4)$$

where λ_B is the center wavelength and n is the fiber index.

The spectra of the PM FBG pair around 1064 nm have $\Delta\lambda_B$ of 0.26 nm as shown in Figure 2.7. In order to provide both polarization and wavelength selection, the fast axes wavelength of the high reflection (HR) FBG is matched to the slow axis wavelength of the output coupler FBG.

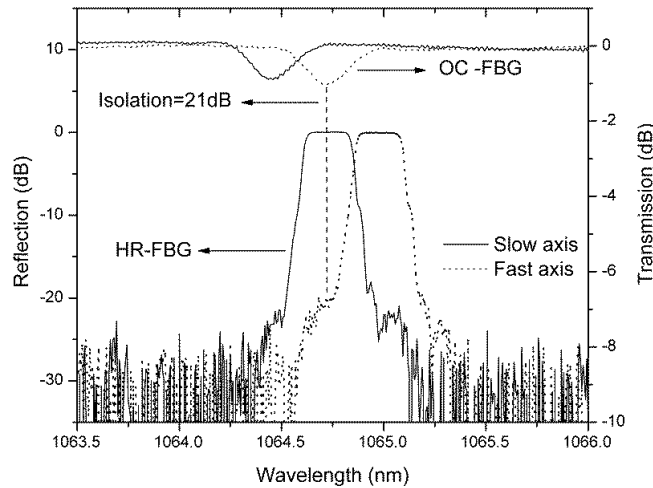


Figure 2.7: Typical Fiber Bragg Grating pair spectra design written on PM fiber at 1064 nm band and used in the proposed fiber laser.

The maximum mismatch allowed between both wavelengths is around 30-40 pm. The high isolation between the two FBG axes is a key factor to have a laser output with high extinction ratio. In order to maintain high isolation, the FBGs 3dB bandwidth should not exceed the Bragg wavelength separation of the PM fiber. Writing FBG with a broader bandwidth will lower the

isolation and may lead to dual polarization operation. On the other hand a too narrow bandwidth will make the wavelength matching difficult. In terms of splicing, high reflection FBG is co-spliced (where both PM fibers are spliced with both their slow axes are parallel to each other) to one end of the active fiber. The output coupler FBG is cross-spliced (where both PM fibers are spliced with their slow axes are perpendicular to each other) to the other end of the active fiber as previously illustrated in Figure 2.1.

2.3. Fiber Laser Assembly

Fiber laser assembly consists of two procedures, fiber splicing and fiber routing. Different types of splicing points and recoating types involved in assembly will be discussed in this section.

Two types of splices were implemented as shown in the laser schematic in Figure 2.1. The first is between multimode fiber and PM fiber (The point between the laser diode output or the bandpass filter (BPF) and the HR FBG). This type of splicing is performed with an Ericson FSU-975 arc fusion splicer.

The second type is between two PM fibers using a Fujikura FSM-20PMII arc fusion splicer. It has a program to splice two PM fibers at any desired angle. In the proposed laser module, the PM fiber splicing has two orientations; co-splicing or cross splicing. Co-splicing two PM fibers is shown in Figure 2.8.

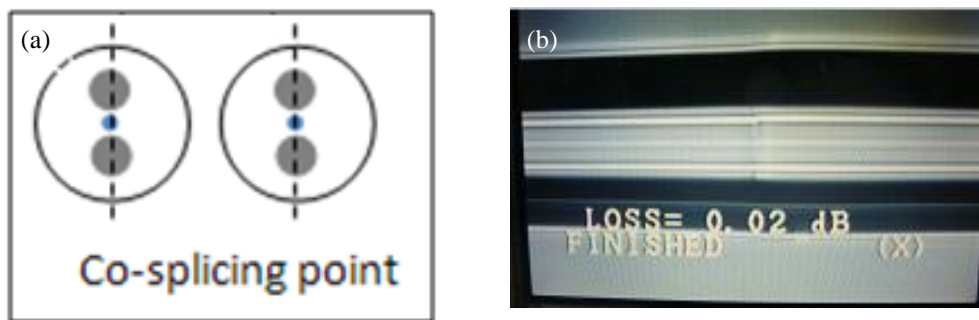


Figure 2.8: (a) Schematic for co-splicing two PM fibers. (b) Photo for X-view direction for co-splicing two PM fiber using Fujikura FSM-20PMII machine.

On the other side, cross-splicing of two PM fibers, is splicing the two PM fibers with their slow axes are perpendicular to each other as shown in Figure 2.9.

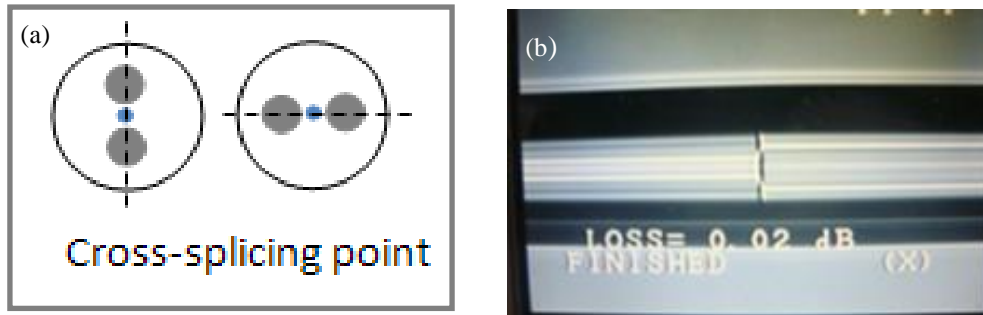


Figure 2.9: (a) Schematic for cross-splicing two PM fibers. (b) Photo for X-view direction for cross-splicing two PM fiber using Fujikura FSM-20PMII machine.

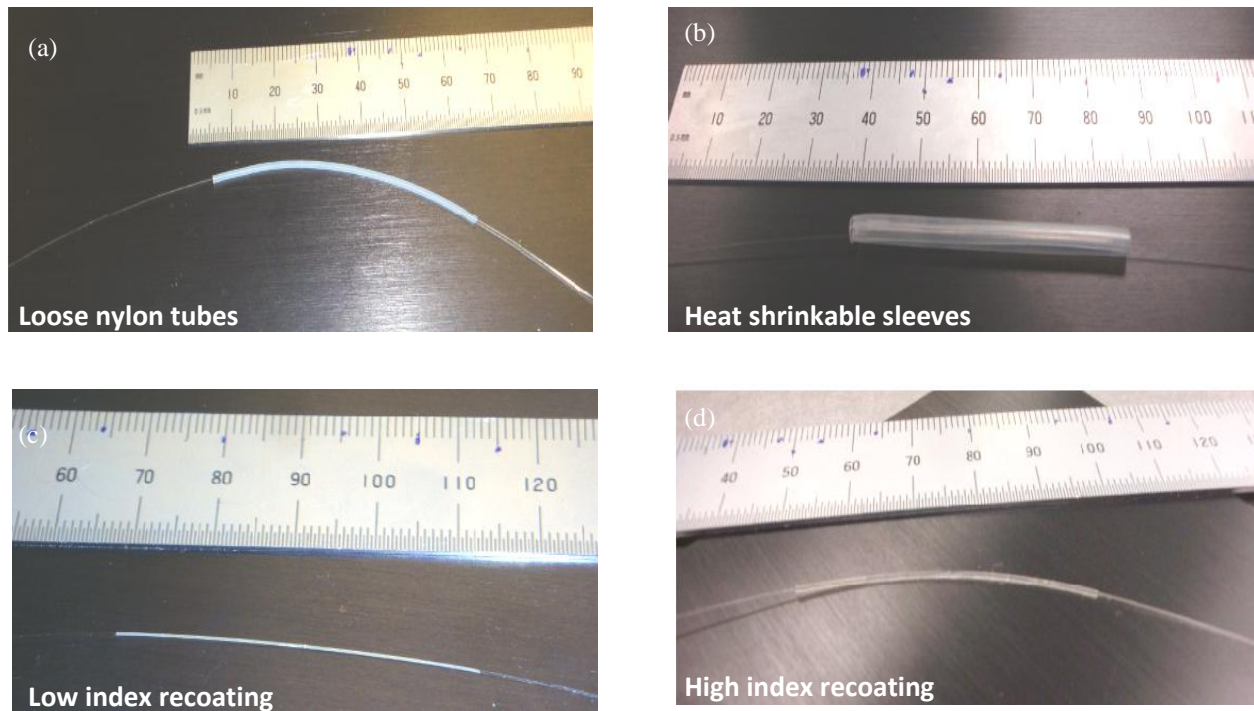


Figure 2.10: (a) Loose nylon tubes (b) Heat shrinkable sleeves with metal support (c) Low index recoating (d) High index recoating.

Fiber recoating is used to protect splicing point or FBG section. There are several options used to protect splicing points such as 0.9mm loose tubes, or heat shrinkable sleeves [64]. Low index recoating is performed with a Vytran PTR-200-MRC recoater (Coating material: UV- curable acrylate DSM950-200 with index around 1.4) while the high index recoating is performed with a filament fusion splicing station, Vytran FFS-2000.

Choosing a proper recoating type depends on the location of the splicing point in the designed laser. Photos of different types of fiber protection styles are shown in Figure 2.10. The positions of the splicing points are marked with "x" label as shown in Figure 2.1. Most of the splicing points inside the laser cavity are recoated with low index material. These points are normally exposed to high inter-cavity power density and power leakage should be minimized. The splicing point between the output coupler FBG and output pigtail is normally recoated with high index material. This is done on purpose to strip out any unabsorbed pumping light.

2.4. Fiber Laser Measurements

In this section, measurements related to the proposed linearly polarized mode-locked fiber laser will be presented. The laser power and polarization measurements will be described in Sec 2.4.1. Pulse measurements including both optical and electrical equipments will be discussed in Sec.2.4.2.

2.4.1. Power & Polarization Measurements

Two different power meters are used; the first is the OPHIR power meter with a thermal sensor head, which can measure the power up to 30 W. The other is the Thorlab PM100D power meter with a Thorlab-S145C integrated sphere photodiode power sensor, which uses an InGaAs photodiode. It operates in the wavelength range from 800 nm to 1700 nm and can measure up to 3 W maximum power. The Thorlab power meter is wavelength calibrated. In addition to power measurements, the proposed laser emits a linearly polarized beam that will be also characterized. The degree of linear polarization is normally quantified by the Polarization Extinction Ratio (PER). This is defined as the ratio of the optical power in two orthogonal polarization directions and in the unit of decibels (dB). The experimental setup used to measure the polarization extinction ratio is shown in Figure 2.11.

The polarization measurement setup is composed of a rotatable fiber holder, a collimating lens (with a focal length=58 mm), a 1 inch polarization cube beam splitter and two power meters. The collimated laser beam incidents on the 45° surface of the beam splitter, which separates the beam into two polarization directions. The power of the two beams (one passing through the cube and the other reflecting from it) are measured with the two power meters as shown Figure 2.11. The output fiber can be rotated to null the laser power transmitted through the cube. The

power ratio between the reflected powers to the transmitted power gives the polarization extinction ratio.

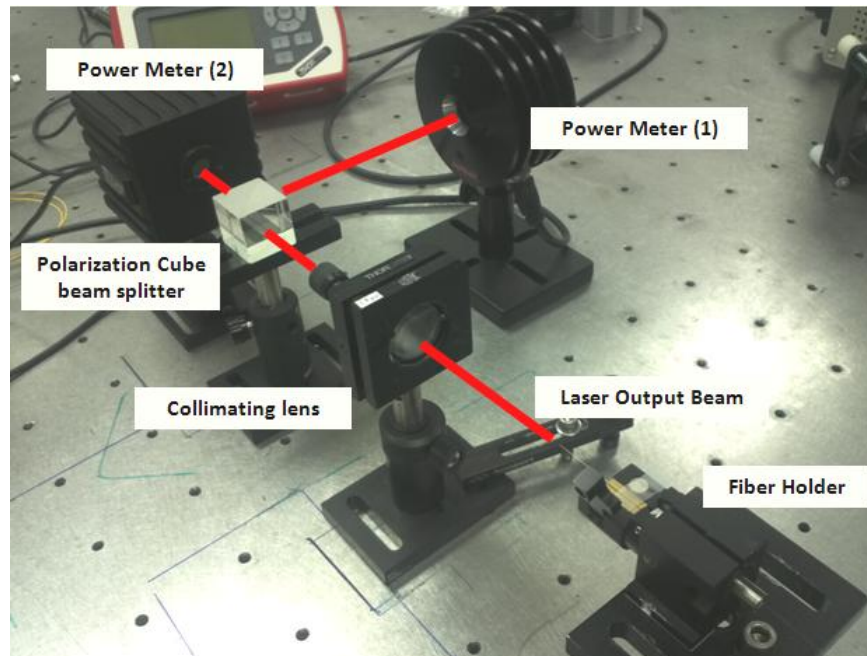


Figure 2.11: Experimental setup for measuring polarization extinction ratio (PER).

In the lab, two types of polarization cube beam splitter are used. One is a Thorlab-PBS253 polarization cube beam splitter, operating from 900 nm to 1300 nm and with an extinction ratio of 1000:1. The other is Edmund, Techspec™ NT48-580 operating in C-band with an extinction ratio of 1000:1. The beam splitters can also be mounted on a rotational optic holder to measure the output power as a function of the polarizer angle (Malus' curve).

2.4.2. Pulse Measurements

With advancement of high transmission-rate systems and short-pulse laser, many applications require high speed optical pulse detection system. Optical pulses and optical pulse trains can be characterized as follows:

- **Pulse repetition rate:** measured with a fast photodetectors and a fast oscilloscope.
- **Pulse width:** can be measured with various methods, fast photodetectors and oscilloscope, or an autocorrelator.
- **Pulse energy:** can be calculated by dividing the average power by the repetition rate of optical pulses.

- **Pulse peak power:** can be calculated from the pulse energy, pulse duration and shape.
- **Laser output spectral shape:** can be measured with an optical spectrum analyzer.
- **Other parameters such as Chirp, Timing jitter and Coherence:** can also characterize optical pulse for special applications [13].

Optical pulse measurement consists of a photodetector and oscilloscope connected by an SMA cable. However, even if the optical signal of interest is very fast, and the photodetector or scopes may not have an enough bandwidth, the measured pulse will be broadened. That means, it not only requires a fast detector, that will convert the fast optical signal to fast electrical signal, but also fast oscilloscopes to observe them. As a consequence, the bandwidth of each component in the pulse measurement system has to be carefully chosen to match the measured output pulse width.

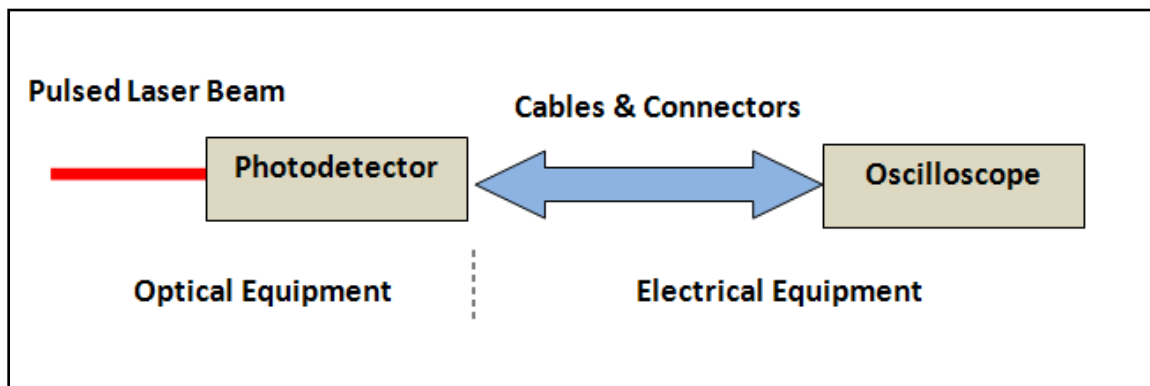


Figure 2.12: Experimental setup schematic for optical pulse measurements.

(a) **Fast Photodetectors:** Photodetectors are essential component in pulse detection system where the optical signal is converted to electrical signal. There are different kinds of photodetectors such as the most well-known photodiodes (based on p-i-n junctions), Metal semiconductor metal (MSM) (based on Schottky diodes), phototransistors, photoresistors and photomultipliers (based on vacuum tubes) [1]. The main properties that characterize photodetectors for pulse detection are:

- **Operating wavelength range:** where the detector acquire constant responsivity.
- **Detector speed or bandwidth:** can be used to estimate the minimum pulse width measured by detector.

- **Maximum power capability:** indicating the maximum power (peak or CW) can be measured without damaging the detector.
- **Impulse response time:** shortest pulse at the output of the detector.
- **Detector conversion gain:** given in V/W and tells how much output voltage will result from given optical power. The conversion gain value is the product of the photodetector responsivity, amplifier's gain and input impedance.
- **CW saturation power:** The point at which the output of photodetector becomes nonlinear.

The detector conversion gain and CW saturation power can be multiplied to estimate the **optical saturation level** of the photodetector. This value should not be exceeded for good accuracy in pulse width measurements.

As of Fourier transform limited pulse rule, the minimum pulse width ($\tau_{equipment}$); assuming a Gaussian shape; that can be detected by certain equipment with a bandwidth f_{3dB} is:

$$\tau_{equipment} = \frac{0.4}{f_{3dB}} \quad (2.5)$$

Several optical photodetectors are used in pulse measurements with a bandwidth that varies from 1 GHz to 45 GHz. The following tables lists the detectors used and their main specifications

Table 2.6: Specifications of general purpose detectors

Detector name	New focus 1811 IR-DC-125MHz	Newfocus 1611 IR-DC-1GHz
Operation wavelength	900-1700 nm	900-1700 nm
Maximum power	4 mW or 6 dBm	4 mW or 6 dBm
Gain	4×10^4 V/W	700 V/W
CW saturation power	55 μ W	1 mW
Optical input	FC	FC
Output connector	SMA	SMA
Detector speed	125 MHz	1 GHz
Minimum measured pulse width (FWHM)	3 ns	400 ps

Table 2.7: Specifications of high speed detectors

Detector name	Newport AD-10ir	Newfocus-1024
Operation wavelength	950-1650 nm	950-1650 nm
Maximum power	4 mW,6 dBm	1 mW,0 dBm
Gain	180 V/W	10 V/W
CW saturation power	>>200 mW	1 mW
Optical input	FC	FC
Output connector	Wiltron-V	Wiltron-K connector
Detector speed	43 GHz	26 GHz
Minimum measured pulse width (FWHM)	10 ps	12ps

(b) Cables and Connectors: The optical signal converted to electrical signal using photodetectors, is transmitted via SMA cables and interfacing connectors to the scopes.

Cables: Regular cables are the RG-58. There are also some versions which are good up to 50GHz.

Connectors: Different type of connectors can be used for pulse measurements depending on the required bandwidth. The BNC connectors most abundant in the labs are good up to 2 GHz, while the SMA ones are up to 24GHz. The 3.5 mm ones, which can be mated with SMA is good up to 34 GHz. The Wiltron-K or 2.95 mm is good to 40GHz, the 2.4 mm up to 50 GHz while the 1.85 mm or Wiltron-V is good up to 65 GHz. The measurement setup in the lab used a 50 cm long RG-58 cable with an SMA connector on the detector side and BNC on the scope side.

(c) Oscilloscopes: In pulse measurement, three scopes are used, two sampling scopes with 500 MHz bandwidth and a real-time scope with 12GHz bandwidth. The 500 MHz scopes are Tektronix TDS-3054 (maximum 10,000 sample points) and Tektronix TDS-5054 (can reach up to 2 million sample points). For detecting picosecond pulse width, faster scope, Agilent Infinium DSO-81204A, with 12GHz bandwidth is used. By applying Eq.(2.5), the minimum pulse width can be measured with 500 MHz scopes is 800 ps and 34 ps for the 12 GHz ones. The details of instruments bandwidths effect on pulse measurement are illustrated in Appendix A.

2.5. Design Specifications

The main guidelines used in designing the mode-locked fiber lasers can be stated as follows:

(a) Active Fiber:

- Dopant type: Yb-doped for emission in 1 μ m band.
- Core diameter: 5 μ m core fibers are used and further scaled to 10 μ m to scale-up the average power level.
- Double-clad PM fiber: provides a birefringent medium with high power levels to induce Kerr nonlinear effect.
- Polarization-dependence of the gain was not given by the manufacturer, so it is assumed that the fast and slow axes gain are equal. In the laser cavity, the signal is amplified along the fast axis.
- Length of active fiber:
 - Chosen to realize sufficient pump absorption. The minimum required pump absorption for an efficient fiber laser is around 10-12dB. (For 5 μ m fiber with 2 dB/m cladding absorption at 975nm, minimum fiber length of 5 m was used while for 10 μ m fiber with 5dB/m cladding absorption, minimum fiber length of 2.5m was used).
 - Maximum length of 10m with 50dB absorption was used. Longer lengths of active fiber with the rated absorption level will not be efficiently pumped (as verified by solving fiber laser rate equations shown in Appendix B) and thus wastes relatively expensive gain fiber. That's why 10m length of active fiber was not exceeded.
 - The length of the active fiber determines the repetition rate of the mode-locked pulses. Mode-locking repetition rate in the range of 10-40MHz were realized in the experiments.

(b) PM-FBG pair:

- The PM-FBG pair provides both wavelength and polarization selection for the laser. It is a key component to realize an output with high PER.
- Matching HR-FBG fast axis and OC-FBG slow axis wavelengths within no more than 30-40pm.
- Designing HR-FBG with flat top rectangular spectrum with required isolation of 20dB or more between the two FBG axes.
- The FBG is fabricated on PM fiber with a birefringence wavelength separation of 0.26 nm. This limits the maximum FBG 3dB bandwidth to 0.2-0.24 nm.
- The total fiber length on which FBG was written is around 50-55cm where the FBG has a length of 6mm.
- The laser output is coupled through an APC pigtail was used to reduce backward reflections.

(c) Fiber Splicing :

- All the splicing points are protected with low index material to minimize light leakage at these points.
- A high index recoating is used to protect the splicing point between APC pigtail and OC-FBG. This type of recoating is chosen to strip any unabsorbed pump power for proper output power measurements. It is preferable that high index recoating point to be located out of the cavity with lower power levels than inside the cavity.

Chapter 3. Experimental Results of Mode-Locked all-PM Fiber Laser

This chapter presents and analyzes the experimental results of the presented mode-locked all-fiber laser. In Sec 3.1, an overview of the laser design is presented. In Sec 3.2, characterization for different laser output parameters is illustrated. Scaling average power and pulse energy is proposed in Sec 3.3. The application of pulsed current sources to pump laser diodes will be presented in Sec.3.4. Finally, results summary and discussions are included in Sec 3.5.

3.1. Laser Design Overview

The laser schematic, shown in Figure 2.1, is fully composed of PM fibers in a Fabry Perot configuration. The laser is pumped with 975 nm fiber-coupled laser diode and operates around 1064 nm wavelength. A PM Yb-doped active fiber is inserted between two PM-FBGs with special spectral design and splicing arrangements as previously illustrated in Sec. 2.2.3 and Sec. 2.4. The laser components and assembly are discussed in details in Chapter 2. The laser with a combination of a birefringent gain medium, polarization selection mechanism and induced nonlinear effects, delivers linearly polarized picoseconds mode-locked pulses.

3.2. Characterization of Laser Performance

This section presents detailed measurements of the mode-locked fiber laser, including average power, spectrum, polarization and pulsed output at different pumping conditions. The effect of varying design parameters such as active fiber length, core diameter and output coupler reflectivity are also included in the following sections.

3.2.1. Power Measurements

The laser is built with an active PM Yb-doped double-cladding fiber with a mode field diameter of 6.9 μm and an NA of 0.13 (Nufern PM-YDF-5/130). The active fiber has a length of 5-5.2 m with a quoted multimode absorption coefficient of 1.7-2 dB/m at the pump wavelength of 975 nm. The FBG pair is written on a matching passive fiber with a mode field diameter of 6.7 μm .

The laser output power is measured through an APC fiber pigtail co-spliced to the output coupler FBG. This splicing point is normally coated with high index material for stripping out any excess pumping light and proper measuring of average power.

The laser output power is measured versus pumping power as shown in Figure 3.1(a). The laser acquires a maximum output power of 4.6 W. The slope efficiency of laser is 84% using best linear fit for nonlinear output power measurements as shown in Figure 3.1(a) and 65% efficiency at maximum output power. The output coupler (OC) reflectivity is also varied from 20% to 75% to study its effect on the self mode-locking (SML) operation. This will be presented in details in Sec.3.2.4. The average power measured using different OCs are compared in Figure 3.1(b). For 5 μ m modules, SML pulses with broader envelopes are measured using 55% (R) output coupler. At this value, the laser acquires a maximum average power of 3.2 W. The corresponding slope efficiency at R=55% with best linear fit is 74% and 52% efficiency at maximum output power.

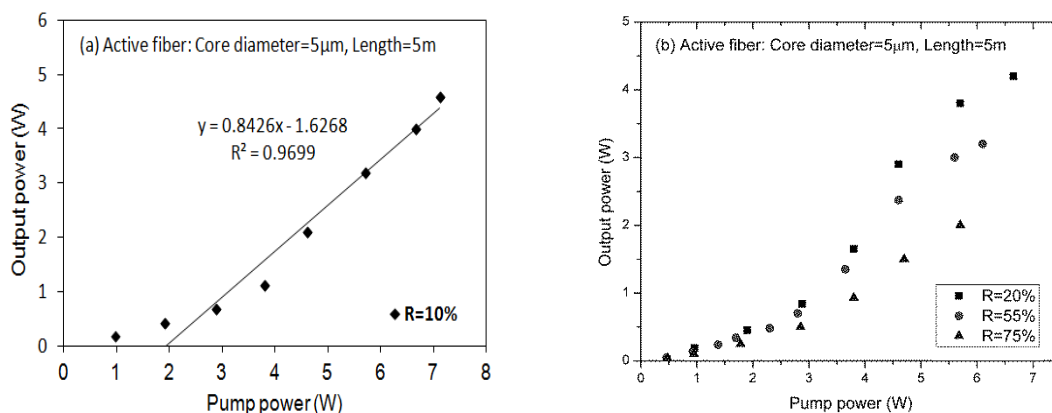


Figure 3.1: Measured output power versus pumping power for 5 μ m core module with 5 m active fiber and using different output couplers (a) R=10% (b)R=20%, R=55% and 75%.

In order to increase the average power level, the 5 μ m core active fiber is replaced with large mode area 10 μ m core PM fiber with a mode field diameter of 11 μ m and an NA of 0.075 (Nufern PLMA-YDF-10/12). The 10 μ m fiber has a higher quoted multimode absorption coefficient of 5 dB/m at 975 nm pump wavelength. The FBGs fiber is also changed to 10 μ m double-clad (Nufern PM085-LNA-FA) to match the new active fiber. Higher pump absorption level and 40% increase in fiber cross-section area are expected to increase the average power level.

For 10 μm core laser modules, active fiber length and output coupler reflectivity are also varied to optimize the laser performance. Average output power versus pumping power is measured using different active fiber lengths and presented in Figure 3.2(a).

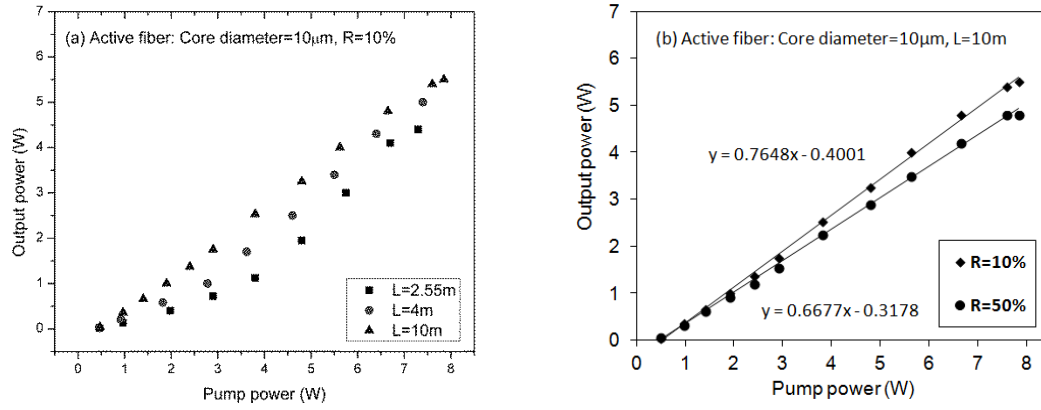


Figure 3.2: Measured output power versus pumping power for 10 μm core modules (a) Output coupler reflectivity, R =10% at different active fiber lengths. (b) Active fiber length, L =10 m at R=10% and R=50%.

The 10 μm lasers acquire higher output power levels compared to the 5 μm core-based ones. The power level increases to 5.5 W with slope efficiency of 76% (70% efficiency at maximum output power). This improvement in power level is attributed to higher pump absorption and larger fiber core area. With 10 m of 10 μm active fiber and 50% output coupler, the output has narrower pulse width and broader envelope width. (Details of temporal measurements are illustrated at Sec.3.2.4). At these settings, the laser has 4.8 W output power at 7.6 W pumping power and 67% slope efficiency as shown in Figure 3.2(b) (62% efficiency at maximum output power).

3.2.2. Spectrum Measurements

The output spectra for both 5 μm and 10 μm laser modules are measured at different lengths of active fiber and output coupler reflectivity. Example for FBG pair spectra used for was used in assembly of 5 μm core laser module is shown in Figure 3.3(a). The high reflectivity FBG (HR-FBG) has a reflectivity of >99% with a 3dB bandwidth of 0.2 nm and fast axis wavelength of 1063.445 nm. The output coupler FBG has a matched slow axis wavelength of 1063.415 nm, 3dB bandwidth of 0.25 nm and 10% reflectivity. The laser normally operates at this matched wavelength as discussed at Sec. 2.2.3.

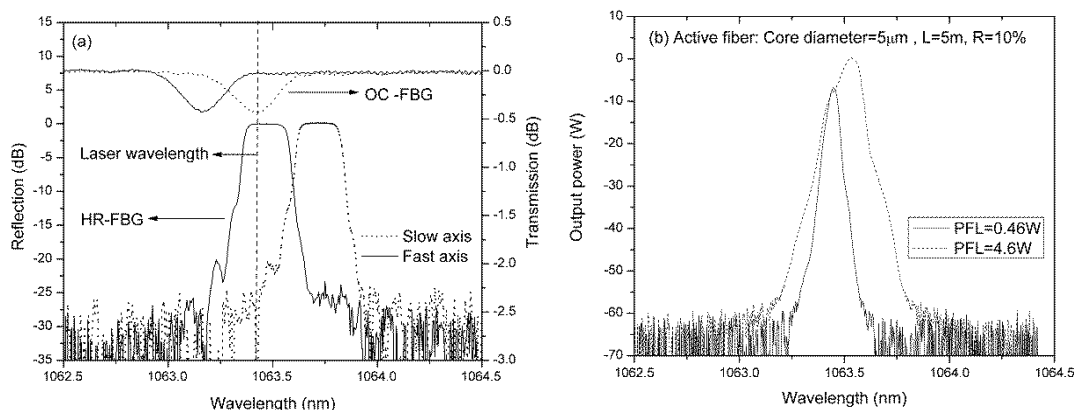


Figure 3.3: (a) Transmission and Reflection spectra for FBG pair with operating wavelength of 1063.4 nm. (b) Output spectrum at 0.46 W and 4.6 W output power of the 5 μm fiber laser.

The 5 μm -core fiber laser emits initially at 1063.4 nm wavelength with 0.46 W output power as shown in Figure 3.3(b). This wavelength corresponds to the grating matched wavelength. The laser shows an excellent Optical Signal to Noise Ratio (OSNR) of 60 dB and narrow 3dB bandwidth of 35 pm. With increasing pumping power, the laser wavelength is shifted to longer side with an 86 pm shift at a maximum output power of 4.6 W. This can be attributed to temperature rising inside the cavity with increasing pumping power. At 4.6 W output level, the laser 3dB bandwidth broadens to 82 pm while preserving its OSNR as shown in Figure 3.3(b).

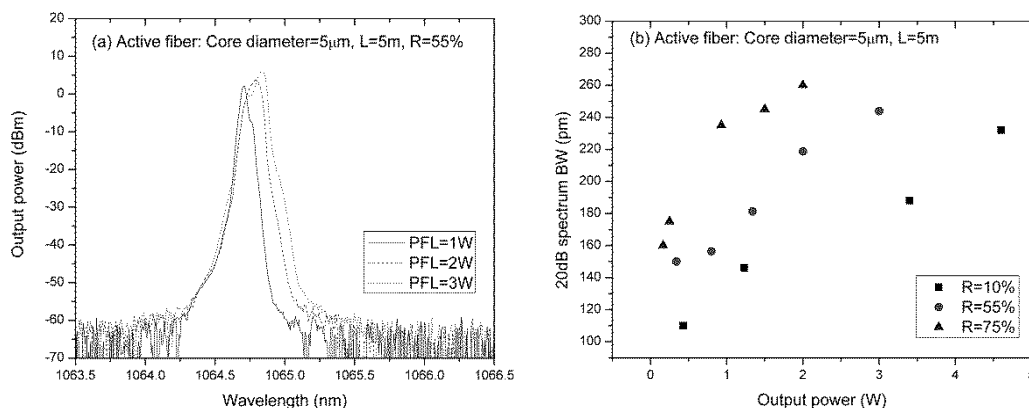


Figure 3.4: Measurements for 5 μm core laser module (a) Output spectra at different output power levels, and (b) 20dB bandwidth versus output power at different output coupler reflectivity.

The output spectrum for 5 μm core laser module using 55% output coupler is shown in Figure 3.4(a). The laser emits a wavelength of 1064.84 nm and 3dB bandwidth of 70 pm. The 5 μm -core laser modules spectra are compared at different output coupler reflectivity as shown in Figure 3.4(b). As shown, the output spectrum broadens with increasing output coupler reflectivity. This

can be explained by the increase in the intra-cavity power levels and induced nonlinear effects such as SPM and XPM. The spectra for 10 μ m-core modules with 10 m active fiber length are plotted in Figure 3.5(a) and (b) using 10% and 50% output couplers respectively. The laser modules keep excellent OSNR of 60-70 dB and 3dB line width of 30-50 pm. It can be also deduced from spectra measurements that the laser bandwidth increases with a ratio of 1.5-1.8 times by changing output coupler reflectivity from 10% to 50%. On the other hand, the laser bandwidth doesn't show any variation with changing active fiber length.

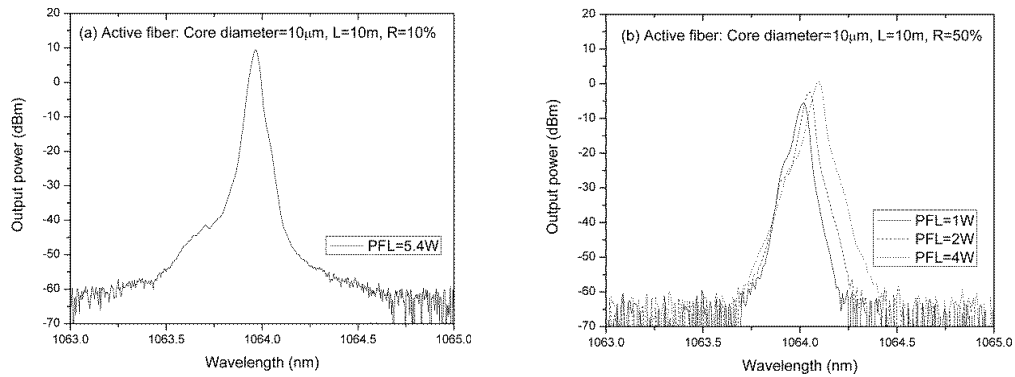


Figure 3.5: Measurements for 10 μ m core laser module with an active fiber length of 10m. (a) Output spectra at maximum power level of 5.4 W and R= 10%. (b) Output spectra at different output power levels using R=50%.

3.2.3. Polarization Measurements

Polarization measurement setup is discussed in Sec.2.4.1. Example of measured extinction ratio and Malus curve are shown in Figure 3.6(a) and (b), respectively. An extinction ratio of 25-30 dB is achieved at different output power levels. All modules share similar PER and Malus curves.

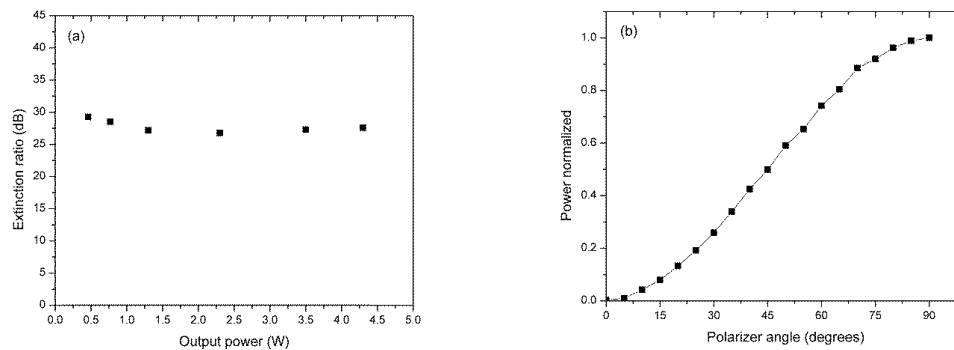


Figure 3.6 Measurements for 5 μ m core laser module with an active fiber length of 5m and R= 10%. (a) Extinction ration in (dB) versus laser output power (b) Malus polarization curve: Normalized output power versus polarizer angle in degrees.

The output coupler FBG was also co-spliced to the gain fiber to test splicing angle effect on polarization selectivity. At such a condition, laser spectrum was measured at different output power levels as shown in Figure 3.7. As expected, the laser shows dual wavelengths corresponding to two polarizations.

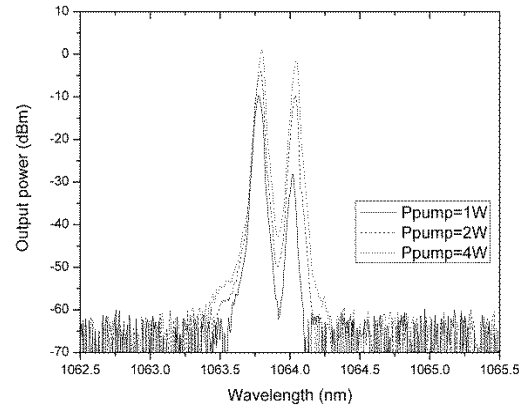


Figure 3.7: Measured laser spectra at different pumping power with co-spliced output coupler FBG.

3.2.4. Pulse Measurements

This section shows detailed measurements of Self mode-locked (SML) pulses with high average power levels. This includes pulse trains and single pulse width measurements for different laser modules. The effect of changing core diameter, output coupler reflectivity and active fiber length on output pulse features is studied. In addition, pulse amplitude envelope phenomena is observed and discussed.

3.2.4.1. 5 μ m-core Laser Modules

The mode-locking operation is studied with a 5 μ m core laser module and an active fiber length of 5 m. The output was measured through a Hi1060 APC-pigtail and detected with a Newport AD-10ir photoreceiver and a 12 GHz Agilent Infinium DCA DS081204A oscilloscope. This set-up can detect pulses down to 34ps (This value is estimated using Eq.(A.1) in Appendix A). The laser has a pulse repetition rate of 17.8 MHz which matches its round trip time of 56 ns as shown in Figure 3.8(a) with temporal SNR of 4:1. The laser has pulse width of 83ps with Time-Bandwidth Product (TBP) of 1.09 as shown in Figure 3.8 (b). It is observed that the mode-locked pulses amplitude is modulated with an envelope as shown in Figure 3.8(a). The envelope parameters will be studied using different laser configurations.

Mode-locked pulses, pulse and envelope widths are measured using different output couplers. The pulses measured with 55% output coupler, are shown in Figure 3.9(a) and (b). The output measured through PM980 APC-pigtail using a Newfocus 1611 IR-DC-1GHz detector and a 500MHz Tektronix TDS-3054 oscilloscope. The pulses show 54 ns roundtrip with 4:1-7:1 temporal SNR. The pulses amplitude is still observed with an envelope with increasing pumping power. The mode-locked pulses with an envelope is measured at 3 W output power and plotted in Figure 3.9 (b). The envelope width is measured using different output couplers and at different output power levels as shown in Figure 3.10(a).

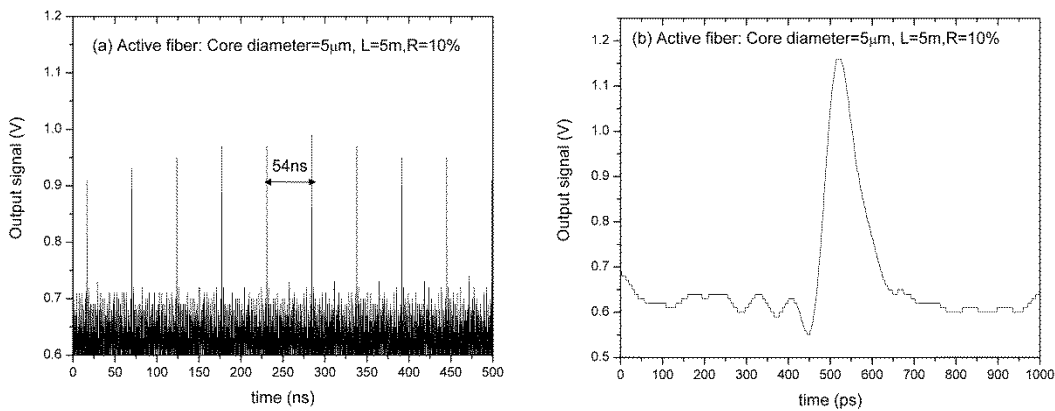


Figure 3.8: Measurements for 5 µm core laser module with an active fiber length of 5 m and output coupler of 10% (a) Mode-locked pulse train at output power of 2 W (b) Single pulse width of 83 ps at 2 W output power.

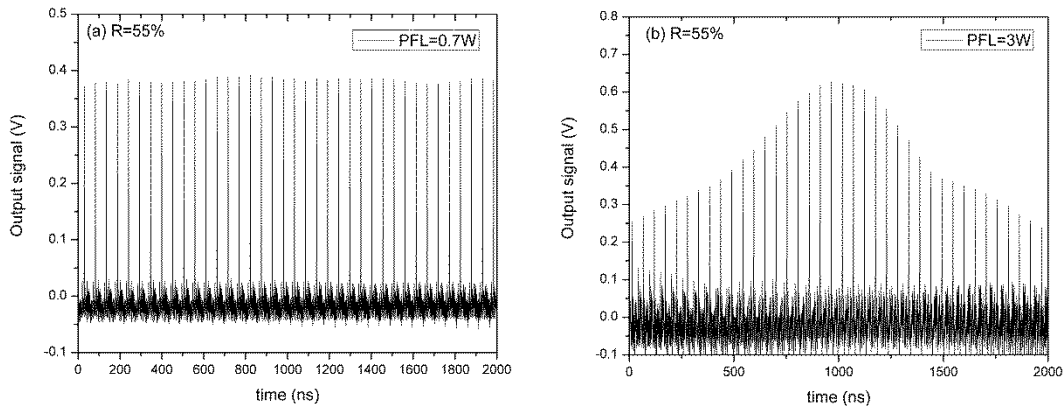


Figure 3.9: Mode-locked pulse train for 5 µm core laser module with an active fiber length of 5 m and R =55% with 54 ns round trip time (a) PFL=0.7W. (b) PFL=3W. PFL is the fiber laser output power.

Different design parameters have been varied to study and analyze its effect on the pulses envelope width. The envelope is approximately fitted with a Gaussian shape and its width is measured at FWHM of the Gaussian fit. All envelope recordings are measured with a Newfocus

1611 IR-DC-1GHz detector and a 500MHz Tektronix TDS-3054 or oscilloscope. From the envelope measurements, it can be concluded that:

- Broader envelope width is measured with increasing output coupler reflectivity and at lower pumping levels.
- At each power level, the envelope width is measured five times with $\pm 2\mu\text{s}$ variations for measured envelope widths.
- From $5\mu\text{m}$ core modules, there is a pumping range where the envelope width increases till reach certain threshold from which start to decrease. This pumping range decreases with higher OC reflectivity .
- The envelope width decreases with a faster rate by increasing OC. This can be attributed to higher induced nonlinear effects due to increasing intra-cavity power levels with higher OC reflectivity..
- A $43\mu\text{s}$ envelope width is measured from $5\mu\text{m}$ core modules and using 75% output coupler. Though this is the broadest envelope obtained but limited within very narrow power range. At this core diameter, better performance is reached with 55% output coupler with approximately $40\mu\text{s}$ envelope width.

The pulse width is also measured for the $5\mu\text{m}$ core module with 55% output coupler as displayed in Figure 3.10(b) using a Newport AD-10ir photoreceiver and a 12 GHz Agilent Infinium DCA DS081204A oscilloscope. At each power level, the pulse width is measured four times and has an average width of $80\pm 10\text{ps}$ (TBP=1.05). This laser acquires an average power of 3.2 W and repetition rate of 18.8 MHz.

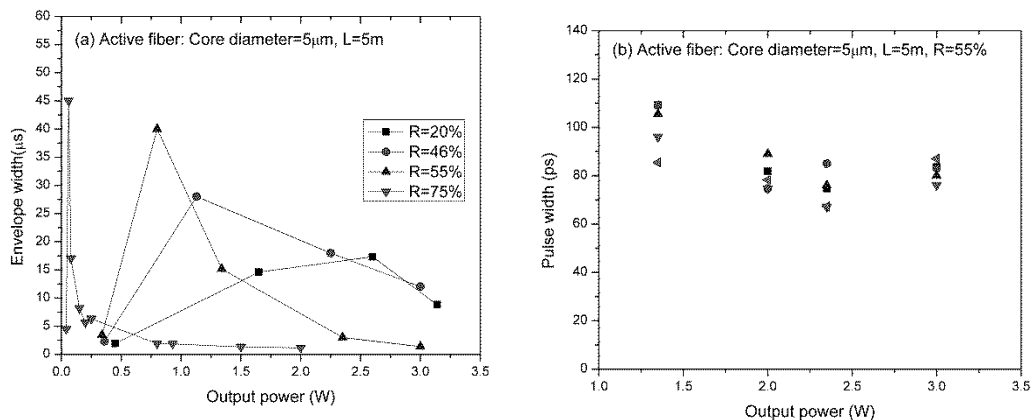


Figure 3.10: Measurements for $5\mu\text{m}$ core module with 5m active fiber (a) Envelope width versus output power and $R = 20\%$, 46%, 55% and 75%. (b) Measured pulse width versus output power and 55% output coupler.

3.2.4.2. 10 μ m-core Laser Modules

For further scaling average power and pulse energy, active fiber core diameter of 10 μ m is used. Higher average power of 5.5 W is achieved using 10 m of active fiber of 10 μ m core. Also narrower pulse width is obtained using the 10 μ m core lasers. Single pulse width is measured using two different lengths of active fiber and compared in Figure 3.11(a). At each power level, the pulse width is measured four times. It has an average width of 55 ± 5 ps (TBP=0.73) using 10 m active fiber compared to 65 ps (TBP=0.86) using 2.55 m. Single pulse measurements for 10 μ m core laser and 10% output coupler is shown in Figure 3.11 (b).

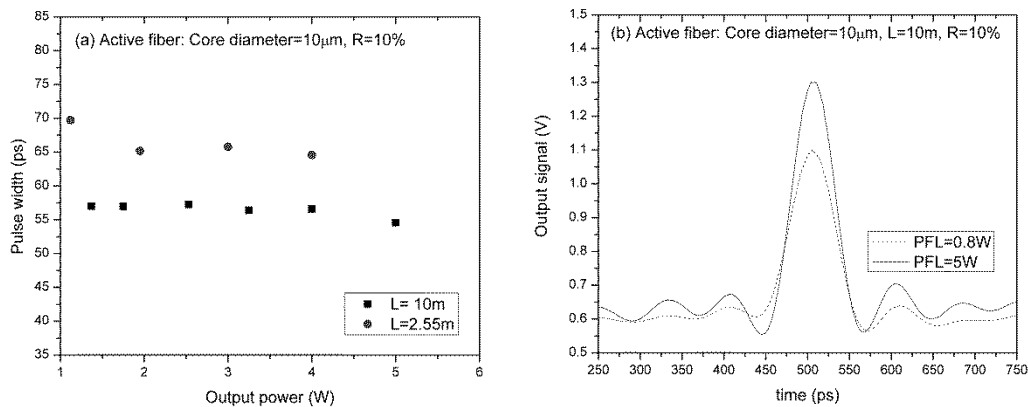


Figure 3.11: Measurements for 10 μ m core laser module with R =10% (a) Pulse width measurements at different output power with active fiber length of 2.55 m and 10 m. (b) Pulse width at 0.8 W and 5 W output power.

The 10 μ m core module with 10 m active fiber shows improved performance in terms of pulse width, average power as well as broader envelope width. Both 5 μ m and 10 μ m core modules share the same characteristics for their pulse amplitude envelope. Further experiments with 10 μ m core fiber modules were conducted to study the envelope behaviour. The envelope width is recorded using different active fiber lengths and output couplers. Summary of these results are shown through Figure 3.12(a)-(c).

From the above measurements, the following trends for pulse envelope can be concluded:

- The longer the active fiber, the broader the envelope width as shown in Figure 3.12(a).
- At each power level, the envelope width is measured five times with $\pm 2\mu$ s variations for recorded values.

- At a fixed active fiber length, the envelope width increases with increasing output coupler reflectivity as shown in Figure 3.12(b) and (c).
- The broadest envelope width is $45\mu\text{s}$ measured using 10m active fiber and a 50% output coupler. At each power level, the pulse width is measured four times with an average width of $55\pm 5\text{ps}$ (TBP=0.73) recorded at different power levels as shown in Figure 3.12(d).

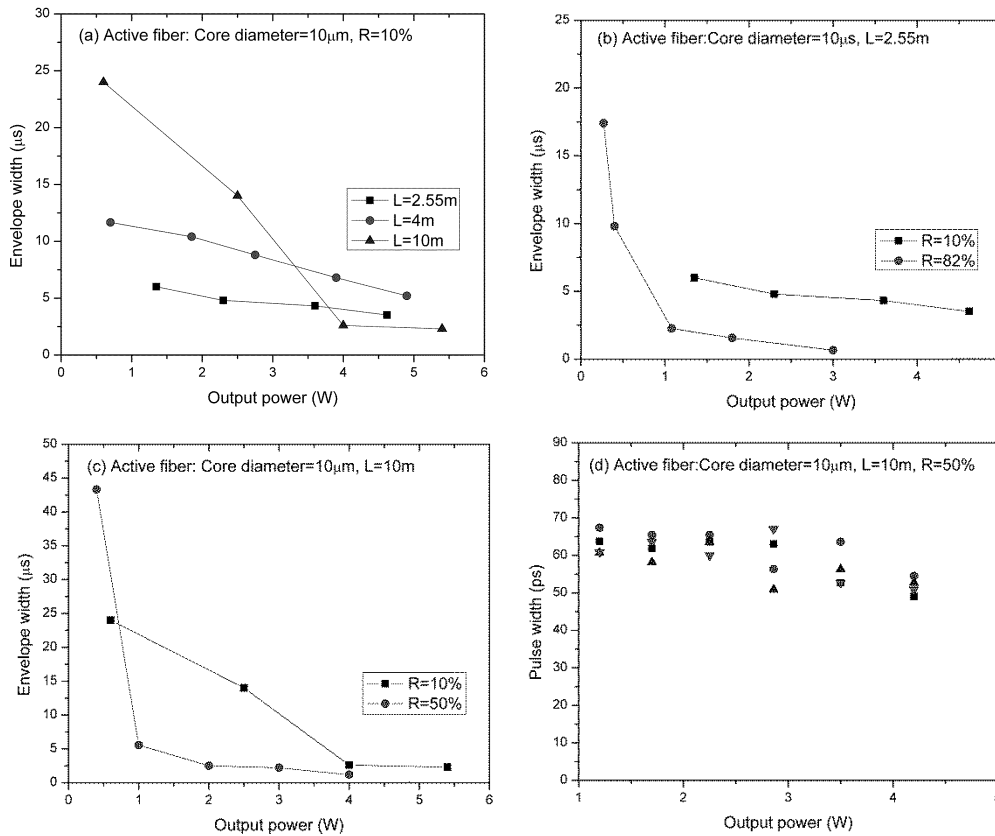


Figure 3.12: Measurements for 10 μm core laser modules. (a) Envelope width versus output power with R=10% and active fiber length of 2.55 m, 4 m and 10 m. (b) Envelope width versus output power with 2.55 m active fiber at R=10% and 82%. (c) Envelope width versus output power using 10 m active fiber at R =10% and R=50% .(d) Single pulse width versus output power with 10 m active fiber and R=50% .

Examples of the pulse amplitude envelope evolution are shown in Figure 3.13. The figures are measured for 10μm core laser module with 10m active fiber and 50% output coupler at different output power levels.

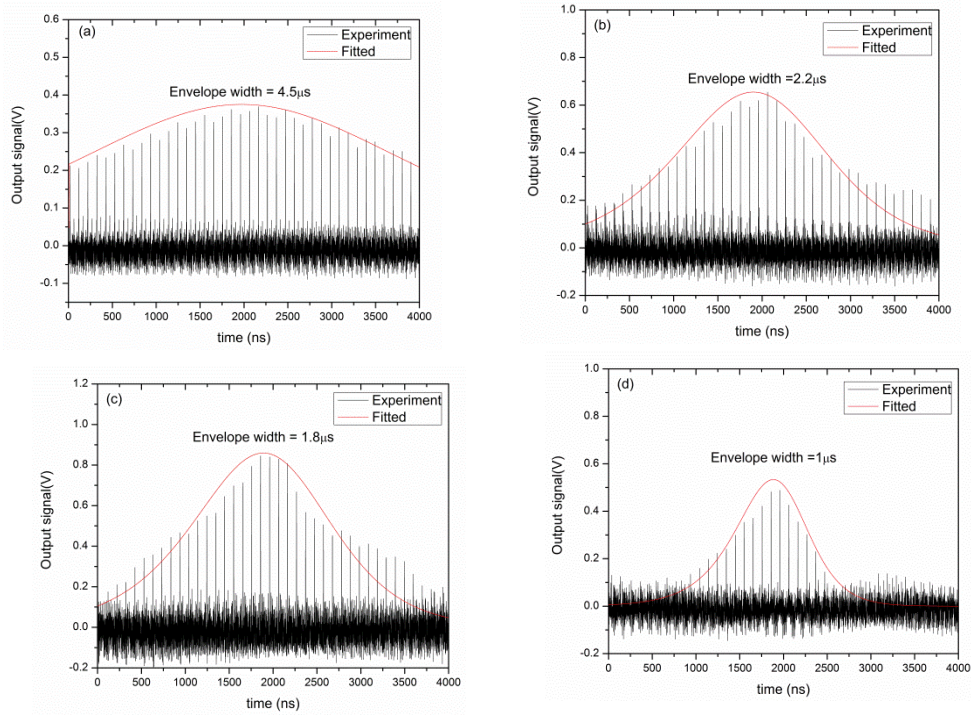


Figure 3.13 Oscilloscope trace for SML pulses with an amplitude envelope. (a) PFL=1 W, $P_{pump}=2.5$ W. (b) PFL =2 W, $P_{pump}=4$ W. (c) PFL=3 W, $P_{pump}=6$ W. (d) PFL=4W, $P_{pump}=8$ W.

Broadening pulse envelope: It has been proved experimentally that introducing a cross-splicing point in the mid of the active fiber as shown in Figure 3.14 will broaden the pulse envelope.

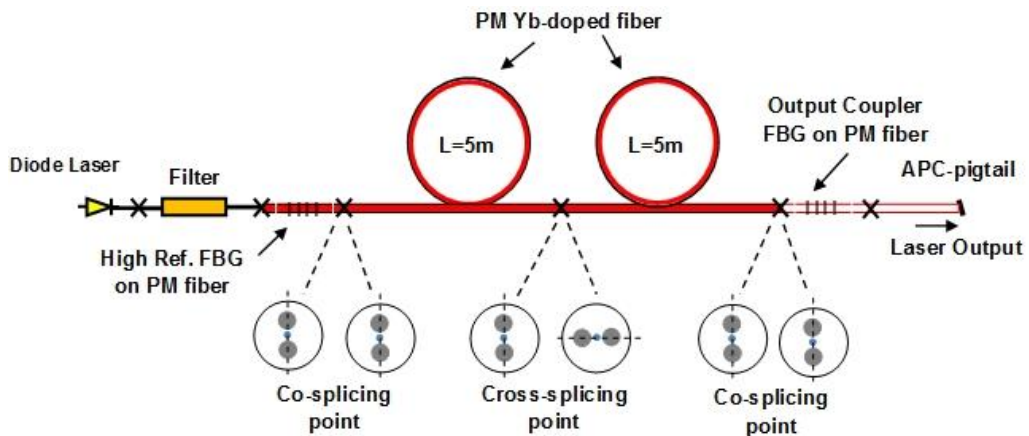


Figure 3.14: All-fiber mode- locked laser schematic with mid cross-splicing point for the active fiber. This module has a total PM Yb-doped active fiber length of 10 m with R= 50%..

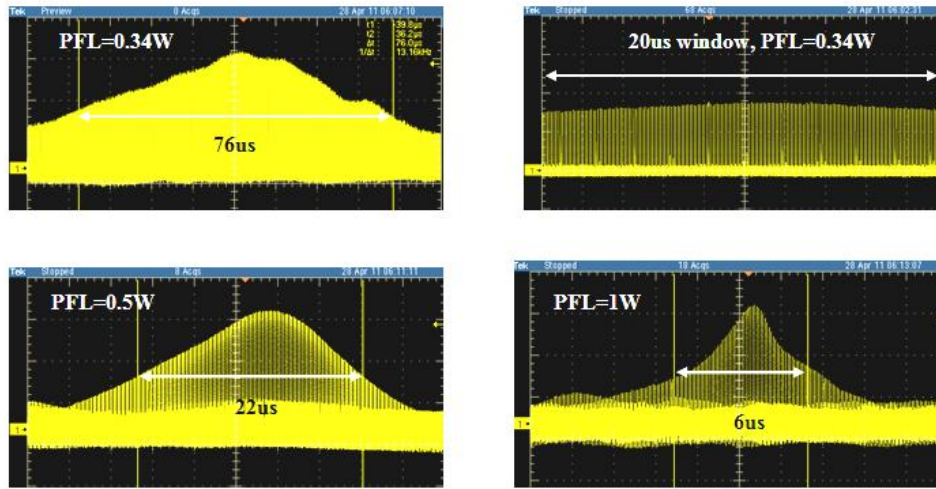


Figure 3.15: Oscilloscope traces for envelope measurements from 10 μ m core laser module with active fiber length of 10 m with mid cross-splicing and $R = 50\%$ at different output power levels.

This new splicing averages out the linear birefringence in the cavity [59] and improves the pulse trace stability. The new splicing scheme and measurements are presented as follows. The laser has a slope efficiency of 58% and a maximum average output power of 4.2 W at 7.8 W pumping level. The laser operates at the grating wavelength of 1063.9 nm with a narrow 3dB bandwidth of 50 pm and OSNR of 70 dB. The extinction ratio, measured at different output power levels, has an average value of 24 dB

Pulse envelope at different output power levels are shown through Figure 3.15(a)-(d). The total length of the cavity is around 10 m with a repetition rate of 10 MHz and 10:1 temporal SNR as displayed in Figure 3.15(b). The envelope widths measured at different output power levels are compared in Figure 3.16(a). The cross-splicing in the middle of the active fiber significantly broadened the envelope width to 75 μ s compared to 45 μ s at low output power levels. On the other hand, the envelope has same widths starting 1W output power. This can be explained as follows: the phase shift induced in the gain medium is the sum of both linear birefringence and nonlinear phase shift. At low pumping power, linear birefringence phase shift has dominant role over the nonlinear one. The linear birefringence phase shift, subjected to fluctuations due to temperature and polarization variations, can degrade the mode-locked stability [59]. By averaging out the linear birefringence, broader envelope width is realized. At high output power, nonlinear phase shift has higher contribution so the envelope width remains unchanged.

With the new cavity configuration, the laser has an average pulse width of 50 ps (TBP=0.66) as shown in Figure 3.16(b). The laser acquires picosecond pulse at high average power of 4 W.

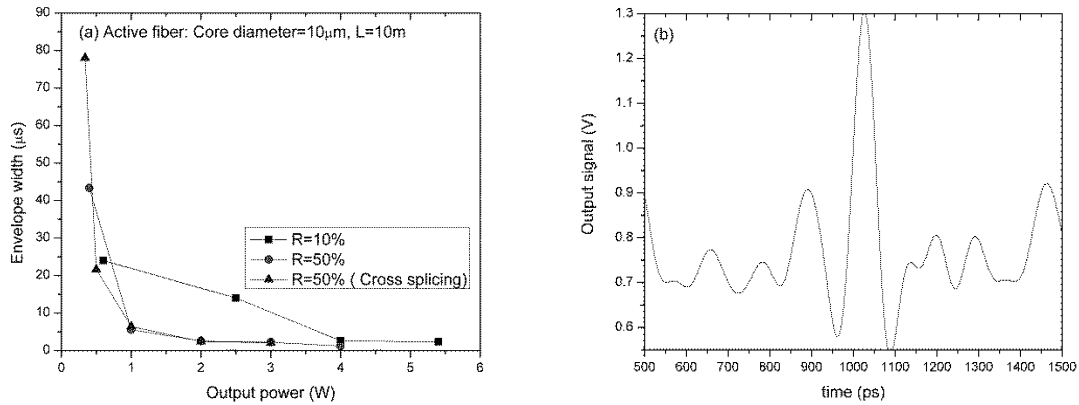


Figure 3.16: Measurements for 10 μm core laser module with an active fiber length of 10 m with mid cross-splicing and R=50% (a) Envelope width at different output power at R=10%, R=50% without and with active fiber mid cross-splicing. (b) Single pulse width measured at 4W output power.

3.3. Scaling Pulse Energy and Average Power

The proposed fiber laser succeeds to deliver SML pulses with high average power and energy. This is realized with a single stage module without using any amplifier stage or adjustable PC. Further pulse energy scaling will be presented in this section. This will be implemented via cavity length extension or building a fiber-amplifier. Most of the power and energy scaling techniques are applied to 5 μm core modules.

3.3.1. Cavity Length Extension

One of the well-known techniques to scale up pulse energy is to extend the cavity length while keeping average output power. Extending cavity length will reduce pulse repetition rate and consequently increases pulse energy. The 5 μm core laser cavity with 5 m active fiber and 10% output coupler is extended with a 50 m PM980 passive fiber. The passive fiber will be inserted between the active fiber and the output coupler FBG. The 55 m laser cavity has a maximum output power of 4 W as shown in Figure 3.17. The laser has an efficiency of 55% with 55 m cavity compared to 65% with 5 m one (slope efficiency of 74% with 55m compared to 84% with 5m using best linear fit for nonlinear output power curves). The linearly polarized output pulses have an extinction ratio of 30 dB.

The extended cavity operates around 1063.4 nm wavelength with a 70 dB OSNR as shown in Figure 3.18(a). With increasing the pumping power (cavity length of 55 m), the laser bandwidth was increased from 20 pm to 240 pm at maximum output power level of 4 W. A sample for mode-locked pulse train is plotted in Figure 3.18 (b). The pulse train has a round trip time of 592 ns and a corresponding repetition rate of 1.68MHz. By extending the cavity length, the repetition rate is reduced by 10 times and consequently the pulse energy is increased by almost same ratio.

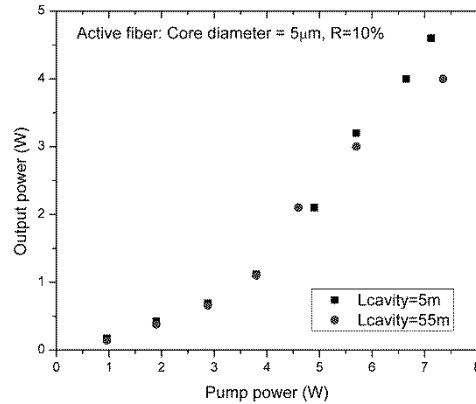


Figure 3.17: Output power versus pumping power for 5 μ m laser module operating at 1 μ m wavelength with 10% output coupler and cavity length of 5 m and 55 m.

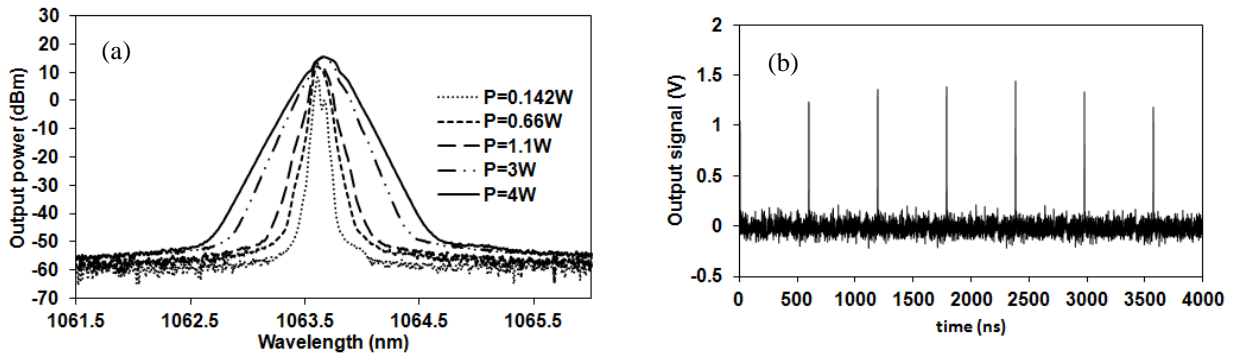


Figure 3.18: Measurements for 5 μ m laser module with 55 m cavity length and 10% output coupler (a) Laser output spectra at different output power (b) Mode-locked pulse train at 1.1 W output power.

3.3.2. Amplifier Stage

Scaling up average power is realized by adding an amplifier stage. The schematic for a seed laser followed by the amplifier stage is shown in Figure 3.19. The seed laser was the same one

described in Sec 3.2.4. The seed laser is tested up to 4 W pumping power and acquires a corresponding maximum output power of 1.7 W. The seed laser was chosen to operate at low pumping power range which has the broadest envelope width to be amplified.

In order to add the amplifier stage, an isolator is spliced between the seed laser and amplifier as shown in Figure 3.19. The amplifier is composed of (2+1) x1 PM-combiner with two input pump ports and one signal port. Both pump ports are connected to 25 W lasers diodes at 975 nm wavelength. The combiner signal input port is spliced to the isolator output while the output port is spliced to the amplifier active fiber. This fiber is a PM Yb-doped with 15 μm core diameter and 8 m length. This large mode area fiber is quoted with 6 dB/m absorption at 975 nm wavelength. The output end of amplifier active fiber is angle cleaved for proper pulse measurements.

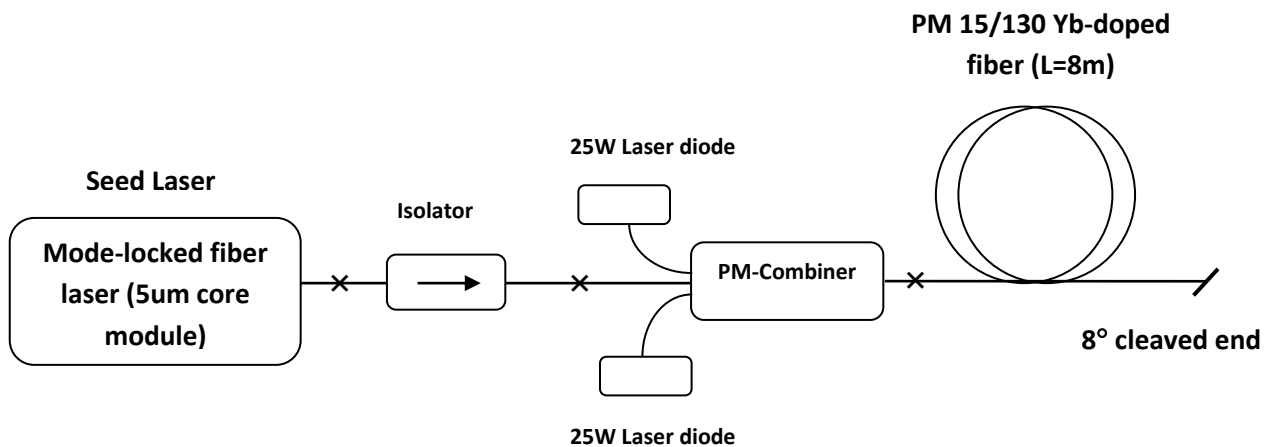


Figure 3.19: Amplifier schematic connected to 5 μm core module as seed laser.

The seed laser output power at different locations are tested and plotted in Figure 3.20(a). An output power of 0.65 W is measured after the isolator compared to 0.76 W out of the seed laser with 14% power loss at the isolator. At the same pumping power, the output reduces to 0.3 W measured at the output of the 15 μm core PM active fiber (before turning on amplifier). The seed laser operates at 3 W pumping power with a broadest envelope width of 32 μs and 0.65 W output power. The pulse train, applied to the amplifier input is presented at Figure 3.20(b). This train has 54.4ns round trip time and 18.5MHz repetition rate.

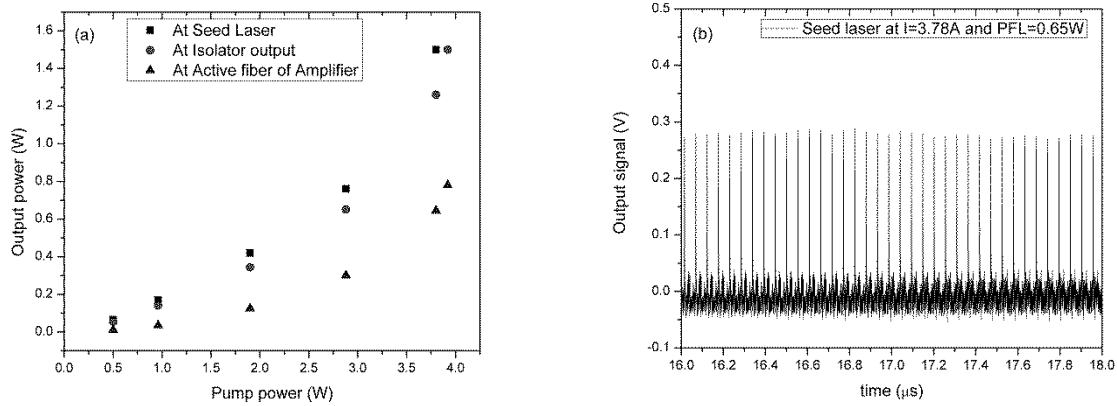


Figure 3.20: (a) Measurements of seed output power versus seed pump power at different positions before turning on amplifier. (b) Seed laser pulse train at 0.65 W output power.

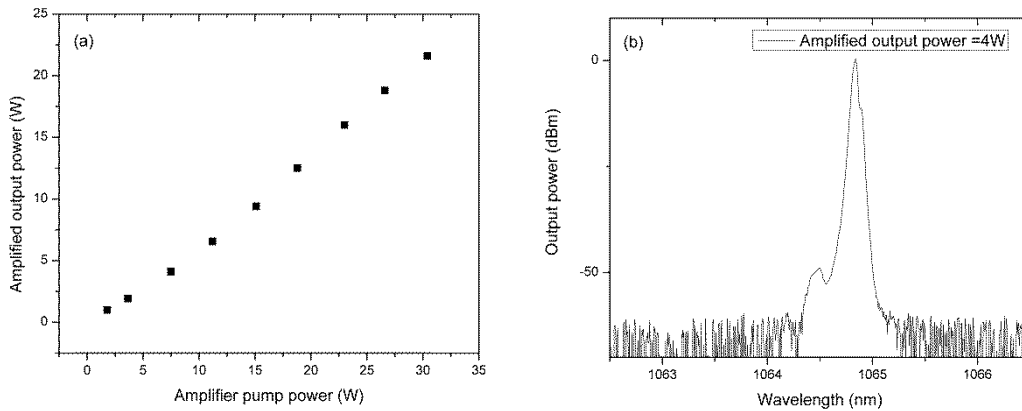


Figure 3.21: (a) Amplified output power versus amplifier pump power. (b) Output spectrum at 4 W amplified output power.

By adding an amplifier, the laser achieves maximum average power of 21.5 W with slope efficiency of 74% as shown in Figure 3.21(a). The amplified output spectrum at 4 W is shown in Figure 3.21(b). The laser operates at 1064.84 nm with 60 dB OSNR. The mode-locked pulses are also recorded at different amplified output power levels as shown in Figure 3.22. The proposed laser, with an amplifier stage generates mode-locked pulses with 21 W average power and 10:1 temporal SNR from an all-fiber module.

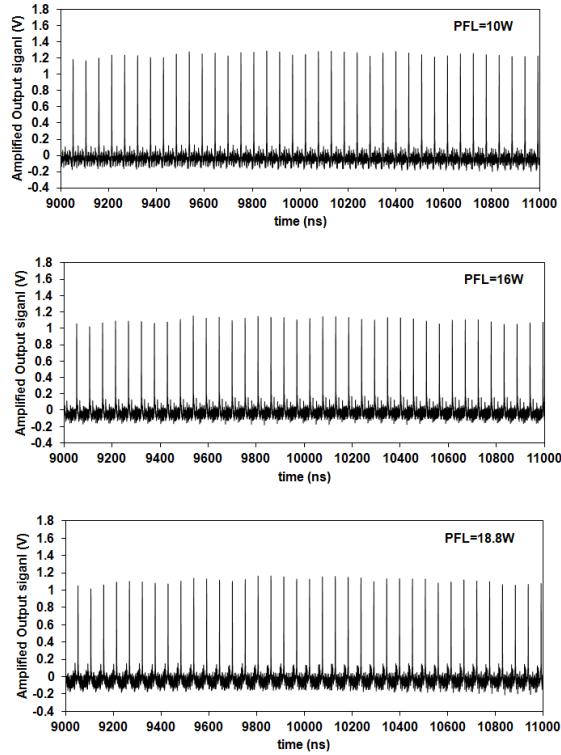


Figure 3.22: Amplified mode-locked pulse train at 10 W, 16 W and 18.8 W average output power.

3.4. Regulation of Mode-Locked Pulses

As shown in previous sections, the presented fiber laser generates SML pulses but with a modulated envelope. An approach to broaden the pulse envelope had been tested experimentally by reducing the linear birefringence phase shift in the cavity. This is implemented by transferring the cross splicing point to the middle of the active fiber. By cross-splicing two fiber sections of equal lengths, the linear birefringence Δn will change sign in the second of fiber due to reversing axes. As a result, the linear birefringence phase shift in the cavity will be averaged out [59]. This technique succeeds to broaden the pulse envelope but cannot totally eliminate it. Though, the laser acquires picoseconds pulses the observed envelope affects its stability. In order to take advantage of generating mode-locked pulses from such a simple cavity structure, an approach to regulate the mode-locked pulses is presented. This is implemented by applying a pulsed current to pump the laser diode. This method successfully stabilizes the mode-locked pulses underneath a Q-switched pulse train as shown in this section.

3.4.1. Experimental Setup

The pulsed current source is applied to a laser setup similar to what is shown in Figure 3.14. The laser uses a fiber-coupled 25 W LUMICS laser diode as pump source. The fiber laser cavity is composed of a total 5 m Yb³⁺ doped fiber (Nufern PLMA-YDF-10/125) and an output coupler with reflectivity value of 16%. Both active and FBG fiber are of double-clad PM type and has a 10 μ m core diameter. All pulse measurements in this section are measured with Newfocus' 1611 IR-DC-1GHz detector and 500 MHz Tektronix TDS-3054 or 500MHz Tektronix TDS-5054 oscilloscope. Another set up composed of a Newport AD-10ir photoreceiver and a 12 GHz Agilent Infinium DCA DS081204A oscilloscope is alternatively used to measure single pulse widths in picosecond range.

3.4.2. Experimental Results

The current source pumping the laser diode can work in either CW or pulsed modes. The laser output in both modes is measured and characterized. In CW mode, the laser has a maximum output power of 8.8 W with slope efficiency of 68% as shown in Figure 3.23(a). As previously discussed, the mode-locked pulses amplitude is modulated with an envelope whose width changes with pumping power. The mode-locked pulses at 6.75 W output power are shown in Figure 3.23(b).

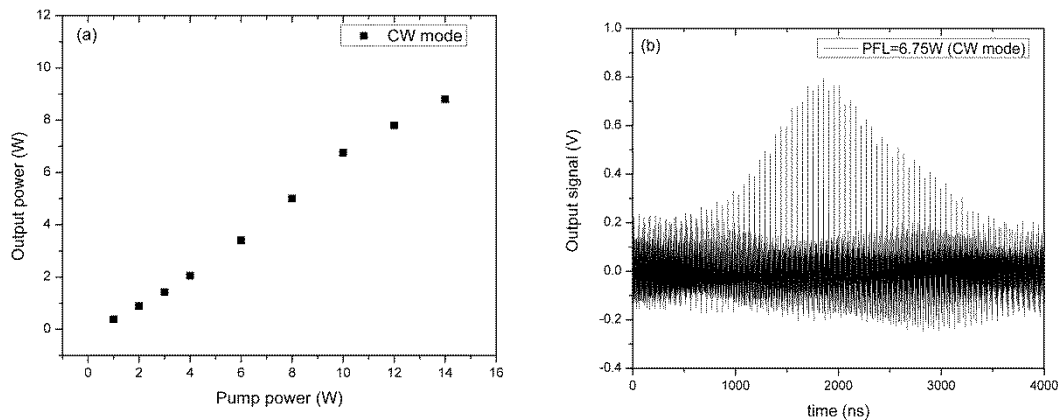


Figure 3.23: (a) Average power versus pump power at CW mode. (b) Mode-locked pulses at output power of 6.75W

In the pulsed mode, the current source has a maximum repetition rate of 100 KHz with an adjustable duty cycle. AC and DC current levels can be also controlled separately. The laser is tested at different pumping conditions and repetition rates from 10 KHz to 100 KHz. By

applying pulsed current to laser diodes, the laser output has a Q-switched form with a repetition rate determined by the current signal. The details of single Q-switch pulse is shown in Figure 3.24(a), in which, mode-locked pulses have duration corresponding to the cavity round trip on top of a Q-switching background. Different pulse parameters are defined in Figure 3.24(a) to characterize the output pulse, where Q_h represents the height of Q-switching background while M_h represents the mode-locked pulses height. The pulse width of the pump current is optimized to reduce Q_h . Figure 3.24 (b) presents the percentage ratio of the Q-switch background to mode-lock pulses heights (Q_h/M_h) at different current pulse widths. At each repetition rate, an optimum current pulse width is recorded with minimum Q_h/M_h ratio.

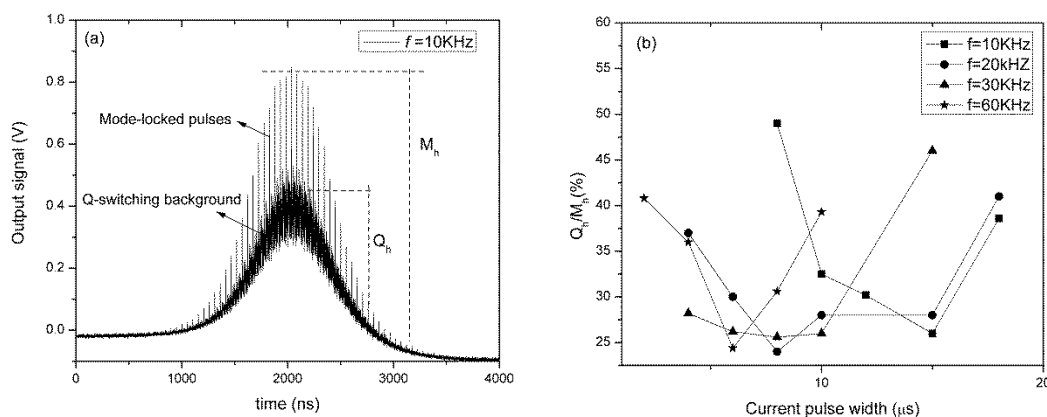


Figure 3.24: (a) Details of Q-switch pulse measured at repetition rate of 10 KHz and electronic pulse width (τ_{EPW}) of 8 μ s. (b) Q-switching background height versus τ_{EPW} at different repetition rates.

At the optimum current signal pulse widths, the output is measured at different time scales as shown through Figure. 3.25(a)-(i). The left column represents Q-switched pulse train, the middle represents details of single Q-switched mode-locked (QML) pulse while the right one represents the measurements of single mode-locked pulse width.

From the above measurements, applying pulsed current sources has stabilized the mode-locked pulses underneath a Q-switch pulse envelope. The laser output mostly follows the repetition rate of the pulsed current as shown in the above figures. A Q-switching background is observed and which reduces part of the mode-locked pulses energy. It can be also deduced that higher average power level can be obtained at higher current repetition rate as shown in Figure 3.. The mode-locked pulse width has a FWHM in the range of 80-120 ps while Q-switch pulses are in 1-1.3 μ s range. Average power of 1.6 W is achieved at 100 KHz with output pulses shown in Figure

3.26(a)-(c). The experimental measurements and estimated pulse energy using pulsed current source for the 10 μ m core fiber module are summarized in Table 3.1.

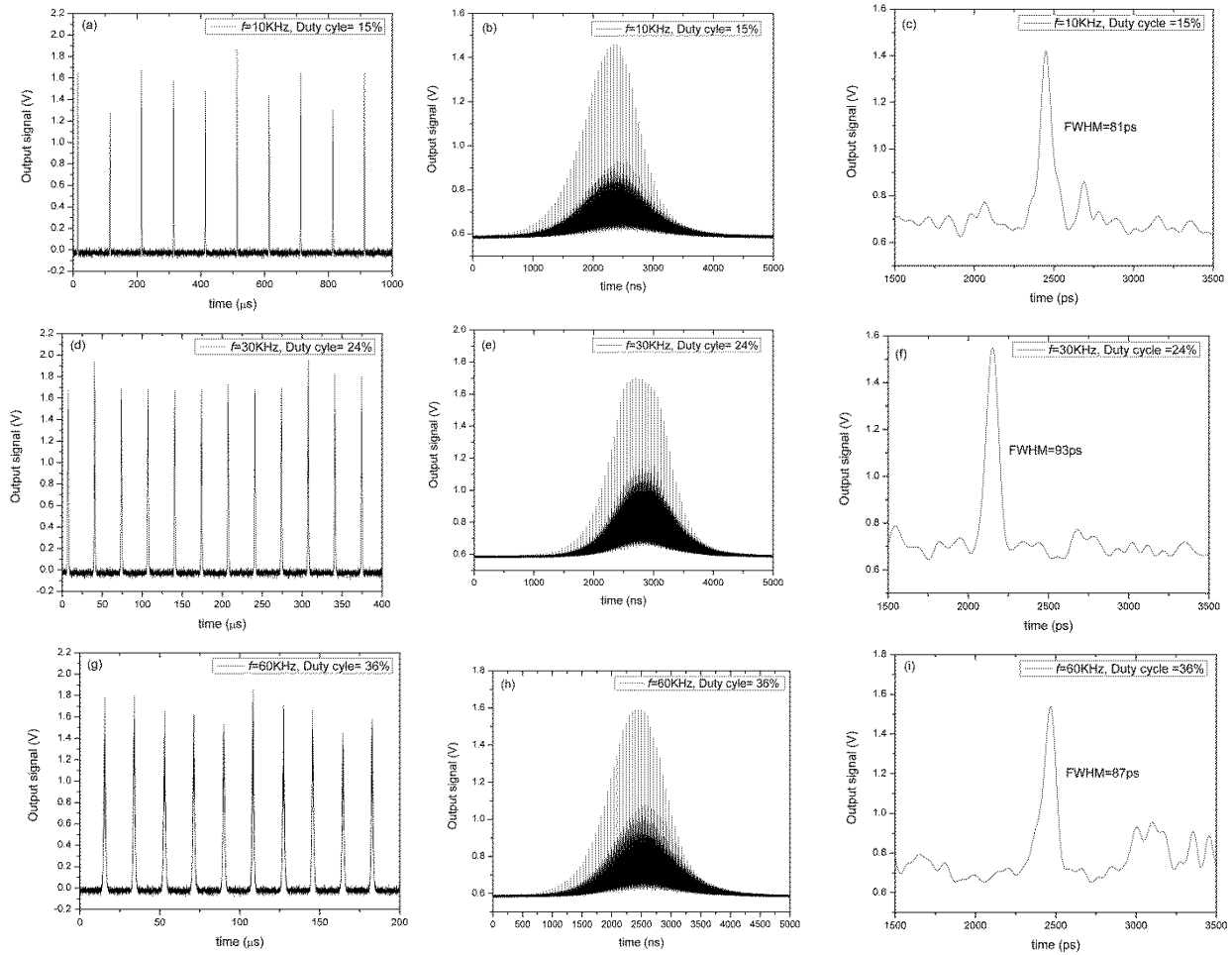


Figure. 3.25: Pulse measurements where left column is Q-switch pulse train, middle column is QML pulse and the right column is mode-locked pulse width for (a)-(c) $f=10$ KHz, (d)-(f) $f=30$ KHz, (g)-(i) $f=60$ KHz.

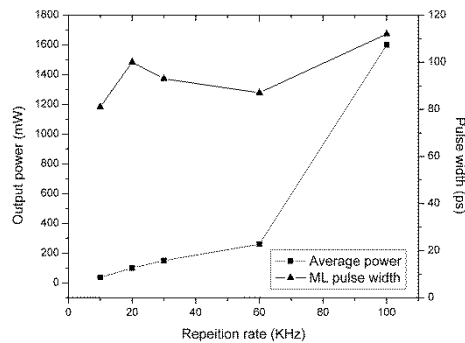
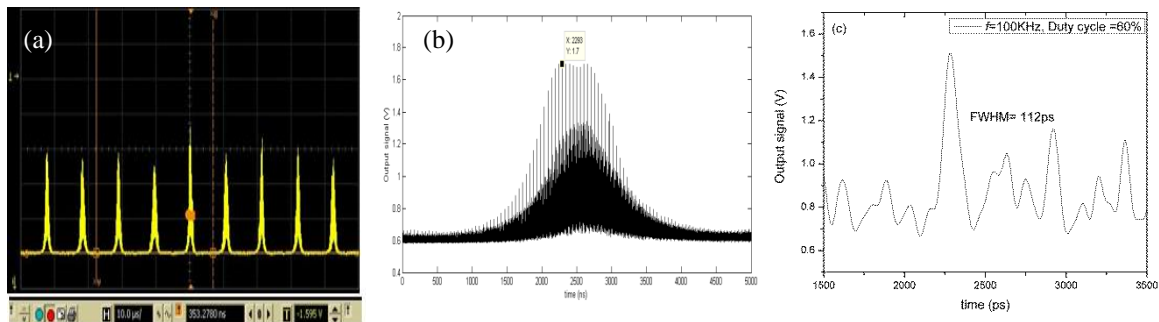


Figure 3.26: Average power and mode-locked pulse width versus repetition rate.

Table 3.1: Laser output parameters at different repetition rates

	f=10KHz	f=20KHz	f=30KHz	f=60KHz	f=100KHz (Fig.3.28)	f=100KHz (Fig.3.29)
Average power (P_{av})	0.037W	0.1W	0.15W	0.26W	1.6W	100mW
Pump current (I_{pump})	2.12A	2.52A	1.96A	1.84A	2.52A	0.7A
Pump power (P_{pump})	0.4W	0.55W	0.69W	0.92W	3.4W	3.4W
Mode Lock width (ps)	81	100	93	87	112	N/A
Electronic pulse width (τ_{EPW})	15 μ s	8 μ s	8 μ s	6 μ s	6 μ s	9 μ s
Laser frequency	10KHz	20KHz	30KHz	60KHz	100KHz	50KHz
Mode-locked envelope width (τ_{MLEW})	1.23 μ s	1.13 μ s	1.05 μ s	1.24 μ s	1.15 μ s	3.53 μ s
Ratio of Q-switched pulse height to mode-lock pulse height (Q_h/M_h)	26%	24%	25.6%	24.44%	50%	4.5%
Q-switched pulses amplitude variations	32%	26.2%	14-16%	16%	20%	10.8%
Q-switched Energy	3.7 μ J	5 μ J	5 μ J	4.3 μ J	16 μ J	2 μ J
Percentage of pedestal energy	33%	-	43%	45%	52%	4%
Total Mode-locked pulses energy	2.45 μ J	-	2.85 μ J	2.38 μ J	7.68 μ J	1.92 μ J
No. of Mode-locked pulses underneath Q-switch envelope	60	-	60	60	60	200
Mode-locked pulse energy (excluding background)	40.8nJ	-	47.5nJ	39.6nJ	128nJ	9.6nJ
Mode-locked peak power	0.49KW	-	0.5KW	0.5KW	1.1KW	-

**Figure 3.27:** Pulse measurements at $f=100$ KHz (a) Q-switch pulse train. (b) Q-switch pulse with mode-locked pulses (c) single mode-locked pulse width.

From the above measurements summarized in Table 3.1, it can be deduced that:

- Optimum output has been realized at $f=30\text{-}60$ KHz with a minimal Q_h/M_h of 24-25% and pulse amplitude variations of 14% with pulse energy of 47nJ peak power of 0.5KW
- Higher pulse energy and peak power are realized at $f=100$ KHz but with higher Q_h/M_h of and pulse variations
- Using pulsed current source at different repetition rates, pulse energy of 50 to 128 nJ and peak power of 0.5 to 1.1 KW are realized using single fiber laser module.

Further experiments are conducted to reduce the observed Q-switching background and improve the output energy. This is implemented by optimizing duty cycle, AC and DC component of the current at repetition rate of 100 KHz. By setting electronic pulse width (EPW) to $9\mu\text{s}$, the Q_h/M_h ratio is reduced to 4.5% compared to 24% as shown in Figure 3.28(a)-(b). The laser has a repetition rate of 50 KHz with an average power level of 100mW. Some variations in pulse heights are attributed to limitations of the number of sampling points (10,000 pts) offered by the oscilloscope.

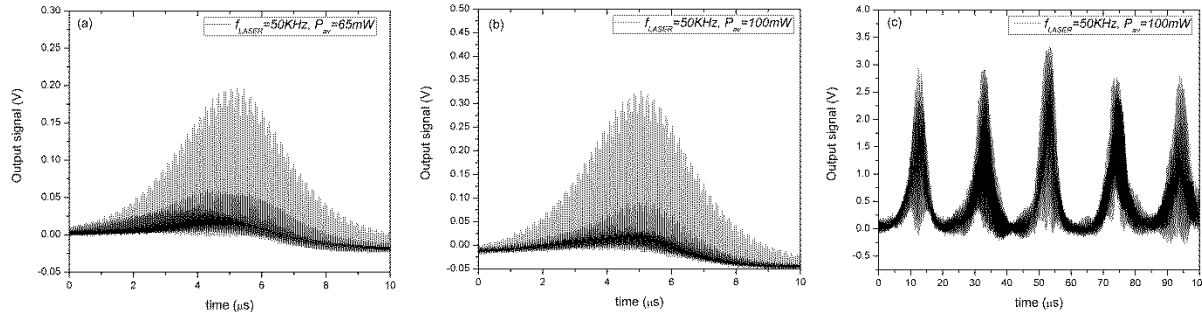


Figure 3.28: Pulse measurements with current repetition rate of 100 KHz . (a) QML pulse at EPW=8 μs (b) QML at EPW= 9 μs . (c) Q-switched mode-locked pulse train at EPW=9 μs .

3.5. Summary & Discussions

In this chapter, experimental results of the proposed fiber laser have been presented. The laser generated mode-locked pulses from an all-fiber structure. This is implemented by combining both birefringent medium and polarization selection mechanism in one cavity. The module worked for both 1 μm and 1.5 μm (1.5 μm results are not presented in the thesis) with high extinction ratio of 25 dB and higher. This can be attributed to high isolation of PM FBGs. Double-clad pumping lead to the high average output power level up to 5.5 W. The laser has a

narrow line width of 30-50 pm with excellent 60-70 dB OSNR and a pulse width of ~50 ps. In addition, more experiments were conducted to increase average output power. This was implemented by or adding amplifier stage to 5 μ m core laser modules. With an amplifier, the SML pulses are measured with 21 W average power.

With increasing pumping power, an envelope modulates the mode-locked pulse amplitude. The envelope width decreases with increasing output power. Different design parameters such as active fiber length, diameter and output coupler reflectivity were varied to study the envelope behaviour. Broadest envelope was obtained with a longer active fiber and higher output coupler reflectivity. The envelope width reaches its broadest width of 76 μ s using 10 m active fiber (10 μ m core), 50% output coupler and introducing a cross-splicing in the middle of the active fiber. This splicing arrangement averages out linear birefringence and broadens envelope width.

The pulse envelope phenomenon is detrimental to a stable mode-locked fiber laser. By incorporating double-clad fiber in the laser cavity, we believe that intra-cavity power must reach a level from which nonlinearities play a role in envelope and pulse formation. This envelope cannot be related to SBS or SRS as no evidence had been shown in the output spectra. SBS has been reported as a main mechanism to generate pulses with cavity mode separation in [65-67]. Typical measured SBS pulse width is 2 ns [65] which is broader than our recorded pulse width. This requires us to develop a numerical model to describe and understand the pulse envelope which is the topic of the next chapter. The origin of this envelope as well as mode locking mechanism will be investigated in Chapter 4.

Finally, The SML pulses were regulated using pulsed current source for the laser diodes. This approach had been tested experimentally in which the mode-locked pulses falls underneath Q-switched pulse train. This Q-switch pulses has a repetition rate equal to the one applied to the current. Different current signal parameters are varied to optimize the laser operation. It has been found, that high average power is achieved at higher repetition rate with average mode-locked pulse width of 100 ps. This approach successfully stabilizes the SML pulses and achieves pulse energy between 50 to 128 nJ and peak power of 0.5 to 1.1 KW using different current settings. High power fiber lasers multiple KHz and peak power in the range of 50-400W are suitable for laser welding of medical devices.[9]. In addition, Material processing including cutting, marking and wafer processing can be accommodated with the realized peak power [4].

Chapter 4. Numerical Modelling of All-PM Mode-Locked Fiber Laser

This chapter mainly presents theoretical modelling for the SML all-fiber laser. In Sec 4.1, an overview on different factors affecting the pulse propagation in a fiber is presented. In Sec 4.2, the main numerical techniques used in simulating pulsed fiber lasers are illustrated. This includes brief explanation for Nonlinear Schrödinger equation (NLSE) and split step Fourier method (SSFM). Different theoretical approaches are presented in Sec. 4.3 to explain SML mechanism and envelope formation. Finally the laser mode-locking mechanism is explained in Sec.4.4.

4.1. Nonlinear Pulse Propagation in Fiber

The performance of picoseconds and femtosecond mode-locked fiber lasers particularly in terms of pulse energy, peak power and pulse quality is controlled by the nonlinearities, dispersion and the gain of the fiber. In order to analyze the pulse formation and stabilization inside optical fiber, it is useful to introduce two length scales, known as the dispersion length L_D and the nonlinear length L_{NL} [59] as shown in Eq.(4.1)

$$L_D = \frac{T_o^2}{|\beta_2|} \quad , \quad L_{NL} = \frac{1}{\gamma P_o} \quad (4.1)$$

where T_o is the initial pulse width and P_o is the initial pulse peak power. The nonlinear coefficient γ , can be calculated from:

$$\gamma = \frac{\omega_o n_2}{c A_{eff}} \quad (4.2)$$

where n_2 is the nonlinear index parameter of a fiber and has a typical range values of 2.2-3.4 $\times 10^{-20}$ m²/W. From Eq. (4.2), it can be deduced that the γ can be calculated using the fiber effective area, A_{eff} , and the operating wavelength.

Based on the definition of dispersion and nonlinear length, two regimes for fiber and pulse interaction can be explained as:

(a) Dispersion dominant regime In this regime, the fiber length $L \ll L_{NL}$ but $L \sim L_D$. The pulse evolution is governed by group velocity dispersion (GVD) and the nonlinear effects play a minor role.

(b) Non-linearity regime: In this regime the fiber length $L \ll L_D$ but $L \sim L_{NL}$. The dispersion has negligible effects compared to nonlinear term.

When the fiber length L is longer or comparable to both L_D and L_{NL} , dispersion and nonlinearity both act together as the pulse propagates along the fiber. The interplay of the dispersion and nonlinear effects can lead to a different behaviour [68] compared with the expected from dispersion or nonlinear alone [68, 69]. Nonlinear effects in optical fibers are particularly important when considering the propagation of short pulses (from 10 ns to 10 fs).

Fiber nonlinearities can be classified into two main categories: stimulated scattering effects (Raman and Brillouin) and effects from the nonlinear index of refraction [70]. Stimulated scattering is manifested as intensity-dependent gain or loss while the nonlinear index gives rise to an intensity-dependent phase of the optic field [70]. Stimulated Raman Scattering (SRS) results from the interaction between the photons and the molecules of the medium with wide gain bandwidth on the order of 100 nm. This leads to the transfer of the light intensity from the shorter wavelength to the longer wavelengths. Stimulated Brillouin Scattering (SBS) with a peak gain coefficient over 100 times greater than Raman makes it more dominant process. It originates from the interaction between the pump light and acoustic waves generated in the fiber. It introduces a strong wave propagating in the opposite directions with a narrowband gain of 20 MHz [70].

The intensity-dependent refractive index of silica gives rise to three effects: Self-Phase Modulation (SPM), Cross-Phase Modulation (XPM) and Four-Wave Mixing (FWM). More insight into some of the fiber non-linearities such as SPM, XPM and NPR will be discussed in the following sections.

4.1.1. Self Phase Modulation (SPM)

One of the important roles played by nonlinear index in fiber is the phenomena of self-phase modulation (SPM). The temporal shape and frequency spectrum of the propagating pulse are influenced by changing in the index that varies with the pulse intensity [71] as shown in Eq. (4.3):

$$n^{SPM} = n_o + n_2 I \quad (4.3)$$

where n_o is the linear index of refraction, n_2 is a nonlinear index coefficient and I is the intensity in the fiber.

To understand the effect of SPM on a propagating pulse, an initial pulse propagating in z -direction is defined as:

$$E = \frac{1}{2} E_o(z, t) \exp(-ink_o z) \exp(i\omega_o t) \quad (4.4)$$

Then, the nonlinear refractive index shown in Eq. (4.3) is substituted into Eq. (4.4) yielding,

$$E = \frac{1}{2} E_o(z, t) \exp(-in_o k_o z) \exp(i\omega_o t - i\varphi(z, t)) \quad (4.5)$$

Here Eq. (4.3) & Eq. (4.5) show that SPM develops an intensity-dependent phase shift $\varphi(z, t)$ with unaffected pulse shape. The additional phase shift can be represented as:

$$\varphi(z, t) = \frac{2\pi n_2 z}{\lambda} I(z, t) \quad (4.6)$$

where z is the distance propagated by the pulse in a fiber.

The maximum phase shift φ_{max} which occurs at the pulse peak is defined in Eq. (4.7), where P_o is the peak power of the pulse.

$$\varphi_{max} = \frac{2\pi n_2 L}{\lambda} \frac{P_0}{A_{eff}} = \gamma P_0 L \quad (4.7)$$

The time variation of phase shift arising from nonlinearities has the effect of introducing new frequency components to the pulse that was not present before. The spectral broadening of the pulse due to SPM is determined by its own power temporal variation. It also affected by the dispersion (GVD) nature inside fiber whether it is normal or anomalous.

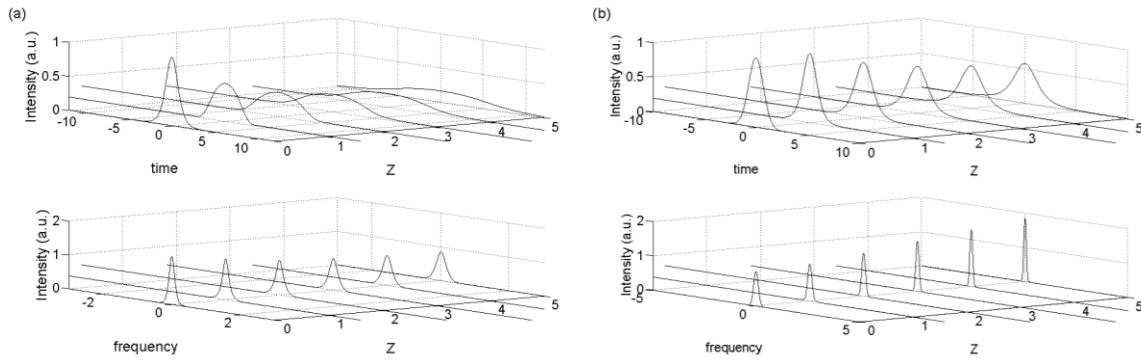


Figure 4.1: MATLAB simulation of a Gaussian pulse after passing through fiber length of 5 m with including SPM with GVD effects (a) $\beta > 0$ (Normal dispersion) (b) $\beta < 0$ (Anomalous dispersion).

The pulse temporal shape and spectrum shown in Figure 4.1 are simulated in both normal and anomalous dispersion regimes in conjunction with SPM. This is conducted with a MATLAB-based program (SSPROP) presented by a research group in Maryland University [72] and the output is shown in Figure 4.1. In normal dispersion, both temporal pulse and spectral broadening can be observed. While with anomalous conditions, the pulse undergoes less temporal broadening rate. The spectrum is narrowed rather than broadened as expected from SPM [71].

4.1.2. Cross Phase Modulation (XPM)

Cross phase modulation (XPM) is similar to SPM [68]; except that it involves two overlapping but distinguishable pulses of either different frequencies or polarizations. The spectral broadening of the pulse is due to the influence of other pulses propagating at the same time in the fiber. The nonlinear index is effectively doubled in XPM over that associated with SPM. The nonlinear coefficient is expressed by Eq. (4.8) [68].

$$n^{XPM} = n_o + 2n_2I \quad (4.8)$$

Each polarization components develop a nonlinear phase shift whose magnitude is the sum of the SPM and XPM contributions. The phase shift in both x and y direction is expressed by Eq. (4.9) for the two components.

$$\varphi_x = \gamma \left(P_x + \frac{2}{3}P_y \right) L, \quad \varphi_y = \gamma \left(P_y + \frac{2}{3}P_x \right) L \quad (4.9)$$

The first term in Eq. (4.9) represents SPM while the second term represents XPM. The nonlinear phase shift acquired by one polarization component depends on the intensity of the other polarization component [68, 71]. The quantity of practical interest is the relative phase difference given by Eq. (4.10).

$$\Delta\varphi_{NL} = \varphi_x - \varphi_y = \frac{1}{3}\gamma(P_x - P_y)L = \gamma P_o L/3 \cos(2\theta) \quad (4.10)$$

where P_o represents the peak power, L the length of the fiber and θ is the angle of incidence of light on the fiber. The nonlinear phase shift term by XPM component is responsible for asymmetric spectral broadening of co-propagating optical pulses.

4.1.3. Nonlinear Polarization Rotation (NPR)

One of the most popular techniques for mode-locking fiber lasers is the Nonlinear Polarization Rotation (NPR). The NPR can be treated as a kind of artificial saturable absorption to achieve the passive mode locking in a fiber laser [73].

NPR technique can be explained as follows:

- If the light intensity incident on a birefringent fiber is strong, the nonlinear optical Kerr effect in the fiber must be considered and introduces extra changes to the light polarization. The polarization change introduced by the optical Kerr effect depends on the light intensity. The orientation and the final light polarization are also determined by the fiber length and its birefringence.
- If a polarizer is placed after the fiber, the transmission through this polarizer will become intensity dependent. Through appropriately selecting the orientation of the polarizer or the length of the fiber, the light with higher intensity will experience lower losses at the polarizer. An artificial SA effect with ultra-fast response could be realized with such a system and is used to passively mode-lock the fiber lasers.

The evolution of the two polarization components will be tracked by a column matrix for the electric field and a 2×2 matrix for the resonator elements. The electric field 2×1 column matrix can be represented as follows:

$$\begin{pmatrix} E_x \\ E_y \end{pmatrix} \quad (4.11)$$

The propagation through a birefringent fiber of length L is represented by two terms; the linear propagation phase (φ_L) and nonlinear phase modulation (φ_{NL}). The resulting matrix is thus a product of two matrices, and the field vector is given by [73]:

$$\begin{pmatrix} E_x(L) \\ E_y(L) \end{pmatrix} = \begin{pmatrix} e^{i\varphi_{NLx}} & 0 \\ 0 & e^{i\varphi_{NLy}} \end{pmatrix} \begin{pmatrix} e^{i\varphi_L} & 0 \\ 0 & e^{i\varphi_L} \end{pmatrix} \begin{pmatrix} E_x(0) \\ E_y(0) \end{pmatrix} \quad (4.12)$$

$$\begin{pmatrix} E_x(L) \\ E_y(L) \end{pmatrix} = \begin{pmatrix} e^{i\varphi_x} & 0 \\ 0 & e^{i\varphi_y} \end{pmatrix} \begin{pmatrix} E_x(0) \\ E_y(0) \end{pmatrix} \quad (4.13)$$

$$\varphi_x = \frac{2\pi nL}{\lambda} \left[|E_x|^2 + \frac{2}{3} |E_y|^2 \right] - \frac{2\pi \Delta n L}{\lambda} \quad (4.14(a))$$

$$\varphi_y = \frac{2\pi nL}{\lambda} \left[|E_y|^2 + \frac{2}{3} |E_x|^2 \right] + \frac{2\pi \Delta n L}{\lambda} \quad (4.14(b))$$

where Δn represents the birefringence of the PM fiber. The first term in Eq. (4.14) represents nonlinear phase shift due SPM and XPM while the second term represents linear phase shift due to fiber birefringence. Other components of the round-trip model like gain, saturable absorption, mirrors, etc., usually do not distinguish between the two polarization components. From the analysis in [73], the transmission coefficient for a pulse passing through a birefringent fiber and a polarizer can expressed in Eq. (4.15), where θ is the angle of incidence of light on the fiber.

$$T(t) = \frac{1}{2} \left[1 - \cos \left(\Delta\varphi_{NL}(t) \right) \right] \sin^2(2\theta) \quad (4.15)$$

4.2. Numerical Modelling

4.2.1. Nonlinear Schrödinger Equation (NLSE)

NLSE comes in a variety of forms based on the system being studied. Its generalized time domain form can be represented in Eq. (4.16) [59]:

$$\frac{\partial A}{\partial z} = -i \frac{\beta_2}{2} \frac{\partial^2 A}{\partial t^2} + i\gamma(|A|^2)A + \left(\frac{g}{2}\right)A + \left(\frac{gT_2^2}{2}\right)\frac{\partial^2 A}{\partial t^2} \quad (4.16)$$

where A is the electromagnetic field amplitude of the optical pulse, z is the spatial coordinate along the fiber length and t is relative time in the moving pulse frame of reference. The pulse propagates in the cavity is subjected to Kerr nonlinearity (γ) and second-order dispersion (β_2). It will experience additional saturated gain (g) with a finite bandwidth when passing through gain fiber. T_2 is the gain dispersion coefficient which accounts for the decrease of the gain coefficient at the wavelength located far from the gain peak and inversely proportional to the gain bandwidth ($\Delta\nu_g$). The derivation of NLSE starting from Maxwell equation is illustrated in details

in [55]. If more than one polarization presents inside the fiber, the Eq. (4.16) will be changed to represent the two polarizations inside fiber. The time-domain Coupled NLSE (CNLSE) for high birefringence fiber is shown as follows [74]:

$$\frac{\partial A_x}{\partial z} = -\frac{\Delta\beta_1}{2} \frac{\partial A_x}{\partial t} - i \frac{\beta_2}{2} \frac{\partial^2 A_x}{\partial t^2} + \frac{\beta_3}{3} \frac{\partial^3 A_x}{\partial t^3} + i\gamma \left(|A_x|^2 + \frac{2}{3} |A_y|^2 \right) A_x + \left(\frac{g}{2} - \frac{\alpha_o}{2} \right) A_x \quad (4.17)$$

$$\frac{\partial A_y}{\partial z} = \frac{\Delta\beta_1}{2} \frac{\partial A_y}{\partial t} - i \frac{\beta_2}{2} \frac{\partial^2 A_y}{\partial t^2} + \frac{\beta_3}{3} \frac{\partial^3 A_y}{\partial t^3} + i\gamma \left(|A_y|^2 + \frac{2}{3} |A_x|^2 \right) A_y + \left(\frac{g}{2} - \frac{\alpha_o}{2} \right) A_y \quad (4.18)$$

where β_3 represents third order dispersion and α_o is the cavity losses. Third order dispersion is not considered in our simulations.

4.2.2. Split Step Fourier Method

One of the powerful methods to solve NLSE is known as split-step Fourier method (SSFM) which is the technique of choice for solving NLSE due to its easy implementation and speed compared to other methods especially time-domain finite-difference method [75, 76]. It assumes that mathematical terms due dispersion and nonlinearity can act separately and independently over short piece of fiber [75, 76]. With the above assumption, the NLSE can take the following form:

$$\frac{\partial A}{\partial z} = (\widehat{D} + \widehat{N}) A \quad (4.19)$$

where $A(z,t)$ is the complex field envelope at step z and time t . \widehat{D} is the differential operator that represents dispersion and absorption in a linear medium and \widehat{N} is the nonlinear operator representing nonlinear effects on the propagating pulse as shown in Eq.(4.20) [75, 76].

$$\widehat{D} = -\frac{\alpha}{2} - i \frac{\beta_2}{2} \frac{\partial^2}{\partial t^2}, \widehat{N} = i\gamma(|A|^2) \quad (4.20)$$

Other terms such as β_1 and β_3 shown in Eq. (4.17) and Eq. (4.18) for CNLSE are added to differential operator \widehat{D} if considered in the simulation. The SSFM is an iterative process that determines the field solution for spatial steps of h . This performed for each step for the entire length of the fiber. The procedure during one step is illustrated in Figure 4.2. The fiber of length L is divided into $s_L=L/h$ steps of length h [76]. The field propagation $A(jh, t)$ per spatial step h at the step jh ($j=1, 2, s_L$) for the entire fiber length can be represented by the following relation:

$$A(jh, t) = \mathcal{F}^{-1} \left\{ \exp \left(h\widehat{D}(i\omega) \right) \mathcal{F} \left\{ \exp \left(h\widehat{N} \right) A((j-1)h, t) \right\} \right\} \quad (4.21)$$

where $A((j-1)h, t)$ is the field solution from the previous step. The operation of nonlinear operator \widehat{N} occurs in the middle of the step. It is the first operator to act on $A(jh, t)$. The effect of dispersion is determined in the frequency domain. The field solution is Fourier transformed, operated on by \widehat{D} and then back transformed to give solution $A(jh, t)$ at step jh . The field solution contains both intensity and phase information.

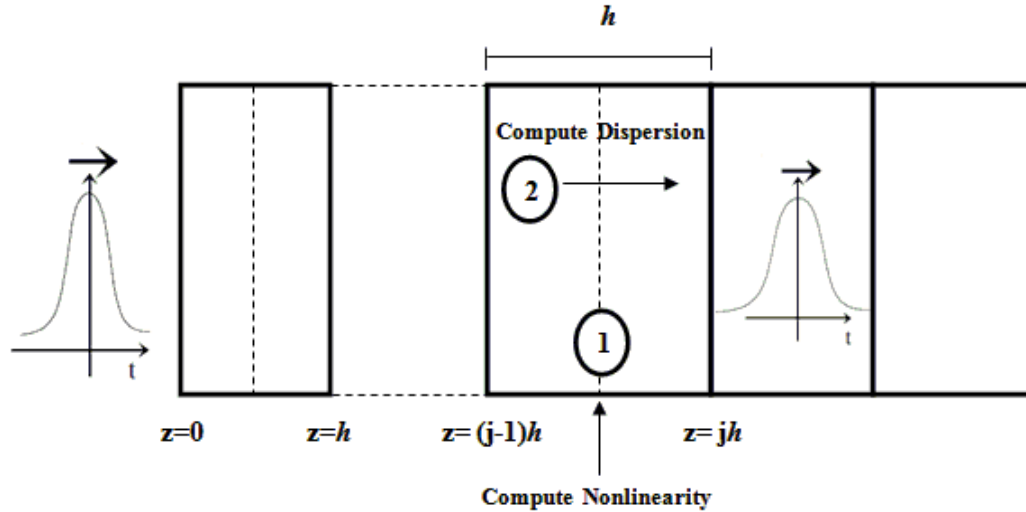


Figure 4.2: The SSFM for one iteration of step h starting at $z = (j-1)h$. The initial pulse $A(0, t)$ enters the medium of length L . The length is divided into $s_L=L/h$ steps of length h .

The iterative steps to produce field solution can be expressed as follows [76]:

1. Calculate the nonlinearity at the midpoint of the step: $\left\{ \exp \left(h\widehat{N}(i\omega) \right) A((j-1)h, t) \right\}$

2. Calculate the dispersion over step h in the frequency domain:

$$\left\{ \exp \left(h\widehat{D}(i\omega) \right) \mathcal{F} \left\{ \exp \left(h\widehat{N}(i\omega) \right) A((j-1)h, t) \right\} \right\}$$

3. Calculate solution at $z=jh \Rightarrow$

$$A(jh, t) \approx \mathcal{F}^{-1} \left\{ \exp \left(h\widehat{D}(i\omega) \right) \mathcal{F} \left\{ \exp \left(h\widehat{N}(i\omega) \right) A((j-1)h, t) \right\} \right\}$$

4. Repeat iterations till $z=s_L, h=L$ where L is the length of the fiber, for the final solution $A(L, t)$.

The fast computation speed of SSFM compared to other methods can be related to:

- Avoiding any numerical derivatives by calculation the dispersion in the frequency domain.
- Using Fast Fourier Transform (FFT) to go between the frequency and time domains.
- Elimination of carrier frequency from the derivation of the NLSE.

Other methods are reported to solve NLSE such as inverse scattering method and frequency domain technique known as total field transformation. These two methods are difficult to be numerically implemented and need significant computation capabilities [61].

4.3. Numerical Simulations

In this section, the numerical analysis of the SML fiber laser with an amplitude modulated envelope is presented. The output pulses shape changes with pumping power. Every scheme will be investigated to understand the mode-locking mechanism of the laser. The model simulates fiber laser cavity built with 10 μ m core fibers. The active fiber has 10 m length with an equivalent 100 ns cavity round trip time. Both cavity FBGs has bandwidth of 0.2-0.25 nm and OC reflectivity of 50%.

4.3.1. Pulsing origin

In order to study the laser self pulsing, the output is characterized at different pumping levels. The self-pulsing as observed in experiment starts with relaxation oscillations as shown in Figure 4.3. The simulation and the estimation of the relaxation oscillation frequency using fiber laser rate equations are shown in Appendix B.

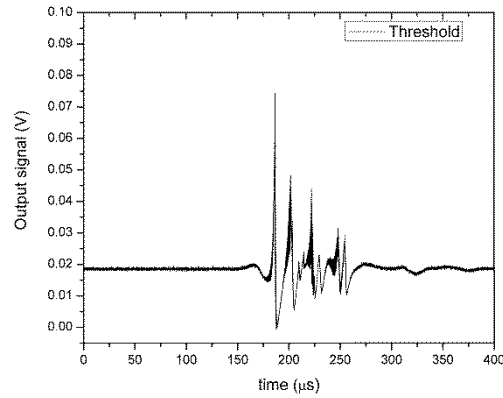


Figure 4.3: Measured pulsing start-up near threshold with relaxation oscillation structure.

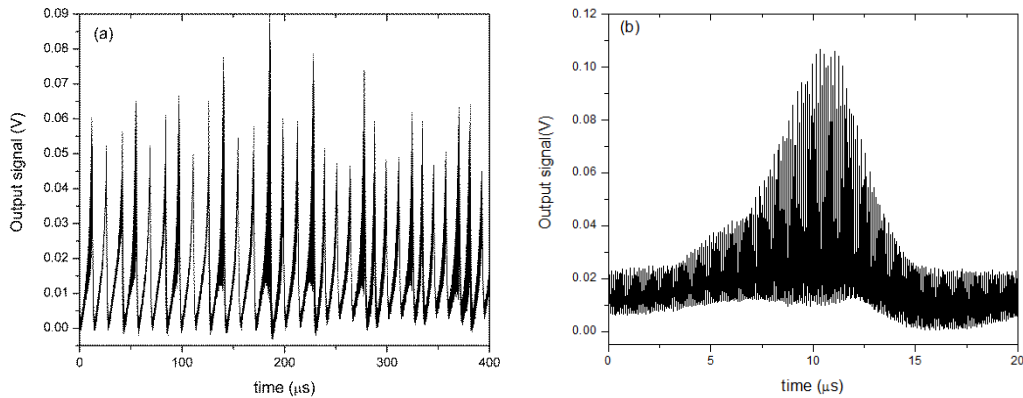


Figure 4.4: (a) Oscilloscope trace for Self-Q switching pulses at low pumping power near threshold. (b) Details of single Q-switched pulse.

As observed in experiment, by increasing the pumping power, the laser output delivers sustained Q-switched pulses as shown in Figure 4.4(a). SML pulses evolve underneath these Q-switched pulses as shown in Figure 4.4(b). The SML pulses has a repetition rate of 10 MHz which matches $L=10$ m cavity mode separation $c(2nL)^{-1}$. With further increasing pumping power, the Q-switching repetition rate increases until it reaches a threshold from which only SML pulses are

distinguished. Examples for evolution of Q-switch like pulses and mode-locked pulses at different pumping levels are shown through Figure 4.5 (a)-(h). These plots are measured from 5 μm core module with an active fiber length of 5m (round trip time of 50 ns) and output coupler reflectivity of 46%. Similar pulse evolutions are observed for 10 μm core modules.

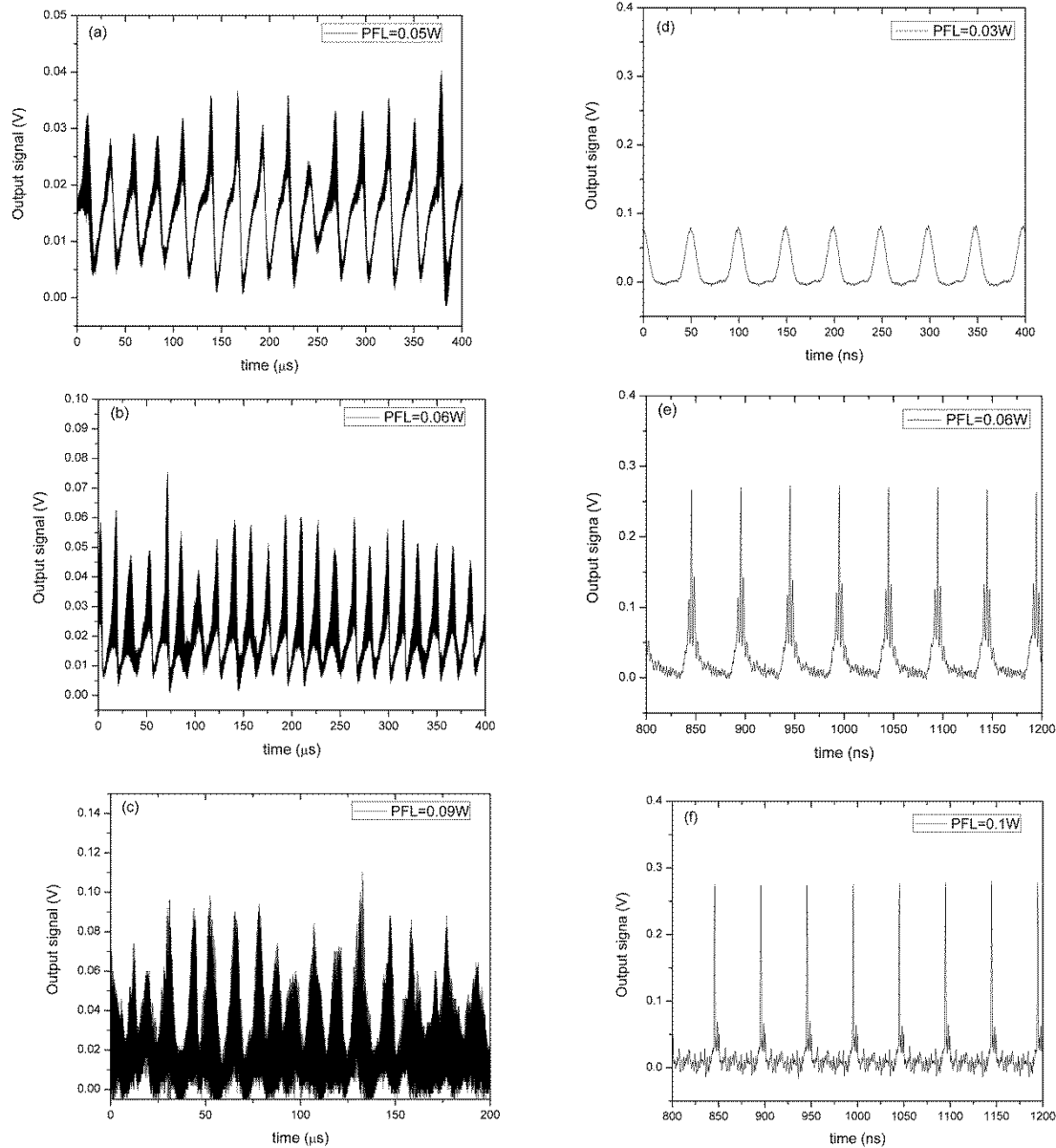


Figure 4.5: Measurement of 5 μm core fiber laser module with 5 m active fiber and R=46% (a)-(c) Evolution of Q-switched like pulses (d)-(f) Evolution of SML pulses underneath Q-switched pulses.

4.3.2. Mode-locked Pulses Simulation

A NLSE-based theoretical model is developed in the following section to explain the mode-locking with a modulated amplitude envelope.

4.3.2.1. Simulation Model

The fiber laser cavity (Figure 4.6(a)) is divided into the sections and modeled as shown in Figure 4.6(b). The proposed simulation model considers the following:

1. NLSE is used to simulate the laser cavity
2. Two sections of single mode fiber (SMF) are included in the cavity modelling (on which FBG is written).
3. Any FBG in the laser represents Spectral filtering component.
4. The OC-FBG acts also as an output coupler.

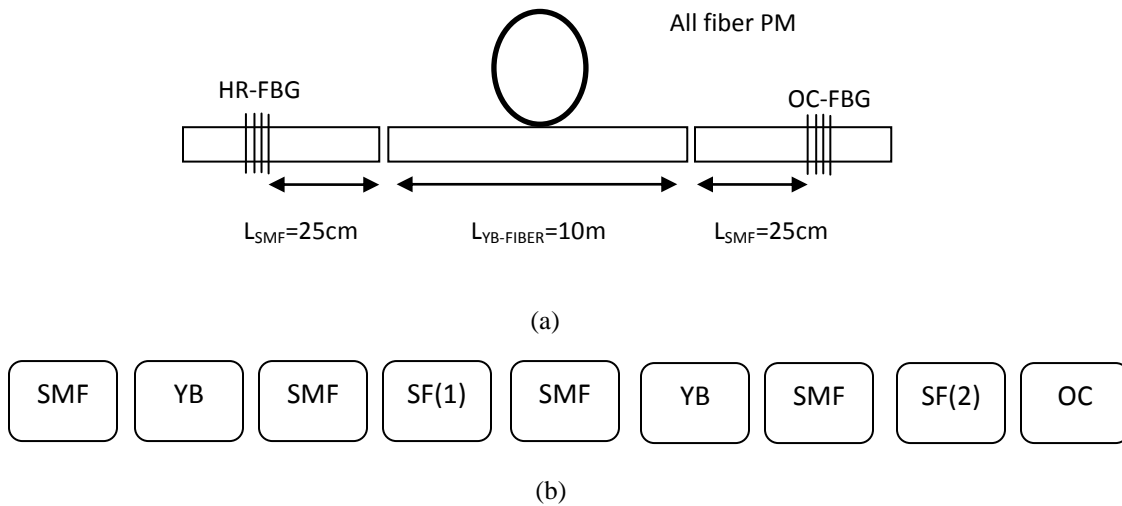


Figure 4.6 : (a) Fiber laser schematic (b) Simulation model schematic; where SF (1) is the HR-FBG and SF (2) is the OC-FBG.

Following the approach in [77, 78], the operator, C , describing the round trip for the linear cavity can be represented as follows:

$$C = F G e^{i\varphi} F R_{HR} F G e^{i\varphi} F R_{OC} \quad (4.21)$$

Where, F and G represent the propagation through the SMF and the gain fiber. φ is a cavity related phase shift. R_{HR} and R_{OC} are the reflectivity of the HR and OC FBGs respectively. Each component model will be explained as follows:

(a) Fiber Sections

In the simulation, the pulse propagation through SMF and gain fiber represented by F and G are solved by NLSE [shown as Eq. (4.16)] using a split-step Fourier method. The gain saturation model is given in Eq. (4.22), where g_0 is the small signal gain coefficient (related to dopant concentration), E is the instantaneous pulse energy and E_{sat} is the gain saturation energy which is pump-power dependent. For the non-gain single mode fiber, saturated gain factor g is set to zero to eliminate the influence of the gain effect.

$$g = \frac{g_0}{1 + \frac{E}{E_{sat}}} \text{ and } T_2 = \frac{2}{\Delta\omega_g} \quad (4.22)$$

If two polarizations are included in the cavity simulation, NLSE is replaced by CNLSE. The model assumes equal gain for the two polarizations and the high Birefringence fiber Jones matrix [79] is given as:

$$T = M_{Hi-Bi} = \begin{pmatrix} e^{-i(2\pi \cdot \Delta n \cdot L)/\lambda} & 0 \\ 0 & e^{i(2\pi \cdot \Delta n \cdot L)/\lambda} \end{pmatrix} \quad (4.23)$$

Where L is the length of the fiber, Δn is the fiber birefringence and λ is the operating wavelength. Other components of the round-trip model like gain, saturable absorption, mirrors, etc., usually do not distinguish between the two polarization components. The output signal after gain fiber [80, 81] will be:

$$\begin{pmatrix} E_x^{out} \\ E_y^{out} \end{pmatrix} = \sqrt{G} * \begin{pmatrix} e^{-i(2\pi \cdot \Delta n \cdot L)/\lambda} & 0 \\ 0 & e^{i(2\pi \cdot \Delta n \cdot L)/\lambda} \end{pmatrix} * \begin{pmatrix} E_x^{in} \\ E_y^{in} \end{pmatrix} \quad (4.24)$$

Regarding the SSFM, the nonlinear operator should be changed to:

$$\widehat{N}_x = i\gamma(|A_x|^2 + 2/3|A_y|^2) \quad (4.25(a))$$

$$\widehat{N}_y = i\gamma(|A_y|^2 + 2/3|A_x|^2) \quad (4.25(b))$$

(b) Cavity phase shift component

The cavity phase shift, φ induced from the gain fiber section and represents the polarization rotation, is expressed as shown in Eq. (4.26).

$$\varphi = \varphi_L + \varphi_{NL} = \frac{-2\pi\Delta n L_{yb}}{\lambda_o} + \gamma_{Yb}L_{Yb}|A|^2 \quad (4.26)$$

where Δn is the birefringence of the PM fiber. L_{yb} and γ_{yb} are the length and nonlinear coefficient of the gain fiber respectively. λ_o is the center wavelength. The first term in Eq. (4.26) represents the linear birefringence of the PM fiber [82, 83] while the second is a nonlinear phase shift proportional to the intra-cavity field power. This term in the model is part of the pulse phase shift evolution and rotation that plays a major role in the performance of the SML laser.

If two polarizations are included in the cavity simulation, NLSE should be replaced by CNLSE. At such as case, a new cavity phase shift for each polarization will be introduced as:

$$\varphi_x = \frac{-2\pi\Delta n L_{yb}}{\lambda_o} + \gamma_{Yb}L_{Yb}(|A_x|^2 + 2/3|A_y|^2) \quad (4.27(a))$$

$$\varphi_y = \frac{2\pi\Delta n L_{yb}}{\lambda_o} + \gamma_{Yb}L_{Yb}(|A_y|^2 + 2/3|A_x|^2) \quad (4.27(b))$$

(c) FBG (Spectral filtering components and Output coupler)

Both HR-FBG (R_{HR}) and OC-FBG (R_{OC}), their reflectivity spectra are modeled with a Gaussian function with a bandwidth of 0.2 nm and center wavelength λ_o of 1064 nm. The output is taken at the 50% OC-FBG. The filter function is represented in frequency domain [80] as shown in Eq. (4.28). That is the reason to apply FFT for the input signal before applying to filter section. At the filter output, IFFT operation is applied to the output signal.

$$SF(f) = \exp\left(-2\ln 2 \frac{f^2}{\Delta f^2}\right) \quad (4.28)$$

where $SF(f)$ is the filter transfer function in frequency domain and Δf is the filter's 3dB bandwidth.

For the two polarization simulations, PM FBG will be modeled with a reflectivity matrix with two wavelengths [67, 68] and spectral filtering component as

$$\begin{pmatrix} A^{out}_x \\ A^{out}_y \end{pmatrix} = SF * \begin{pmatrix} r_1 & 0 \\ 0 & r_2 \end{pmatrix} * \begin{pmatrix} A^{in}_x \\ A^{in}_y \end{pmatrix} \quad (4.29)$$

r_1 and r_2 is the reflectivity of both PM FBG axes.

(d) Initialization Pulse

The simulation is initialized by small amplitude Gaussian pulse of FWHM of 1ns. For the two polarization simulation, two Gaussian pulses will be used to represent each polarization as shown in Eq. (4.30).

$$\begin{pmatrix} E^{ini}_x \\ E^{ini}_y \end{pmatrix} = \begin{pmatrix} E_x \exp\left(-\frac{t}{T_0}\right)^2 \\ E_y \exp\left(-\frac{t}{T_0}\right)^2 \end{pmatrix} \quad (4.30)$$

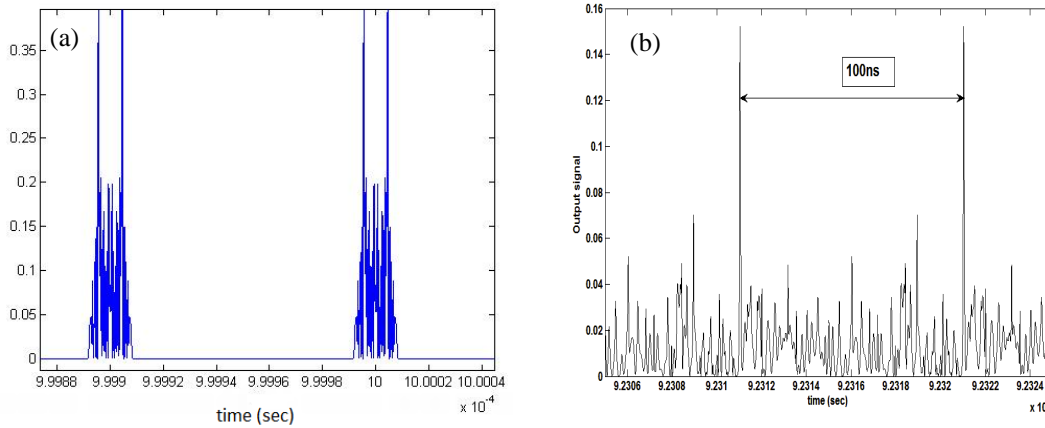
4.3.2.2. Simulation Parameters & Results

The numerical simulation starts with a 1 ns Gaussian pulse as an initial condition and we examine the output after 10000 round trips. In one round-trip, the propagation of the optical pulses is solved in every section of the laser. After one round-trip through the laser cavity, the resulted pulse from simulation was used as the input for the next round-trip calculation. The outcome results of the proposed model are studied at different conditions.

The model is first tested without adding the phase shift parameter to verify its role in pulse formation. The simulation output without and with this term is shown in Figure 4.7(a) and (b). The pulse shape is distorted without adding the phase shift component to the model. The envelope width at E_{sat} of 1 nJ is 72 μ s which is not in the same order of magnitude for the measurements at 1 W pump power. By increasing the saturation energy value, the envelope width at $E_{sat} = 2$ nJ is close to the envelope width at 1 W pumping level.

Table 4.1: Simulation parameters for NLSE-based model.

Gain fiber	SM fiber	FBGs
Fiber Length (L)=10 m	Fiber Length (L)=0.25 m	HR-FBG reflectivity (R_{HR})=0.99
2nd order dispersion (β_2)=0.024 ps ² /m	2nd order dispersion (β_2)=0.024 ps ² /m	OC-FBG reflectivity (R_{OC})=0.5
Nonlinear coefficient (γ)=0.0016 W ⁻¹ m ⁻¹	Nonlinear coefficient (γ)=0.0016 W ⁻¹ m ⁻¹	FBG 3dB BW ($\Delta\lambda_{3dB}$)=0.2 nm
Small signal gain (g_0)= 0.1 m ⁻¹ , Saturation energy (E_{sat})=2 nJ (Pump parameter) Gain bandwidth ($\Delta\omega_g$)= 45 nm	Small signal gain (g_0)=0	Center wavelength (λ_0)=1064 nm
Birefringence (Δn)=3 x10 ⁻⁴	Birefringence (Δn)=3 x10 ⁻⁴	-

**Figure 4.7:** Simulated output pulses (a) without phase shift component (b) with phase shift component.

Since the cavity has high PER, XPM effect is assumed to be small. SPM is only considered as the source of nonlinear phase shift in the simulation model. This assumption is verified by solving CNLE and including the field with two polarization components. By using the two polarization equations illustrated in Sec. 4.3.2.1, the model can be altered to accommodate two polarization simulations. The OC-FBG has 50% reflectivity for both axes. In simulation, one of the FBG axes will have a smaller reflectivity value as shown in Eq. (4.31) compared to the other

one. This is implemented to realize the wavelength matching condition, where the fast axis is matched with the slow axis of other PM-FBG in the simulation [83]. The PM FBGs reflectivity matrices are:

$$R_{HR} = \begin{pmatrix} 0.99 & 0 \\ 0 & 0.99 \end{pmatrix}, R_{OC} = \begin{pmatrix} 0.05 & 0 \\ 0 & 0.5 \end{pmatrix} \quad (4.31)$$

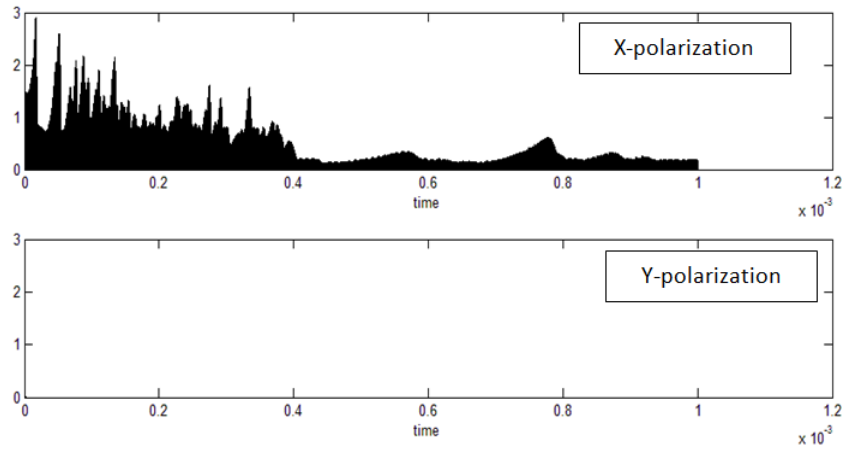


Figure 4.8: Two polarization simulation using CNLSE and PM FBG reflectivity matrices at $E_{sat}=2$ nJ.

The two polarizations simulation with CNLSE using the reflectivity values shown in Eq. (4.31); is shown in Figure 4.8. The y-polarization curve is presented to verify that the output is minimized at this polarization by incorporating the wavelength matching condition shown in Eq. (4.31). Thus the cavity selects one polarization only or the output is linearly polarized. With high PER and similar simulation, only one polarization will be considered in the simulation to reduce the computational time as shown in Figure 4.9(a)..

The simulation output acquires large amplitude variations for the first 4000 round trips (corresponding to time 0.4ms) as shown Figure 4.9(a). After that, the output is changed with some peaks of different amplitudes as shown in Figure 4.9(a).

By examining the details underneath the peak with highest amplitude, it shows mode-locked pulses of width 280 ps as presented in Figure 4.9(b). This matches experimental measurement of 260 ps at equivalent pump power.

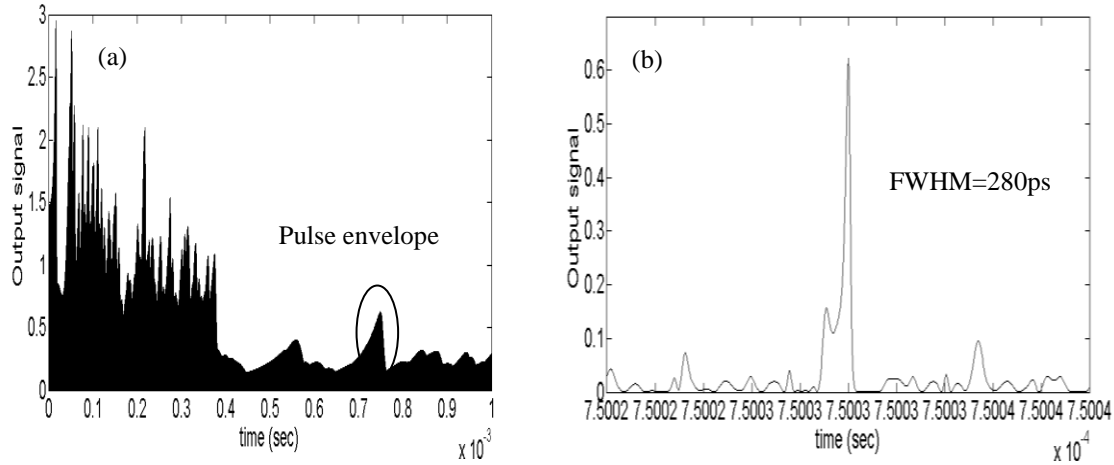


Figure 4.9: (a) Simulation output with phase shift component for $N=10000$ R.T and $E_{sat}=2$ nJ. (b) Single pulse plot underneath the marked envelope shown in Figure 4.9 (a).

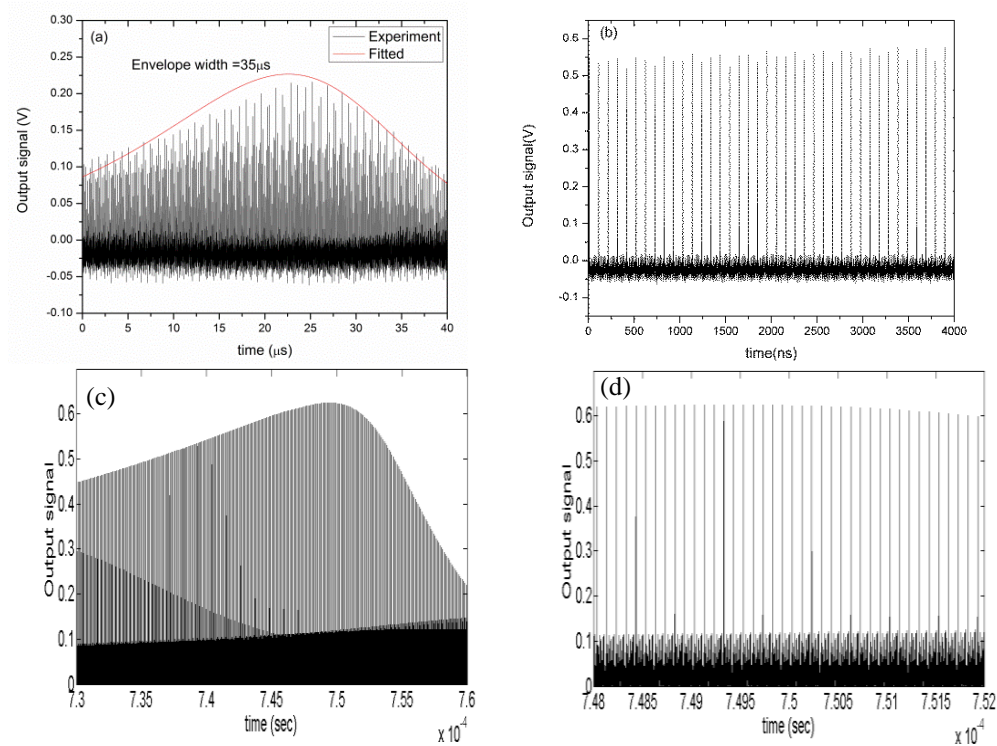


Figure 4.10: (a) Measured pulse envelope at $P_{pump}=1$ W (b) 4 μ s pulse train at $P_{pump}=1$ W (c) Simulated envelope at equivalent $P_{pump}=1$ W, $E_{sat}=2$ nJ (Envelope width=34 μ s). (d) 4 μ s simulated pulse train at equivalent $P_{pump}=1$ W, $E_{sat}=2$ nJ.

The simulated pulse train has an envelope width of $34\mu\text{s}$ which matches the $35\mu\text{s}$ width measured at 1 W pump power. Both measured and simulated outputs are shown in Figure 4.10(a)-(d). As noted in Figure 4.10, differences between simulated and measured envelope shape can be accounted for not considering backward direction propagation and spatial gain distribution in the simulation. This can be a direction for future work to extend the proposed model.

The pump-dependent parameter (E_{sat}) is varied in the simulation to test the envelope width as a function of pump power. In the simulation, E_{sat} has a value of 2 nJ which is considered to be equivalent to 1 W pumping power in the experiment. After which, the saturation energy, E_{sat} is varied in the same pace to study the effect of changing pump power. Simulation outputs at equivalent pumping powers are shown in Figure 4.11(a)-(c).

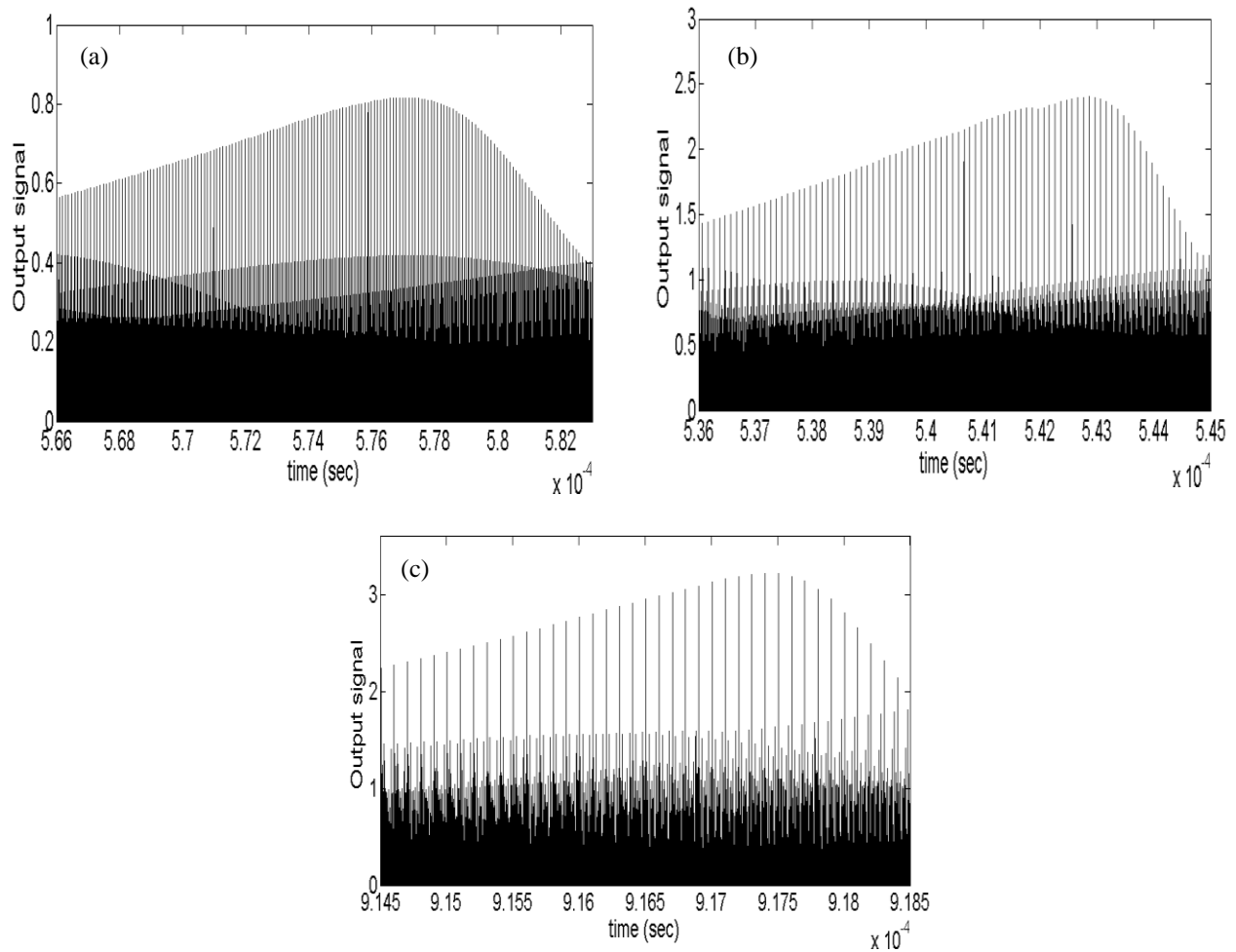


Figure 4.11: Simulated envelope at equivalent (a) $P_{\text{pump}}=2.5\text{W}$, $E_{\text{sat}}=4\text{nJ}$ (b) $P_{\text{pump}}=6\text{W}$, $E_{\text{sat}}=12\text{nJ}$ (c) $P_{\text{pump}}=8\text{W}$, $E_{\text{sat}}=16\text{nJ}$.

At 8 W pumping levels, the simulated output has an envelope width of 2.6 μs (Figure 4.11 (c)) and a single pulse width of 88 ps compared to the measured 55 ps as shown in Figure 4.12 (a). The simulated envelope width matches in same order of magnitude the experimental ones at different pumping levels as presented in Figure 4.12(b). From simulation, the envelope width reaches a maximum width of 72 μs at $E_{\text{sat}}=1\text{nJ}$ (0.5W pumping power). At further lower pumping level the simulated envelope width is reduced.

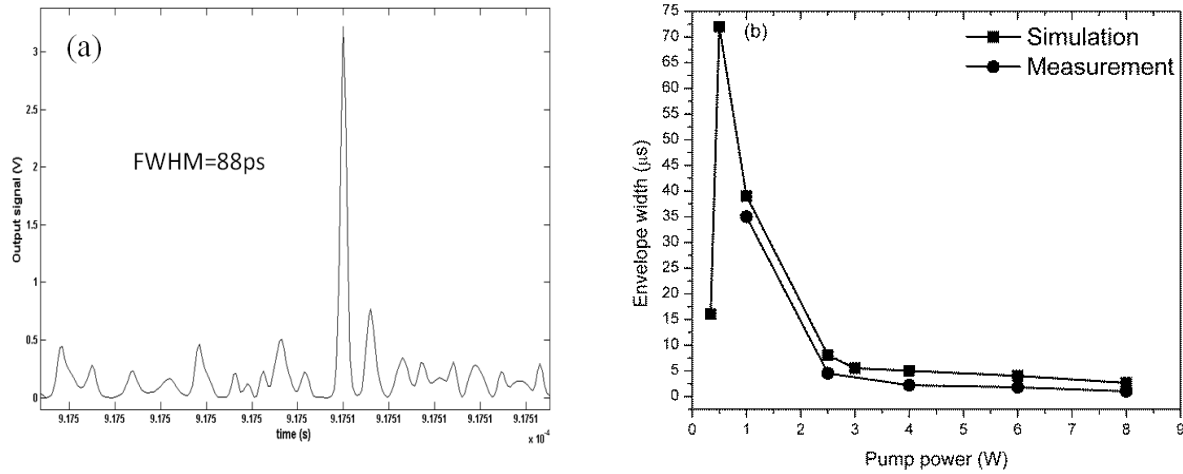


Figure 4.12: (a) Simulated single pulse width at equivalent $P_{\text{pump}}=8$ W, $E_{\text{sat}}=16$ nJ. (b) Measured and Simulated envelope widths versus pumping power.

In the simulation work, several parameters had been changed to explain and understand the envelope phenomena. First, a factor, K , is introduced to the nonlinear phase shift term as shown in Eq. (4.32). This factor, K is changed while fixing all other simulation parameters. The envelope width broaden by decreasing, the factor, K , as shown in Figure 4.13, thus decreasing nonlinear phase shift in the cavity.

$$\varphi_{NL} + \varphi_L = K \gamma_{YB} L_{ybfiber} |E|^2 - \frac{2 \pi \Delta n L_{ybfiber}}{\lambda c} \quad (4.32)$$

This outcome is verified experimentally as broader envelope widths are measured at low power levels. Another way to reduce the nonlinear phase shift and thus broaden the pulse envelope is to use larger core area fibers. This is also proven experimentally with broader envelope widths using 10 μm core fibers compared to 5 μm ones.

Second, the PM-FBGs can have a maximum bandwidth of 0.2-0.24 nm. However both HR –FBG and OC-FBG, bandwidths were also varied to study the effect of spectral filtering bandwidth on the envelope. By increasing the FBGs bandwidths in the range from 5-10 nm, the envelope width is broadened and the pulse amplitude modulation is less dominant. This simulation can point out the role of narrow FBG bandwidth on envelope formation. Other cavity parameters such as the length of the gain fiber, OC-FBG reflectivity effect can be also varied and studied numerically.

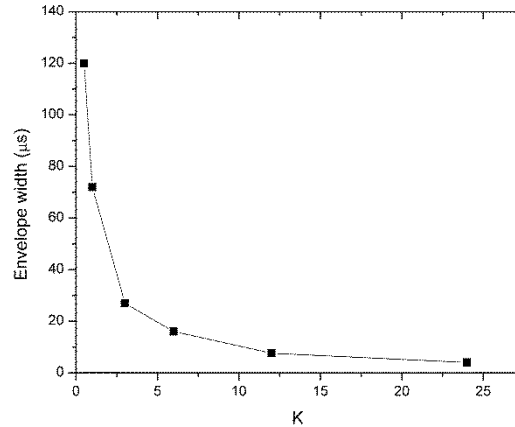


Figure 4.13: Envelope width versus phase factor (K).

4.4. Discussions: Mode-locking Mechanism

The mode-locking mechanism for the proposed laser can be explained using NPR. The laser is designed such that PM-FBG pair selects one polarization which is amplified by the cavity. However, a small component of the other orthogonal polarization can also evolve inside the cavity. The walk-off between the two orthogonal polarizations accumulates while propagating along the cavity. Thus the propagating light will be elliptically polarized and its rotation becomes intensity dependent. When the elliptically polarized light reaches the OC-FBG, the light component aligned with fast axis will only pass it. Thus the laser output is linearly polarized.

The PM-FBG pair in the laser cavity acts as a polarizer through which intensity-dependent rotation is transformed into intensity dependent transmission. This serves as a fast artificial SA and generates mode-locked output pulses [84-86].

Yet, the induced high linear and nonlinear phase shift doesn't help to fully retrieve the pulse after one round trip. The cavity modes are not perfectly locked and the generated mode-locked pulses amplitude is modulated with a microsecond envelope that varies with pump power.

Chapter 5. CW Linearly Polarized ALL-Fiber Laser Sources

5.1. Introduction

High power CW fiber lasers with linearly polarized output are essential for many applications, such as Second Harmonic Generation (SHG), polarized laser beam combining, and interferometer sensing. However, developing such lasers with all-fiber structure, narrow linewidth and high Polarization Extinction Ratio (PER) is a challenge. There are several fiber laser designs reported to have linearly polarized output. Liu et al. reported a linearly-polarized fiber laser with a PER of 17-20 dB using tightly-coiled high-birefringence fiber [87]. Despite its success in achieving a high output power of 405 W, its 1.9 nm linewidth is too broad for SHG. Li et al. reported a high power fiber laser using a single-polarization fiber from Corning for polarization selection and achieved 17-20 dB of PER [88]. Nevertheless, the lasers reported in [87, 88] used dichroic mirrors to separate pump and lasing wavelengths and bulk optics to couple the light in and out of the gain fiber. Therefore they were not all-fiber designs.

An all-fiber laser is designed using a single-polarization fiber for polarization selection and a fiber Bragg grating (FBG) for wavelength selection. This is accomplished by an FBG inscribed on a single polarization (SP) fiber as a high reflection mirror and another piece of the same fiber spliced to the active fiber as an output coupler as shown in Figure 5.1. A PM single-mode Yb-doped double-cladding fiber was used as an active fiber. A narrow linewidth of 0.054 nm, high PER of 28 dB at output power of 1.7 W were obtained [89].

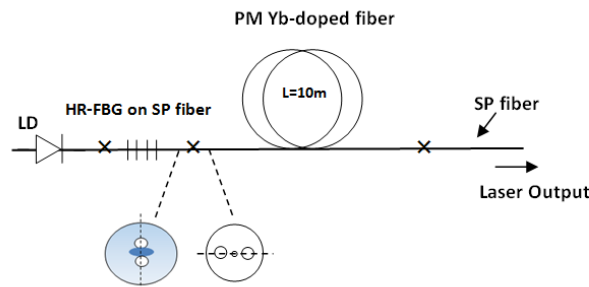


Figure 5.1: A schematic diagram of the linearly polarized fiber laser using SP fiber in 1 μm band [89].

Another compact fiber laser with a linearly polarized output in the C-band is also developed. This is implemented by replacing the PM Yb-doped active fiber with a PM Er/Yb one in the laser schematic shown in Figure 5.1. The linearly polarized laser achieved maximum output power of 1.5 W in the 1.5 μm band. Also it preserves narrow line width of 0.004nm, high SNR of 60 dB and high PER of 25 dB. The lasers using SP fiber acquire high extinction ratio, high optical SNR and narrow line width operation. However the shape mismatching between the elliptic core of the single-polarization fiber and the circular core of the gain fiber caused the light to leak at the splicing point and thereby, limiting the output power scale-up.

Shirakawa et al. pioneered a new fiber laser design for linearly polarized output using two FBGs made on polarization maintaining (PM) fiber with the slow axis wavelength of one FBG matching the fast axis wavelength of the other FBG. The highly reflective FBG was spliced to the gain fiber with its axes aligned while the output coupler FBG was cross-spliced to the gain fiber. In that design only one polarization was selected in the cavity [90]. The laser achieved 8 W of output power and 18 dB of PER. The main drawback of the laser was the requirement of a temperature controller to keep the two wavelengths of FBGs aligned within the narrow bandwidth of the FBGs. The PM FBG cavity design is improved by fabricating the highly reflective FBG with a top-flat, almost rectangular-shaped reflection spectrum. The wavelength of the output coupler FBG on the slow axis matched a highly reflective FBG on the fast axis within 30 pm to ensure 20 dB isolation between two polarizations [91]. As a result, the laser achieved single-polarized output of 20 W, a linewidth of 0.22 nm and a PER of 23 dB with no temperature controlling required. Recently, a similar structure with output power of 100 W at 1120 nm with a PER of 15 dB and a linewidth of 0.21 nm is presented in [92].

While one motivation is to increase the output power of the linearly-polarized output, the other is to design the fiber laser with dual wavelength and single-polarization output. Dual-wavelength fiber lasers also have many interesting applications such as differential frequency generation (DFG) for mid-infrared wavelength which is critical for pollutant chemical detections. In [93], the laser output with two orthogonally polarized wavelengths is realized by matching the wavelengths of two PM-FBGs. Though this technique delivers a narrow linewidth of 0.01 nm and high PER of 25 dB, the maximum wavelength separation is no more than 0.35 nm, limited

by the birefringence of the PM-fiber. In addition, the adjustment of a polarization controller is required to match the wavelengths of FBGs in order to achieve the dual wavelength operation. In [94], a dual wavelength operation is achieved with a maximum tunable separation of 83 nm using two bulk gratings and half wave-plates. An output with a 0.05 nm line width and 20 dB PER were obtained. In [95], a dual wavelength operation with 13 nm separation is obtained in an all-fiber structure by applying compression and tension to the two FBGs used simultaneously with a cantilever beam and translation stage. All the lasers in [93-95] operate in the 1 μm or 1.5 μm band. In [96], a dual wavelength laser operating at 1 μm and 1.5 μm simultaneously is reported using Er/Yb co-doped fiber. The laser output is single polarized with 0.1 nm bandwidth but the output power is limited to 60 mW. The adjustment of bulk optic components is needed to realize the dual wavelength operation.

The above review clearly shows that it is still a challenge to design a stable dual wavelength all-fiber laser with wide wavelength spacing and single-polarized output. In the following section; a compact, stable dual wavelength all-fiber laser simultaneously lasing at 1 μm and 1.5 μm wavelengths is presented. The proposed fiber laser is a novel demonstration of a dual-wavelength fiber-based source, with a fundamental wavelength interval as far as about 500 nm in an all-fiber configuration.

5.2. Dual Wavelength all-PM Fiber Laser

5.2.1. Experimental setup

The schematic diagram of the fiber laser, with all fiber connections fusion spliced, is shown in Figure 5.2. An 8.5 W diode laser at 975 nm with a multimode fiber output was used as a pump source. A PM single-mode Er/Yb co-doped double-cladding fiber of 2 m in length, with a mode field diameter of 6.7 μm and an NA of 0.18, was used as an active fiber (Nufern: PM-EYDF-6/125). This fiber has an Er doping concentration of $N_{\text{Er}} = 2.42819 \times 10^{25} \text{ m}^{-3}$ and Yb doping concentration of $N_{\text{Yb}} = 3.37 \times 10^{26} \text{ m}^{-3}$ respectively (data from the manufacturer) The laser diode was spliced to a low pass filter which passes only the pump wavelength and block the longer wavelength ASE or spontaneously lasing that could burn the laser diode. Although the filter introduced ~7% loss to the pump power, its use is necessary to protect the pump diode from damage.

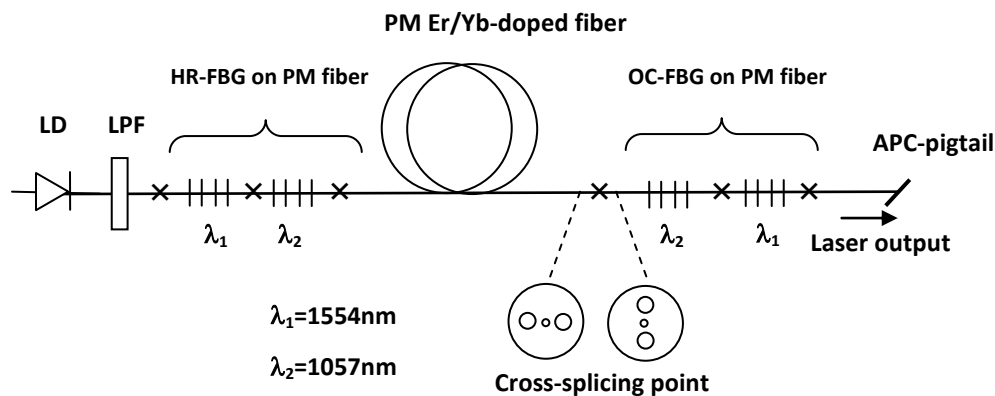


Figure 5.2: A schematic diagram of the dual wavelength linearly polarized Er/Yb-doped fiber laser.

To achieve wavelength and polarization selections, two FBG pairs were fabricated at 1057 nm and 1554 nm respectively, on a PM double-clad fiber with a core diameter of 5 μm and an NA of 0.12, (Nufern: 1060-GDF-5/130). For both wavelengths, FBG pairs were designed such that the slow axis wavelength of output coupler (OC) matched the fast axis wavelength of the corresponding highly reflective (HR) FBGs within 30 pm. FBG pair spectra designed at 1057 nm wavelength are shown in Figure 5.3 with a flat-top and almost rectangular shape for highly reflective FBG. A similar design was used for 1554 nm FBG pair (not shown). The fast and slow axis FBGs are separated by 0.26 nm due to the birefringence of the fiber.

The two FBGs spliced between the laser diode and the active fiber had highly reflectivity of >99% and fast axes wavelengths at 1554.3 nm and 1057.7 nm respectively. The HR-FBGs have an almost rectangular shaped spectrum with 23dB isolation between its two polarizations. This high isolation is a key factor to realize a laser output with high PER. Both highly reflective FBGs were co-spliced to the active fiber, where both PM fibers had their fast axes aligned parallel to each other. The other end of the active fiber was spliced consecutively to two FBGs as OCs with reflectivity of about 10%. The OC-FBGs were cross-spliced to the active fiber, where their slow axes were aligned perpendicular to the slow axis of the active fiber as shown in Figure 5.2. The fiber cavity thus designed selects both wavelength and polarization state. The pigtail of the output coupler was spliced to an angle-polished connector to prevent the reflections from the fiber end. The laser output power was measured using a laser power meter with an integrated

sphere (Thorlabs, Model S145C). A polarizing cube beam splitter (Thorlabs with an extinction ratio of 1000:1) was used to measure the polarization extinction ratio.

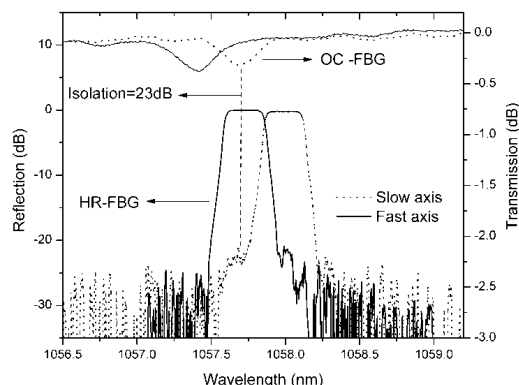


Figure 5.3: Fiber Bragg Grating spectra at 1057 nm show the matching fast and slow axes wavelengths.

5.2.2. Results & Discussions

The laser output parameters, such as its output power, linewidth, PER and temperature tunability are presented as follows. The output power as a function of the diode pump power is shown in Figure 5.4. Since two laser wavelengths emitted from the fiber are collinear, they need to be spatially separated for power measurement. A bulk grating of 180 lines/mm was used which separated the laser beams of 1554 nm and 1057 nm by 5 degrees. The laser output has a maximum output power of 0.67 W and 0.65 W for both 1554 nm and 1057 nm wavelengths respectively at 5.3 W pumping power.

It can be seen from Figure 5.4 that 1057 nm laser power increases rapidly with pump power with a threshold almost 2.5 times higher than that of the 1554 nm emission. This can be explained as follows: the active fiber is optimized so that erbium ions are primarily pumped via energy transfer from ytterbium, so only 1554 nm wavelength lases at low pumping power. At a higher pumping level, a larger number of Yb ions are excited until a level is reached, at which 1057 nm wavelength starts lasing [96]. Above this level, the energy transfer between Yb and Er ions will be less efficient and 1057 nm output power will be increasing rapidly with further increasing pump power. Since the active fiber is optimized for C-band operation, the 1057 nm cavity was made as an inner cavity to reduce its cavity loss in order and better match the power of 1554 nm laser output.

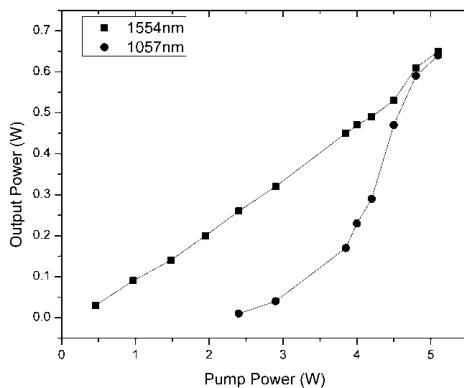


Figure 5.4: Output power versus pump power for both wavelengths of 1554 nm and 1057 nm.

To measure the PER, the laser output pigtail was mounted on a rotating stage and collimated into a parallel beam by a lens. Then the laser polarization was aligned in the horizontal direction and transmitted through a polarization cubic beam splitter. The power of the transmitted beam and the reflected beam were measured respectively when the laser output pigtail was rotated to maximize the power difference. The PER of 200:1 or 23 dB was obtained from the ratio of the two power readings. This high extinction ratio can be attributed to the high isolation between the slow and the fast axes wavelengths of the FBG. Figure 5.5(a) clearly shows that a high extinction ratio was achieved over the whole power range. The stability of the output power was measured for 60 minutes; the power variation of less than $\pm 2.0\%$ was found at 1.3 W.

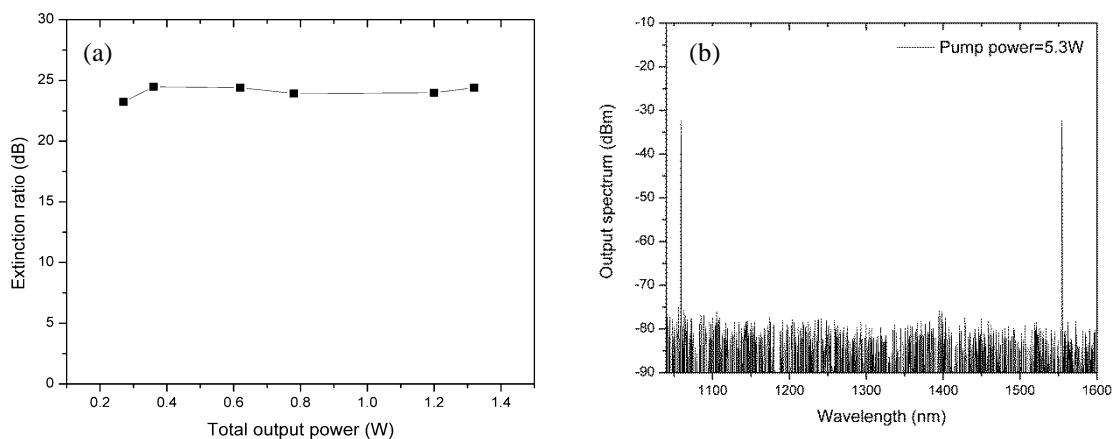


Figure 5.5: (a) Extinction ratio in dB as a function of the laser total output power (b) Laser output spectrum at 5.3 W pump powers.

A narrow bandwidth of the laser output is essential for efficient second harmonic and mid-IR generation using non-linear crystals or periodically poled MgO: LiNbO₃ (PPLN). The output spectrum was measured using an ANDO AO6317 optical spectrum analyzer, and the laser emissions at both 1057.7 nm and 1554.3 nm are depicted in Figure 5.5 (b). Both laser emissions achieved a narrow bandwidth of 26 pm at full-width half-maximum (FWHM) with an optical SNR of over 60dB by separately measuring each band as shown in Figure 5.6.

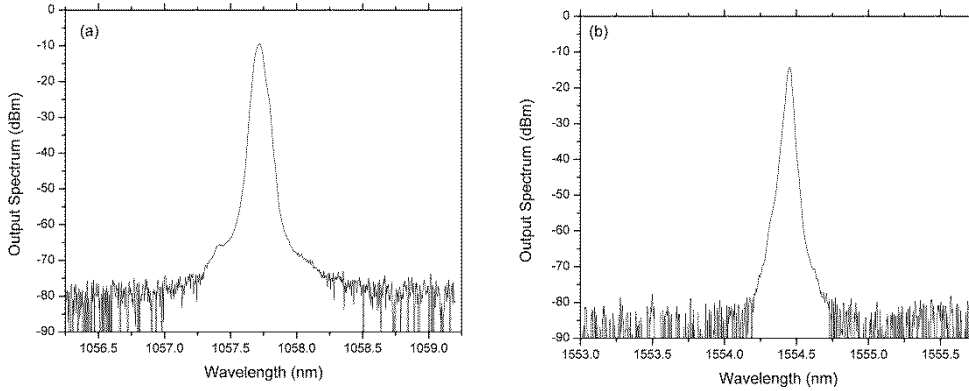


Figure 5.6: Output spectrum at (a) 1057 nm wavelength and (b) 1554 nm wavelength

To characterize the tuning capability of the dual wavelength laser as a pumping source for mid-IR generation, the output wavelength was tuned by varying the temperature of the 1057 nm FBG pair. The output wavelength can be tuned over 0.6 nm bandwidth by varying the temperature from 25.3°C to 96.1°C as shown in Figure 5.7(a).

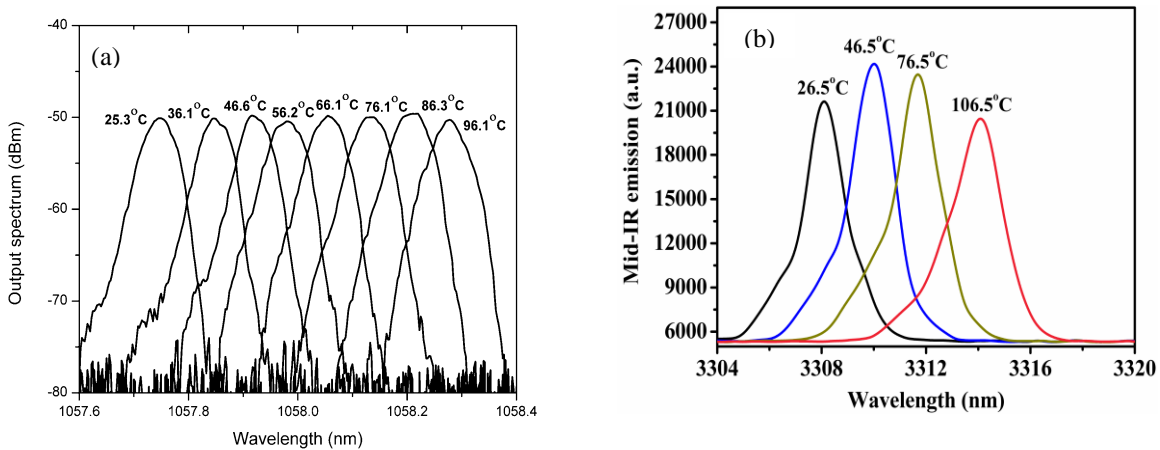


Figure 5.7: Output spectrum tunability by varying temperature of 1057 nm FBG pair (b) Mid-IR spectra tuned at different temperature.

The proposed dual wavelength fiber laser was implemented successfully as a compact tunable pumping DFG source for 3.3 μm mid-IR generation (Ref. [2] in publications list). The laser successfully generates mid-IR emission of 0.23 mW at 3371 nm. By tuning the temperature of 1057 nm FBG pair from 26.5 to 106.5°C, the wavelength of the mid-IR emission could be continuously tuned by ~ 6 nm as shown in Figure 5.7(b), which is sufficient to cover several vibration-rotational absorption lines for methane detection.

This design is well-suited for a compact fiber-based DFG pumping source for mid-IR generation. It can replace conventional DFG-pumping technique using two separate fiber lasers as recently reported in [54-57]. The dual-wavelength emissions from the same cavity and gain fiber offer more stable output and smaller foot print.

Chapter 6. Conclusions and Future Directions

6.1. Conclusions

This thesis presented the design and development of two novel high power linearly polarized all-fiber cavity lasers. Both lasers have a linear cavity structure with all components made of PM fibers. They use specially designed FBG pair inscribed on PM fiber to form the laser cavity. The two matching FBGs are designed to provide both wavelength and polarization selection. The improved PM FBG pair design with high isolation is a key component to realize a laser output with high PER.

The following can be concluded, based on extensive experimental and numerical analyses presented in this thesis:

(A) Mode-locked all-fiber laser:

- Experimental work shows that this design could generate linearly polarized mode locked pulses in the 1 μ m region with an extinction ratio up to 30 dB. Mode-locking is achieved with a compact design that has neither free space nor adjustable components. In addition, double-clad fibers and cladding pumping technique allow the generation of picosecond mode-locked pulses with high average output power up to 5.5W. The mode locked pulses showed a modulated amplitude envelope with increasing pumping power.
- The factors that control the mode locking operation were identified by detailed experimental parametric study. Shorter pulse widths and broader envelope widths were realized with longer active fiber and high output coupler reflectivity.
- A novel theoretical model was developed and implemented to conduct numerical simulations that study self-mode locking in an all-PM fiber laser with a Fabry-Perot configuration. The output pulses are modulated with an envelope which is studied by solving NLSE with additional phase shift term. The phase shift represents SPM which was proven to play an important role in pulse-shaping and formation. With the proposed

approach, the simulation succeeds to explain and retrieve the mode-locked pulse envelope at different pumping levels. The developed model can be also used to simulate relevant linear fiber laser cavities with pulsed output.

- Further scaling for pulse energy and average power is implemented by building and adding an amplifier stage. The laser acquires mode-locked pulses with high average power pulse up to 21W. Though modulated with an envelope, it shows good capabilities in metal marking and cutting when combined with an amplifier.
- Pumping laser diodes with a pulsed current source was proven experimentally to stabilize the acquired mode-locked pulses. The SML pulses were regulated underneath Q-switched pulse train with kHz repetition rates. This approach helps to generate mode-locked pulses with energy of 50-130 nJ and peak power of 0.5-1.1 kW.

(B) CW all-fiber, dual-wavelength laser:

Another design of dual-wavelength emission with a 500 nm separation and 1.3W output power was demonstrated. The CW laser used two pairs of the specially designed FBG to achieve a linearly polarized output with a high extinction ratio of 23 dB. The laser emission has an excellent SNR of over 60dB and a narrow bandwidth of 26 pm at 1057 nm and 1554 nm respectively. This design is well-suited for a compact fiber-based DFG pumping source for mid-IR generation. The dual-wavelength emission from the same cavity and gain fiber offer more stable output and compact packaging.

Though the dual wavelength laser shares some similarities in structure with the mode-locked laser, it conveys a CW output. This difference is proved by experimental measurements. Different reasons can explain the difference in output nature. One reason is that the dual wavelength laser setup has two cavities to generate the two wavelengths. Each wavelength sees different cavity round trip time. Even if the cavity setup can generate mode-locked pulses for single wavelength, these pulses will not be temporally overlapped and are not synchronized [97, 98]. With different dispersion and cavity losses at each wavelength, it is harder for the dual wavelength cavity to generate similar mode-locked pulses. Another reason, is that within the applied pumping region and given cavity parameters, nonlinear effects may not be strong enough and to mode-lock the output.

Investigating the possible operating conditions at which the dual wavelength laser can generate mode-locked pulses can be a part of future research.

6.2. Directions for Future Research

In continuation to the work presented in this thesis, the following research directions are proposed:

- Characterize the polarization-dependent gain for PM active fibers.
- Explore using PM FBGs to design circularly polarized all-fiber laser sources.
- Investigate the power leakage through the HR-FBG at high output power levels.
- Include backward-propagation direction and small signal gain spatial distribution as extension to the theoretical model.
- Develop polarized version for time dependent fiber laser rate equations.
- Improve output power level for dual-wavelength fiber laser by optimizing cavity design parameters and theoretical modeling.

Appendix. A: Effect of Instruments Bandwidth on Pulse Measurement

1. Estimating the minimum temporal response of measurement setup

The minimum pulse width (τ_{\min}) expected from a measurement setup can be calculated using Eq. (A.1) [99]. The bandwidths of all the measurement equipments should be included, i.e. scope, detectors and cables. The temporal response for each equipment is calculated using Eq.(2.5), and given the equipment bandwidth.

$$\tau_{\min} = \sqrt{\tau_{\text{oscilloscope}}^2 + \tau_{\text{detector response}}^2 + \tau_{\text{cables}}^2} \quad (\text{A.1})$$

2. Actual pulse width measurement

The measured pulse width is a convolution of the real optical pulse width, the detector impulse response, all electrical components response (scopes, cables and connectors) and sometimes any jitter noise [49]. In order to estimate the contributions of all above stated components, sum of square law technique can be used as shown in Eq.(A.2), from which real optical pulse width can be calculated.

$$\tau_{\text{measured}} = \sqrt{\tau_{\text{optical pulse}}^2 + \tau_{\text{photodiode}}^2 + \tau_{\text{electrical}}^2 + \tau_{\text{jitter}}^2} \quad (\text{A.2})$$

Where:

- τ_{measured} is the measured pulse width
- $\tau_{\text{optical pulse}}$ is the real pulse width
- $\tau_{\text{photodiode}}$ is the detector impulse response
- $\tau_{\text{electrical}}$ is the electrical equipment impulse response (oscilloscope and cable bandwidth).
- τ_{jitter} is the timing jitter noise.

For example, the measured output pulse width ($\tau_{measured}$) of 55 ps using a photodiode with impulse response ($\tau_{photodiode}$) of 10 ps and, 12GHz bandwidth oscilloscope ($\tau_{oscilloscope} = 34\text{ps}$) and 24GHz bandwidth of SMA cables and connectors ($\tau_{cables \ \& \ connectors} = 17\text{ps}$) has a real pulse width($\tau_{optical \ pulse}$) of 38 ps using Eq. (A.2) and considering zero timing jitter noise.

Appendix. B: Time Dependent Fiber Laser Rate Equations

The self-pulsing as observed in experiment starts with relaxation oscillations like structure as shown in Figure B.1 (b). A set of coupled time dependent steady-state equations shown through Eq. (B.1)-(B.4) are solved to estimate relaxation oscillation frequency [52]. P_p represents the pump while E_s^\pm is the signal in both forward and backward direction

$$\pm \frac{\partial P_p}{\partial z} + \frac{1}{v_g} \frac{\partial P_p}{\partial t} = \Gamma_p \{ \sigma_{ep} N_2 - \sigma_{ap} N_1 \} P_p - \alpha_p P_p \quad (B.1)$$

$$\pm \frac{\partial E_s^\pm}{\partial z} + \frac{1}{v_g} \frac{\partial E_s^\pm}{\partial t} = \Gamma_s / 2 \{ \sigma_{es} N_2 - \sigma_{as} N_1 \} E_s^\pm - \alpha_s / 2 E_s^\pm + f_{sp}^\pm + i\gamma \left(|E_s^\pm|^2 + 2 |E_s^\mp|^2 \right) E_s^\pm \quad (B.2)$$

$$\frac{\partial N_2}{\partial t} = -\frac{N_2}{\tau_{21}} - \frac{\lambda_p \Gamma_p}{hc A_{eff}} \{ \sigma_{ep} N_2 - \sigma_{ap} N_1 \} P_p - \frac{n_g \lambda_s \Gamma_s}{2hc Z_o} \{ \sigma_{es} N_2 - \sigma_{as} N_1 \} \{ |E_s^+|^2 + |E_s^-|^2 \} \quad (B.3)$$

$$N_1 = N - N_2, \quad f_{sp}^\pm = \frac{4 Z_o \Gamma_s \sigma_{es} h \nu N_2}{A_{eff} n} \quad (B.4)$$

Table B.1: Basic parameters used in fiber laser rate equations.

Parameter	Value	Parameter	Value
Pump Wavelength (λ_p)	975nm	Signal scattering loss (α_s)	0.005 m ⁻¹
Signal Wavelength (λ_s)	1064nm	YB upper state life time (τ_{YB})	850μs
Pump Absorption Cross section (σ_{ap})	25 x 10 ⁻²⁵	Doping concentration (N)	4.25 x 10 ²⁵ m ³
Pump Emission Cross section (σ_{ep})	25 x 10 ²⁵ m ⁻³	Effective core area (A_{eff})	7.854 e ⁻¹¹ m ²
Signal Absorption Cross section (σ_{ap})	0.01e-24 m ⁻³	Nonlinear coefficient (γ)	0
Signal Emission Cross section (σ_{ep})	0.35e-25 m ⁻³	Active fiber length (L)	10 m
Power fill factor for pump (Γ_p)	0.0064 ^{sc} / 0.0016 ^{dc}	High reflective FBG reflectivity (R_{HR})	99%
Power fill factor for signal (Γ_s)	0.85	Output coupler FBG reflectivity (R_{OC})	50%
Pump scattering loss (α_p)	0.006 m ⁻¹		

The model parameters used in rate equations are justified by matching both experimental and simulation output power levels as shown in Figure B.1 (a). The output power is calculated by time-independent rate equation presented in [100, 101]. The basic parameters for modelling Yb-doped active fiber for pumping wavelength of 975nm and lasing wavelength of 1064nm are listed in Table B.1. Both measured and simulated output has similar oscillating period of approximately $16 \mu\text{s}$.

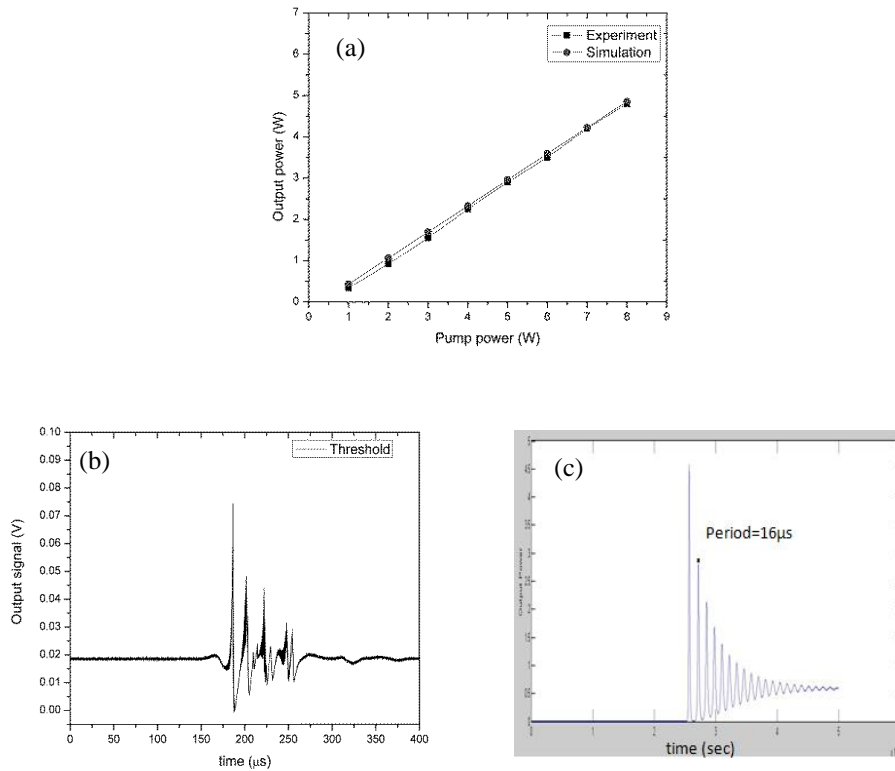


Figure B.1: (a) Measured and simulated output power versus pump power. (b) Measured pulsing start-up near threshold with relaxation oscillation like structure. (c) Simulated Relaxation oscillation.

Appendix. C: MATLAB Codes

The following MATLAB code is utilised for solving the developed model:

```

clear all;
close all;
clc;

global df
    global dt
    global fmax
T=50e-9;
%T=1000e-12;
%dt=0.0001*T;
dt=0.0005*T;
%dt=0.001*T;
fmax=1/dt/2;
df=1/(2*T);
fr=[-fmax:df:fmax];
t=-T:dt:T;
trt=100e-9;
dn=3e-4;
global A;
A=length(fr);

%%%%%%%%%%%%%%%%%%%%%%%%%%%%%%%%%%%%%%%%%%%%%%%%%%%%%%%%%%%%%%%%%%%%%%%%5
c=3*10^8;
lc=1064e-9;
dfr=(2*fmax)+1;
dlr=((dfr)/c)*(lc^2);
lr=linspace(lc-(dlr/2),lc+(dlr/2),A);

T0=1e-9;
E_in=0.001e-9;
global y
%y=sech(t./T0);
y=exp(-(1/2)*t.^2/T0^2);
    %y=wgn(A,1,-40,'real');
    %y=y';
global g0
g0=0.1;
global g;
gain_center_wl=1064e-9;
L_yb=10;
beta2_yb=0.024e-24;
%r_yb=0.0016;%
r_yb=0.0016;
global Es
Es=1*1e-9;
c=3*10^8;
dw_l=45e-9;
w_l=gain_center_wl;
k=2*pi/w_l;
global T_2
%T_2=2*pi/(k^2*(dw_l)*c);

```

```

T_2=((w_1^2)/pi)*(1/((dw_1)*c));
%T_2=100e-15;
global E_pulse
E_pulse=E_in;

beta2_SMF=0.024e-24;
r_SMF=0.0016;
%global P
evolution=[];
evolution2=[];
nx=1.45015;
ny=1.44985;
FACTOR=1;

N=10000;
for round_number=1:1:N
tt=t+(round_number*trt);
y=SMFP(beta2_SMF,r_SMF,0.25);

% Transmission=1-l_0./(1+(abs(y).^2)/P_sat);
% y=y.*(Transmission.^0.5);

y=yb_fiberP(beta2_yb,r_yb,L_yb);

%y=y*(exp(-1i*(2*pi*L_yb*dn/lc)));
%y=y*(exp(-1i*(2*pi*L_yb*nx/lc)));
%y=y*(exp(-1i*(2*pi*L_yb*nx/lc))).*(exp(1i*(r_yb*L_yb*((abs(y)).^2))));
%
y=y*(exp(1i*(2*pi*L_yb*dn/lc))).*(exp(1i*(FACTOR*r_yb*L_yb*((abs(y)).^2))));
%y=y.*(exp(1i*(FACTOR*r_yb*L_yb*((abs(y)).^2))));
%y=y.*(exp(1i*(FACTOR*r_yb*L_yb*((abs(y)).^2))));
y=SMFP(beta2_SMF,r_SMF,0.25);

y_inputfitler=fft(y);
lambda3dB=0.2e-9;
f3dB=lambda3dB*(2.649e20);
n=1;%%%%%%%%%fitler order
n=2*n;
K=(1:A)-1;
K(round(A/2+1:A))=K(round(A/2+1:A))-A;
K=K';
temp=log(sqrt(2))*(2/f3dB/dt/A)^n;
c=exp(-temp*(K.^2));
y_outputfitler=(y_inputfitler).*(exp(-temp*(K.^2)))';
y=ifft(y_outputfitler);

y=SMFP(beta2_SMF,r_SMF,0.25);
y=yb_fiberP(beta2_yb,r_yb,L_yb);
%y=y*(exp(-1i*(2*pi*L_yb*dn/lc)));
%y=y*(exp(-1i*(1*pi*L_yb*dn/lc)));
% y=y*(exp(-1i*(2*pi*L_yb*nx/lc)));
%y=y*(exp(-1i*(2*pi*L_yb*nx/lc))).*(exp(1i*(r_yb*L_yb*((abs(y)).^2))));
y=y*(exp(-1i*(2*pi*L_yb*dn/lc))).*(exp(1i*(FACTOR*r_yb*L_yb*((abs(y)).^2))));
%y=y.*(exp(1i*(FACTOR*r_yb*L_yb*((abs(y)).^2))));
% y=y.*(exp(1i*(FACTOR*r_yb*L_yb*((abs(y)).^2))));

```

```

y=SMFP(beta2_SMF,r_SMF,0.25);
%y_inputfitler=fft(y);
lambda3dB=0.2e-9;
f3dB=lambda3dB*(2.649e20);
n=1;%%%%%%%%
n=2*n;
K=(1:A)-1;
%K(A/2+1:A)=K(A/2+1:A)-A;
K(round(A/2+1:A))=K(round(A/2+1:A))-A;
K=K';
temp=log(sqrt(2))*(2/f3dB/dt/A)^n;
c=exp(-temp*(K.^2));
y_outputfitler=(y_inputfitler).*(exp(-temp*(K.^2)))';
y=ifft(y_outputfitler);

R=50/100;
y=y*((R)^0.5);
y1=y;
%
y11=(1*((1-R)/R))*((abs(y1)).^2);
if ~mod(round_number,1)

% subplot(2,1,1);
% plot(tt,y11,'k');
% xlabel('time');
% subplot(2,1,2);
% plot(tt,angle(y1));
% xlabel('time');
% hold on

% plot(tt,y11);
% xlabel('time');
% hold on

% evolution=[evolution;(1*((1-R)/R))*((abs(y1)).^2)];
%
% yfreq=fft(y1);
% I=yfreq.*conj(yfreq);
%
% Ifreq=((1*((1-R)/R))^(1)*(fftshift(abs((I)))));
% evolution2=[evolution2;Ifreq];
end
end

% IfreqdB=10*log10(Ifreq);
% IfreqdBmax=max(IfreqdB);
% Ifreqn=IfreqdB-IfreqdBmax;
% figure;
% plot(lr*1e9,Ifreqn);
% ylim([-80 0])
% xlabel('Wavelength (nm)');
% ylabel('Output signal (dB)');
% Ifreqnn=Ifreqn';
% lrnn=lr';

```

```

function y_out=yb_fiberP(beta2,r,L)
global P y df fmax T_2 Es E_pulse g0 dt g;

dz=0.01;
for z=0:dz:L
E_pulse=sum(abs(y).^2)*dt;
g=g0/(1+E_pulse/Es);
leff_dz=(1-exp(g*dz))/(-g);
phase=(abs(y)).^2*leff_dz*r;
y=y.*exp(i*phase);
xx=4*pi^2*[0:df:fmax].^2*((1*beta2)+i*T_2^2*(1*g));
yy=4*pi^2*[-fmax:df:-df].^2*((1*beta2)+i*T_2^2*(1*g));
%yy=4*pi^2*[-fmax:df:0].^2*(beta2+i*T_2^2*g);
phaseG=[xx,yy];
w=(fft(y).*exp(i*dz*phaseG/2));
y=ifft(w);
G=exp(dz*g);
y=(G^0.5)*y;
end

%y_out=y;

function y_out=SMFP(beta2,r,L)
global P y df fmax;

dz=0.01;
xx=4*pi^2*[0:df:fmax].^2*(beta2/1);
yy=4*pi^2*[-fmax:df:-df].^2*(beta2/1);
%yy=4*pi^2*[-fmax:df:0].^2*(beta2);
for z=0:dz:L
phase=(abs(y)).^2*dz*r;% SPM
y=y.*exp(i*phase);
%GVD+gain_dispersion
phaseG=[xx,yy];
w=(fft(y).*exp(i*dz*phaseG/2));
y=ifft(w);
end
y_out=y;

```

References

- [1] M. E. Fermann and I. Hartl, "Ultrafast fiber laser technology," *IEEE Journal of Selected Topics in Quantum Electronics*, vol. 15, pp. 191-206, 01, 2009.
- [2] D. D. Hudson, "Mode-locked fiber lasers: Development and application," 2009.
- [3] Jeff Hecht, "Fiber lasers: The state of the art," *Laser Focus World*, vol. 48, pp. 57, 2012.
- [4] D. Hull and J. Souders, "Fiber laser applications," *Report from OP-TEC: The National Center of Optics and Photonics Education*, 2011.
(www.optec.org/pdf/Fiber_Laser_Applications).
- [5] http://www.ipgphotonics.com/apps_notes.htm .
- [6] L. Quintino, A. Costa, R. Miranda, D. Yapp, V. Kumar and C. J. Kong, "Welding with high power fiber lasers - A preliminary study," *Materials and Design*, vol. 28, pp. 1231-1237, 2007.
- [7] J. Keller, "High-power fiber laser for defensive military applications is aim of Army research contract to Lockheed Martin.(ELECTRO OPTICS watch)," *Military & Aerospace Electronics*, vol. 22, pp. 43, 2011.
- [8] K. Kincade, "Fiber lasers find opportunities in medical applications," *Laser Focus World*, vol. 41, pp. 76, 2005.
- [9] SPI application notes: www.spilasers.it/medical_device_welding_with_fiber_lasers_.aspx.
- [10] H. Q. Chen "Cutting and Hole Drilling with a Fiber Laser Marker," *Advanced Battery Technology*, vol. 45, pp. 13, 2009.
- [11] D. Carlson, "Laser Processing of Solar Cells," *SPIE Solar Energy & Technology*, pp. 847302, Oct.2012.
- [12] A. V. Babushkin, D. V. Gapontsev, N. S. Platonov and V. P. Gapontsev, "Pulsed fiber laser with 30W output power at 532nm," *Lasers and Applications in Science and Engineering, International Society for Optics and Photonics*, 2006.
- [13] P. Rüdiger, *Encyclopedia of Laser Physics and Technology*, 1ed, Wiley-VCH, 2008.
- [14] L. Goldberg, J. Koplów, D. G. Lancaster, R. F. Curl and F. K. Tittel, "Mid-infrared difference-frequency generation source pumped by a 1.1-1.5- μ m dual-wavelength fiber amplifier for trace-gas detection," *Opt. Lett.*, vol. 23, pp. 1517-1519, 1998.
- [15] M. J. F. Digonnet, *Rare-earth-doped fiber lasers and amplifiers*, 2d ed, Marcel Dekker, vol. 25, 2001.

- [16] O. Svelto and D. C. Hanna, *Principles of Lasers*, Springer, 1998.
- [17] B. E. A. Saleh, M. C. Teich and B. R. Masters, "Fundamentals of Photonics, Second Edition," *John Wiley & Sons*, 1991.
- [18] Y. Wang and C. Xu, "Actively Q-switched fiber lasers: Switching dynamics and nonlinear processes," *Progress in Quantum Electronics*, vol. 31, pp. 131-216, 2007.
- [19] T. Schreiber, C. K. Nielsen, B. Ortac, J. Limpert and A. Tünnermann, "Microjoule-level all-polarization-maintaining femtosecond fiber source," *Opt. Lett.*, vol. 31, pp. 574-576, 2006.
- [20] B. C. Seung, H. Song, S. Gee and Y. K. Dug, "Self-starting passive mode-locked ytterbium fiber laser with variable pulse width," in *Fiber Lasers VII: Technology, Systems, and Applications*, 2010, pp. 75802C (11 pp.).
- [21] B. Ortac, M. Plötner, T. Schreiber, J. Limpert and A. Tünnermann, "Experimental and numerical study of pulse dynamics in positive net-cavity dispersion modelocked Yb-doped fiber lasers," *Optics Express*, vol. 15, pp. 15595-15602, 2007.
- [22] G. H. Jang and T. H. Yoon, "Environmentally-Stable All-normal-dispersion Picosecond Yb-doped Fiber Laser with an Achromatic Quarter-wave-plate," *Laser Physics*, vol. 20, pp. 1463-8, 2010.
- [23] F. Q. Lian, Z. W. Fan, X. F. Wang, Y. T. Huang, K. Huang, Y. F. Ma, G. Niu, X. H. Li and J. Yu, "Ytterbium doped all-fiber-path all-normal dispersion mode-locked laser based on semiconductor saturable mirror," *Laser Physics*, vol. 21, pp. 1103-7, 06, 2011.
- [24] D. Turchinovich, X. Liu and J. Laegsgaard, "Monolithic all-PM femtosecond Yb-fiber laser stabilized with a narrow-band fiber Bragg grating and pulse-compressed in a hollow-core photonic crystal fiber," *Optics Express*, vol. 16, pp. 14004-14014, 2008.
- [25] X. Tian, M. Tang, X. Cheng, P. P. Shum, Y. Gong and C. Lin, "High-energy wave-breaking-free pulse from all-fiber mode-locked laser system," *Optics Express*, vol. 17, pp. 7222-7, 2009.
- [26] R. Song, H. Chen, S. Chen, J. Hou and Q. Lu, "A SESAM passively mode-locked fiber laser with a long cavity including a band pass filter," *Journal of Optics*, vol. 13, 2011.
- [27] J. Liu, J. Xu and P. Wang, "High Repetition-Rate Narrow Bandwidth SESAM Mode-Locked Yb-Doped Fiber Lasers," *IEEE Photonics Technology Letters*, vol. 24, pp. 539-541, 2012.
- [28] Oliver Prochnow, Axel Ruehl, Michael Schultz, Dieter Wandt and Dietmar Kracht, "All-fiber similariton laser at 1 μm without dispersion compensation," *Optics Express*, vol. 15, pp. 6889-6893, 2007.

- [29] K. Ozgören and F. O. Ilday, "All-fiber all-normal dispersion laser with a fiber-based Lyot filter," *Opt. Lett.*, vol. 35, pp. 1296, 2010.
- [30] M. Schultz, H. Karow, O. Prochnow, D. Wandt, U. Morgner and D. Kracht, "All-fiber ytterbium femtosecond laser without dispersion compensation," *Optics Express*, vol. 16, pp. 19562-19567, 2008.
- [31] J. Fekete, A. Cserteg and R. Szipöocs, "All-fiber, all-normal dispersion ytterbium ring oscillator," *Laser Physics Letters*, vol. 6, pp. 49-53, 2009.
- [32] C. K. Nielsen and S. R. Keiding, "All-fiber mode-locked fiber laser," *Opt. Lett.*, vol. 32, pp. 1474-1476, 2007.
- [33] Z. Zhang, M. Zhang, L. Chen, Y. Jiao, Z. Tu, L. Ren, Y. Cai and C. Zhou, "Advances in SESAM and carbon nanotube saturable absorber mode locked fiber lasers," in *2009 Conference on Lasers & Electro Optics & the Pacific Rim Conference on Lasers and Electro-Optics (CLEO/PACIFIC RIM)*, 2009, 2 pp.
- [34] F. Wang, A.G. Rozhin, V. Scardaci, Z. Sun, F. Hennerich, H. White, W.I. Milne and A.C. Ferrari "Wideband-tuneable, nanotube mode-locked, fibre laser," *Nature Nanotechnology*, vol. 3, pp. 738-742, 2008.
- [35] R. Going, D. Popa, F. Torrisi, Z. Sun, T. Hasan, F. Wang and A. C. Ferrari, "500 fs wideband tunable fiber laser mode-locked by nanotubes," *Physica E: Low-Dimensional Systems and Nanostructures*, vol. 44, pp. 1078-1081, 2012.
- [36] Y. Senoo, N. Nishizawa, Y. Sakakibara, K. Sumimura, E. Itoga, H. Kataura and K. Itoh, "Polarization-maintaining, high-energy, wavelength-tunable, Er-doped ultrashort pulse fiber laser using carbon-nanotube polyimide film," *Optics Express*, vol. 17, pp. 20233-20241, 2009.
- [37] N. Nishizawa, Y. Nozaki, E. Itoga, H. Kataura and Y. Sakakibara, "Dispersion-managed, high-power, Er-doped ultrashort-pulse fiber laser using carbon-nanotube polyimide film," *Optics Express*, vol. 19, pp. 21874, 2011.
- [38] Anonymous "A compact, high power, ultrafast laser mode-locked by carbon nanotubes," *Appl. Phys. Lett.*, vol. 95, pp. 253102-253102-3, 2009.
- [39] Y. Hori, Z. Zhang and M. Nakazawa, "1070 NM passively mode-locked ytterbium-doped fiber soliton laser with SWNT/PMMA saturable absorber," in 2011, pp. 1-2.
- [40] K. Kieu and F. W. Wise, "All-fiber normal-dispersion femtosecond laser," *Optics Express*, vol. 16, pp. 11453-11458, 2008.
- [41] J. Peng, L. Zhan, Z. Gu, K. Qian, S. Luo and Q. Shen, "Direct generation of 128-fs Gaussian pulses from a compensation-free fiber laser using dual mode-locking mechanisms," *Opt. Commun.*, vol. 285, pp. 731-733, 2012.

- [42] W. Guan and J. R. Marciante, "Complete elimination of self-pulsations in dual-clad ytterbium-doped fiber lasers at all pumping levels," *Opt. Lett.*, vol. 34, pp. 815-817, 2009.
- [43] B. N. Upadhyaya, U. Chakravarty, A. Kuruvilla, S. M. Oak, M. R. Shenoy and K. Thyagarajan, "Self-pulsing characteristics of a high-power single transverse mode Yb-doped CW fiber laser," *Opt. Commun.*, vol. 283, pp. 2206-2213, 2010.
- [44] A. V. Kir'yanov and Y. O. Barmenkov, "Self-Q-switched Ytterbium-doped all-fiber laser," *Laser Physics Letters*, vol. 3, pp. 498-502, 2006.
- [45] Feng Xiao-xing, C. Bai, Chen Jia-lin, W. Li, Liang Li-ping and Lin Zun-qi, "Study of self-mode-locking in Q-switched and in all-fiber fabry-perot cavity ytterbium-doped fiber laser," in *Passive Components and Fiber-Based Devices*, 2005, pp. 88-95.
- [46] A. Hideur, T. Chartier, C. Özkul and F. Sanchez, "Dynamics and stabilization of a high power side-pumped Yb-doped double-clad fiber laser," *Opt. Commun.*, vol. 186, pp. 311-317, 2000.
- [47] B. Ortaç, A. Hideur, T. Chartier, M. Brunel, G. Martel, M. Salhi and F. Sanchez, "Influence of cavity losses on stimulated Brillouin scattering in a self-pulsing side-pumped ytterbium-doped double-clad fiber laser," *Opt. Commun.*, vol. 215, pp. 389-395, 2003.
- [48] B. N. Upadhyaya, A. Kuruvilla, U. Chakravarty, M. R. Shenoy, K. Thyagarajan and S. M. Oak, "Effect of laser linewidth and fiber length on self-pulsing dynamics and output stabilization of single-mode Yb-doped double-clad fiber laser," *Appl. Opt.*, vol. 49, pp. 2316, 2010.
- [49] Y. H. Tsang, T. A. King, D. Ko and J. Lee, "Output dynamics and stabilisation of a multi-mode double-clad Yb-doped silica fibre laser," *Opt. Commun.*, vol. 259, pp. 236-241, 2006.
- [50] B. N. Upadhyaya, U. Chakravarty, A. Kuruvilla, A. K. Nath, M. R. Shenoy and K. Thyagarajan, "Effect of steady-state conditions on self-pulsing characteristics of Yb-doped cw fiber lasers," *Opt. Commun.*, vol. 281, pp. 146-153, 2008.
- [51] F. Brunet, Y. Taillon, P. Galarneau and S. LaRochelle, "A simple model describing both self-mode locking and sustained self-pulsing in ytterbium-doped ring fiber lasers," *J. Lightwave Technol.*, vol. 23, pp. 2131-2138, 2005.
- [52] Hojoon Lee and G. P. Agrawal, "Impact of Self-Phase Modulation on Instabilities in Fiber Lasers," *IEEE J. Quant. Electron.*, vol. 46, pp. 1732-1738, 2010.
- [53] A. E. Bednyakova, O. A. Gorbunov, M. O. Politko, S. I. Kablukov, S. V. Smirnov, D. V. Churkin, M. P. Fedoruk and S. A. Babin, "Generation dynamics of the narrowband Yb-doped fiber laser," *Optics Express*, vol. 21, pp. 8177, 2013.
- [54] J. Jiang, J. Chang, S. Feng, L. Wei and Q. Mao, "Mid-IR multiwavelength difference frequency generation based on fiber lasers," *Optics Express*, vol. 18, pp. 4740, 2010.

- [55] J. Chang, Q. Mao, S. Feng, X. Gao and C. Xu, "Widely tunable mid-IR difference-frequency generation based on fiber lasers," *Opt. Lett.*, vol. 35, pp. 3486, 2010.
- [56] J. H. Chang, Q. H. Mao, S. J. Feng, J. Jiang, X. L. Li, Y. Y. Tian, C. Q. Xu and W. Q. Liu, "Theoretical and experimental investigations of the Mid-IR DFG tuning property based on fiber laser fundamental lights," *Applied Physics B*, vol. 104, pp. 851-859, 2011.
- [57] Li Xiu-li, Feng Su-juan and Mao Qing-he, "Development of fiber-type widely tunable DFG mid-infrared laser source," *Chinese Journal of Quantum Electronics*, vol. 29, pp. 298-302, 05, 2012.
- [58] A. Méndez and T. F. Morse, *Specialty Optical Fibers Handbook*. 1ed, Academic Press, 2007, pp. 223-224.
- [59] G. P. Agrawal, *Nonlinear Fiber Optics*, 3ed, Elsevier Science Academic Press, 2007, pp. 11-13,63-66,97-104,213.
- [60] D. J. Richardson, J. Nilsson and W. A. Clarkson, "High power fiber lasers: current status and future perspectives [Invited]," *Journal of the Optical Society of America B*, vol. 27, pp. B63, 2010.
- [61] G. C. Valley, "Modeling Cladding-Pumped Er/Yb Fiber Amplifiers," *Optical Fiber Technology*, vol. 7, pp. 21-44, 2001.
- [62] D. T. Nguyen, D. T. Nguyen, A. Chavez-Pirson, A. Chavez-Pirson, Shibin Jiang, N. Peyghambarian and N. Peyghambarian, "A Novel Approach of Modeling Cladding-Pumped Highly Er-Yb Co-Doped Fiber Amplifiers," *IEEE J. Quant. Electron.*, vol. 43, pp. 1018-1027, 2007.
- [63] O. Deparis, O. Deparis, R. Kiyari, S. A. Vasiliev, V. O. I. Medvedkov, E. M. Dianov, O. Pottiez, P. Megret and M. Blondel, "Polarization-maintaining fiber Bragg gratings for wavelength selection in actively mode-locked Er-doped fiber lasers," *IEEE Photonics Technology Letters*, vol. 13, pp. 284-286, 2001.
- [64] A. D. Yablon, *Optical Fiber Fusion Splicing*, Springer series in optical sciences, 2005, pp. 177-180.
- [65] L. Fuyun, Z. Aiting, F. Yaxian, W. Hongjie, G. Shuguang and L. Kecheng, "Study on self-Q-switched double-cladding fiber laser based on SBS," in *Optical Interconnects for Telecommunication and Data Communications*, 2000, pp. 172-5.
- [66] A. Johnstone, W. Lu, J. S. Uppal and R. G. Harrison, "Sustained and bursting oscillations in stimulated Brillouin scattering with external feedback in optical fibre," *Opt. Commun.*, vol. 81, pp. 222-224, 1991.

- [67] M. Salhi, A. Hideur, T. Chartier, M. Brunel, G. Martel, C. Ozkul and F. Sanchez, "Evidence of Brillouin scattering in an ytterbium-doped double-clad fiber laser," *Opt. Lett.*, vol. 27, pp. 1294-1296, 2002.
- [68] R. G. Molla, "Nonlinear fiber optics for Bio-Sensing," M.Sc. Thesis, University of Kansas, 2005 .
- [69] A. Yariv and P. Yeh, *Photonics: Optical Electronics in Modern Communications*, 6ed, Oxford University Press 2007, pp.251-273, 633-637.
- [70] M. F. S. Ferreira, *Nonlinear Effects in Optical Fibers*, Wiley, 2011, pp.2-3,70-74.
- [71] J. A. Buck and I. Jacobs, *Fundamentals of Optical Fibers*, Wiley Series in Pure and Applied Optics, 2ed, 2004, pp. 241-251
- [72] <http://www.photonics.umd.edu/software/ssprop>.
- [73] J. Diels, *Ultrashort Laser Pulse Phenomena*, 2ed, Elsevier Science Academic Press, 2006, pp.63-66, 97-104, 317-318, 381-384
- [74] C. K. Nielsen, "Mode-locked fiber lasers: Theoretical and Experimental Development," PhD. Thesis, University of Aarhus, Denmark, 2006.
- [75] F. O. Ilday, *Ultrashort pulse propagator v.2.2.2 user guide*, Bilkent University, 2001.
- [76] B. Washburn: www.phys.ksu.edu/personal/washburn/pdf/washburn_thesis_chapter4.pdf .
- [77] J. Lægsgaard, "Control of fibre laser mode-locking by narrow-band Bragg gratings," *Journal of Physics B: Atomic, Molecular and Optical Physics*, vol. 41, pp. 095401, 2008.
- [78] E. Paulucci, N. A. Russo, E. E. Sicre and R. Duchowicz, "Numerical and experimental comparison of an all-fiber APM laser with two-coupled linear cavities," *Optics & Laser Technology*, vol. 48, pp. 495-502, 2013.
- [79] A. J. Rogers, *Polarization in Optical Fibers*, The Artech House Applied Photonics Series, 2008 ,pp.94-98, 100-101.
- [80] L. N. Binh and N. Q. Ngo, *Ultra-Fast Fiber Lasers: Principles and Applications with MATLAB Models*, CRC Press, 2010, pp.180-182.
- [81] Y. Zhao, T. Song, D. Wu and Q. Wang, "Research on fiber optic temperature sensor using a novel high-birefringent fiber loop mirror with a reflection probe," *Sensors & Actuators: A.Physical*, vol. 184, pp. 22, 2012.

- [82] R. M. Silva, A. Layeghi, M. I. Zibaii, H. Latifi, J. L. Santos and O. Frazao, "Theoretical and Experimental Results of High-Birefringent Fiber Loop Mirror With an Output Port Probe," *J. Lightwave Technol.*, vol. 30, pp. 1032-1036, 2012.
- [83] F. Yang, Z. Q. Pan, Q. Ye, D. J. Chen, H. W. Cai and R. H. Qu, "Effect of active fiber birefringence on polarization properties of DBR all-fiber laser," *Laser Physics*, vol. 22, pp. 778-783, 2012.
- [84] M. Hofer, M. E. Fermann, F. Haberl, M. H. Ober and A. J. Schmidt, "Mode locking with cross-phase and self-phase modulation," *Opt. Lett.*, vol. 16, pp. 502-504, 1991.
- [85] P. Myslinski, J. Chrostowski, J. A. K. Koningstein and J. R. Simpson, "Self-mode locking in a Q-switched erbium-doped fiber laser," *Appl. Opt.*, vol. 32, pp. 286-290, 1993.
- [86] F. Krausz and T. Brabec, "Passive mode locking in standing-wave laser resonators," *Opt. Lett.*, vol. 18, pp. 888, 1993.
- [87] C. Liu, A. Galvanauskas, V. Khitrov, B. Samson, U. Manyam, K. Tankala, D. Machewirth and S. Heinemann, "High-power single-polarization and single-transverse-mode fiber laser with an all-fiber cavity and fiber-grating stabilized spectrum," *Opt. Lett.*, vol. 31, pp. 17-19, 2006.
- [88] M. - Li, D. A. Nolan, G. E. Berkey, X. Chen, J. Koh, D. T. Walton, J. Wang, W. A. Wood and L. A. Zenteno, "High-performance single-polarization optical fibers," in *Passive Components and Fiber-Based Devices*, 2005, pp. 612-21.
- [89] D. Xue, A. R. El-Damak and X. Gu, "All-fiber single polarized Yb-doped fiber laser with a high extinction ratio," *Opt. Commun.*, vol. 283, pp. 1059-1061, 2010.
- [90] A. Shirakawa, A. Shirakawa, M. Kamijo, M. Kamijo, J. Ota, J. Ota, K. - Ueda, K. - Ueda, K. Mizuuchi, H. Furuya and K. Yamamoto, "Characteristics of Linearly Polarized Yb-Doped Fiber Laser in an All-Fiber Configuration," *IEEE Photonics Technology Letters*, vol. 19, pp. 1664-1666, 2007.
- [91] J. Wang, L. Zhang, J. Hu, L. Si, J. Chen, X. Gu and Y. Feng, "Efficient linearly polarized ytterbium-doped fiber laser at 1120 nm," *Appl. Opt.*, vol. 51, pp. 3801-3, 06/10, 2012.
- [92] J. Wang, J. Hu, L. Zhang, X. Gu, J. Chen and Y. Feng, "A 100 W all-fiber linearly-polarized Yb-doped single-mode fiber laser at 1120 nm," *Optics Express*, vol. 20, pp. 28373, 2012.
- [93] P. Liu, F. Yan, C. Wang, F. Zhang and C. Liu, "A switchable dual-wavelength all-fiber laser based on Panda-type photosensitive polarization-maintaining erbium-doped fiber," *Microwave Opt Technol Lett*, vol. 52, pp. 386-389, 2010.
- [94] D. Liu and C. Wang, "Single linearly polarized, widely and freely tunable two wavelengths Yb³⁺-doped fiber laser," *Opt. Commun.*, vol. 283, pp. 98-103, 2010.

- [95] Ryun Kyung Kim, Suho Chu and Young-Geun Han, "Stable and Widely Tunable Single-Longitudinal-Mode Dual-Wavelength Erbium-Doped Fiber Laser for Optical Beat Frequency Generation," *IEEE Photonics Technology Letters*, vol. 24, pp. 521-523, 2012.
- [96] J. Bouillet, L. Lavoute, A. Desfarges Berthelemot, V. Kermène, P. Roy, V. Couderc, B. Dussardier and A. Jurduc, "Tunable red-light source by frequency mixing from dual band Er/Yb co-doped fiber laser," *Optics Express*, vol. 14, pp. 3936-3941, 2006.
- [97] G. Q. Xie, D. Y. Tang, H. Luo, H. J. Zhang, H. H. Yu, J. Y. Wang, X. T. Tao, M. H. Jiang and L. J. Qian, "Dual-wavelength synchronously mode-locked Nd:CNGG laser," *Opt. Lett.*, vol. 33, pp. 1872-1874, 2008.
- [98] O. Deparis, O. Deparis, R. Kiyon, E. Salik, D. Starodubov, J. Feinberg, O. Pottiez, P. Megret and M. Blondel, "Round-trip time and dispersion optimization in a dual-wavelength actively mode-locked Er-doped fiber laser including nonchirped fiber Bragg gratings," *IEEE Photonics Technology Letters*, vol. 11, pp. 1238-1240, 1999.
- [99] Newport technical note: Insights into high-Speed detectors and high frequency techniques (<http://www.newport.com/Application-Notes/981012/1033/content.aspx>).
- [100] I. Kelson and A. A. Hardy, "Strongly pumped fiber lasers," *IEEE J. Quant. Electron.*, vol. 34, pp. 1570-1577, 1998.
- [101] Ido Kelson and Amos Hardy, "Optimization of Strongly Pumped Fiber Lasers," *J. Lightwave Technol.*, vol. 17, pp. 891-897, 1999.

Publications

1. A.R. El-Damak and X.Gu, "Investigation of self mode-locked picoseconds pulses in an all-PM double-clad Yb-doped fiber laser," *Optic Express*, in review, 2013.
2. A.R. EL-Damak, J. Chang, J. Sun, C. Xu and X. Gu, "Dual-Wavelength, Linearly Polarized All-Fiber Laser With High Extinction Ratio," *IEEE Photonics Journal*, vol. 5, pp. 1501406-1501406, 2013.
3. L. Zhang, A. R. El-Damak, Y. Feng and X. Gu, "Experimental and numerical studies of mode-locked fiber laser with large normal and anomalous dispersion," *Optics Express*, vol. 21, pp. 12014-12021, 2013.
4. D. Xue, A. R. El-Damak, and X. Gu, "All-fiber single polarized Yb-doped fiber laser with a high extinction ratio." *Opt. Commun.*, vol.283, no. 6, pp.1059-1061, 2010.